Enhancement of Frequency Support Capabilities of Type 1 and Type 2 Wind Turbines

Olivare Dzune Mipoung

A Thesis
In the Department
of
Electrical and Computer Engineering

Presented in Partial Fulfillment of the Requirements

For the Degree of

Doctor of philosophy (Electrical and Computer Engineering) at

Concordia University

Montreal, Quebec, Canada

October 2012

© Olivare Dzune Mipoung 2012

CONCORDIA UNIVERSITY

SCHOOL OF GRADUATE STUDIES

This is to certify that the thesis prepared

By: **Olivare Dzune Mipoung**

Entitled: **Enhancement of Frequency Support Capabilities of Type 1 and Type 2 Wind Turbines**

and submitted in partial fulfillment of the requirements for the degree of

DOCTOR OF PHILOSOPHY (Electrical & Computer Engineering)

complies with the regulations of the University and meets the accepted standards with respect to originality and quality.

Signed by the final examining committee:

_____ Chair
Dr. H. Akbari

_____ External Examiner
Dr. J. Meng

_____ External to Program
Dr. M. Paraschivoiu

_____ Examiner
Dr. A. Aghdam

_____ Examiner
Dr. S. Williamson

_____ Thesis Supervisor
Dr. P. Pillay

_____ Thesis Co-Supervisor
Dr. L.A.C. Lopes

Approved by _____
Dr. J.X. Zhang, Graduate Program Director

October 29, 2012

_____
Dr. Robin A.L. Drew, Dean
Faculty of Engineering and Computer Science

ABSTRACT

Enhancement of Frequency Support Capabilities of Type 1 and Type 2 Wind Turbines

Olivare Dzune Mipoung, Ph.D

Concordia University, 2012

Electricity production in remote communities in northern Quebec is still largely based on diesel power supply. Environmental concerns and the cost of electricity are driving the integration of wind energy in such systems. However, due to the stochastic nature of the wind and the highly variable load characteristic in these communities, the displacement of diesel fuel is usually small. In addition to this, when the system operates with high wind penetration, the frequency tends to vary widely, thereby raising some important stability concerns. This research work investigates important technical issues related to the implementation of fixed-pitch wind turbines that present large droop factor in droop-controlled hybrid diesel mini-grids, to enhance the frequency regulation. An assessment of generators for small scale generation is first presented. Next, a concept for implementing a fixed speed (type 1) wind turbine in a hybrid system is developed, using the power-frequency characteristic of the wind turbine. Due to some limitations of the proposed concept, resulting mainly from the fact that wind turbine power-frequency characteristics present a relatively low droop factor, type 1 wind turbines cannot assist to a high extent with the network frequency regulation. Therefore an approach to implement type 2 wind turbines which present a better droop factor has been developed and used to overcome the limitations of the type 1 system. A hybrid wind diesel mini-grid model without storage has been developed and used to validate the analysis. The proposed implementation concepts provide several benefits for the electrification of remote communities, which are highlighted at different stages of the thesis.

ACKNOWLEDGEMENTS

I would like to express my deep and sincere gratitude to my supervisor, **Prof. P. Pillay** for giving me the opportunity to go through the PhD program. He has inspired me in many ways, from the beginning to the end of my research program. It has been an honor for me to be his PhD student. I also would like to thank him for the financial support.

I am deeply grateful to my co-supervisor, **Prof. L. Lopes** for his detailed guidance and constructive advices, from which I have learned and developed important technical skills to become a better researcher in the field of electrical engineering.

My sincere gratitude goes to all my colleagues from the PEER group at Concordia University for being supportive in my PhD journey. I would like to thank the Natural Sciences & Engineering Research Council of Canada and Hydro-Québec for financially supporting the PEER group.

I also wish to express my love and my heartfelt gratitude to my beloved family and friends for their understanding and endless love, throughout the duration of my studies.

Above all, Glory be given to the most Gracious and most Merciful one in who I put my trust. Every day while we are going to bed, there is no guarantee that we will still be alive the following day. Life and time are gifts from above and I thank God for these gifts and for His continued provisions.

TABLE OF CONTENTS

LIST OF FIGURES

LIST OF TABLES

CHAPTER 1

INTRODUCTION

This chapter introduces the research work presented in this thesis. A brief overview of renewable energy sources with emphasis on wind energy technology is given. Some related work done on hybrid wind-diesel systems are presented, leading to the definition of the research goal and research objectives. The chapter ends with the key steps used to address the objectives, the new contribution of the research, and the structure of the thesis.

Electrical energy is an essential component in the development process of remote communities. However these communities are still prone to several electrification problems in many countries. More than one billion people in the world still do not have access to electricity, of which 83% live in isolated areas [1]. Some of the factors increasing the delay of the electrification process in these areas are:

- High population growth;
- High dispersal load distribution in isolated areas;
- Costs associated with grid extensions;
- Poor access to roads in some locations;
- Low profits for most power supply companies who could invest in these locations;

Rural people often rely largely on wood, agricultural residues and animal dung to meet their energy needs. Thus, the following impacts can be observed:

- Increased pressure on traditional energy resources (such as wood) ;
- Limited supply of traditional and commercial energy versus increasing energy demand;

- Heavy dependence on fuel, leading to fossil fuel depletion and increasing environmental pollution etc.

The increasing problem of rural electrification due to the use of conventional and non-renewable energy resources is the main reason why renewable energy sources are becoming better alternatives for isolated communities.

1.1 Renewable energy sources

Renewable energy comes from resources which are naturally replenished and can be classified into the following types:

- Hydro, where electricity is produced from water;
- Biomass, where electricity is produced from the wastes;
- Geothermal, where electricity is produced from naturally occurring steam under the earth's surface;
- Wind, where electricity is produced from the power available in the wind;
- Photovoltaic, where electricity is produced from sunlight;
- Tidal, where electricity is produced from ocean waves.

The use of renewable energy sources can provide the following benefits:

- Low or no negative environmental impact
- No natural resources depletion
- Low or no carbon or other greenhouse gas emission
- Reduced cost of operation
- Sustainable energy

1.3 Research Background

Electricity generation in remote communities in the north of Quebec is still based on diesel power plants. Environmental concerns and the cost of electricity are driving the integration of wind energy in such systems. However, due to the stochastic nature of the wind and the highly variable load characteristics of remote communities, the displacement of diesel fuel is usually small. This research work builds up from the need to adapt fixed-speed (or limited variable speed) wind turbines and diesel generation concepts, to design a suitable low cost hybrid wind-diesel system for remote communities. The energy supply of rural areas requires the design and application of suitable integrated renewable energy systems with analytical matching of needs, resources and technologies [2].

1.4 Hybrid wind-diesel systems

A hybrid power system is a system that combines two or more electrical power sources where at least one source is a renewable energy source. Recent international appeal on environmental issues such as the reduction of CO_2 emissions and fossil fuel depletion has made hybrid power systems to become better alternatives for decentralized power generation. Some of the aspects justifying the importance of hybrid power systems are:

- The need to take advantage of local renewable resources when they are available ;
- It is possible to centrally locate the power plants where electricity is needed;
- It is possible to store some of the energy produced for later use;
- The importance of having backup generators or secondary power supply;
- It is possible to achieve high scale benefits using multiple generation units;
- Renewable energy technology is relatively mature and well understood;

Figure 1.1 represents a typical configuration of a hybrid wind diesel power system.

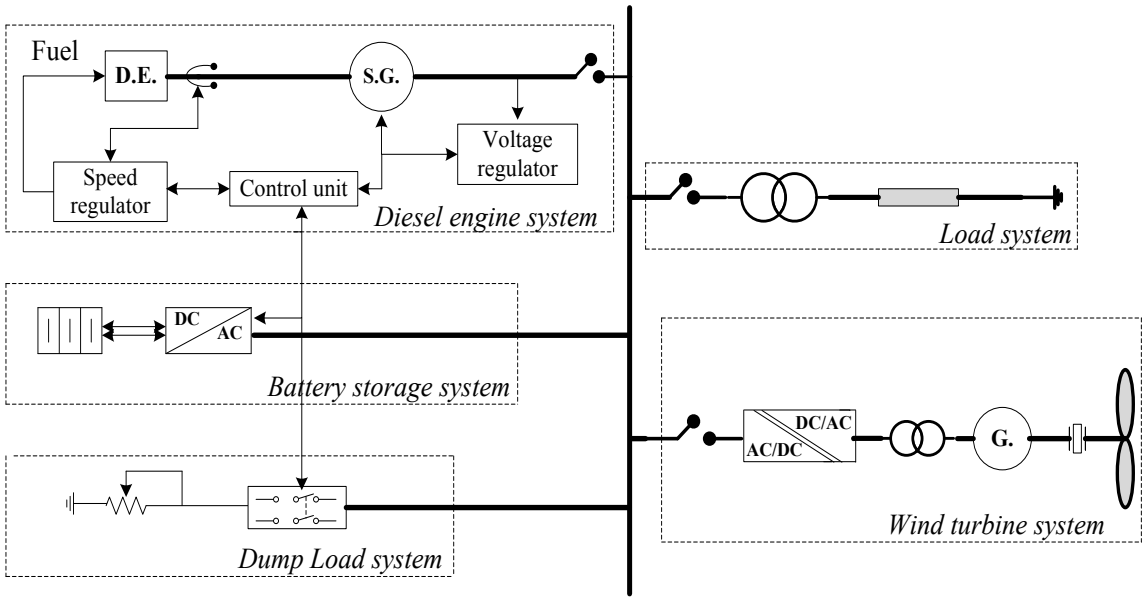

Figure 1. 1 Typical hybrid wind-diesel system

In such as system, both generators would have to share the load demand while the regulation of the system's voltage and frequency is fixed by the diesel-generator set. A dump load could be used to absorb the excess power generated by the wind turbine and, a battery set could be used to meet the energy storage requirements. The system configuration and component size depend on the load characteristic and available wind resource on the site. The level of the power control depends on the level of wind penetration. The wind turbine can be fixed-speed or variable speed.

1.4.1 Fixed speed wind turbines

Fixed-speed turbines operate at almost constant rotor revolutions per minute (rpm) and are optimized for energy capture at a given rotor diameter and at a particular speed in the wind-power curve. Figure 1.2 represents a typical configuration of a fixed-speed wind turbine. In such a system, the electrical generator is directly connected to the grid.

Therefore, only a limited variation of the rotor shaft speed is allowed. This mode of operation has been used in the early 1990s [3].

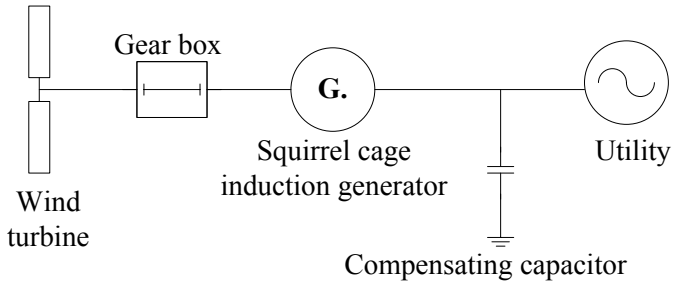

Figure 1. 2 Typical fixed speed wind application

Regardless of the wind speed, the turbine shaft speed is fixed by the gear box ratio, the generator design and the utility frequency. Fixed-speed wind systems are generally equipped with an induction generator (wound rotor or cage rotor) directly coupled to the grid. In typical applications the generator is connected to the grid through a soft starter (at startup) and a capacitor bank is used to provide reactive power compensation. These systems are designed to achieve maximum efficiency at one particular wind speed. In order to increase the power production, the generator of some fixed speed turbines has two winding sets [3]: one used at low wind speeds (typically 8 poles) and the other at medium and high wind speeds (typically 4 to 6 poles). In direct drive applications, the generator shaft is directly connected to the turbine shaft, resulting in a low speed generator with a high number of poles and large diameter. Fixed-speed wind turbines can present the following advantages:

- Simple construction;
- Robust and reliable operation;
- Relatively low cost of the electric parts;
- Well proven technology;

However, the following disadvantages can be highlighted:

- Uncontrollable reactive power consumption;
- Large mechanical loads resulting from torque pulsations due to power fluctuations;
- Limited power quality control;
- In weak grids, power fluctuations lead to voltage fluctuations which may cause flicker problems;

Voltage and power fluctuations resulting from large mechanical loads develop mechanical stresses that decrease the lifetime of the turbines [4]. In fixed speed operation, there is only one wind velocity that results in an optimum tip speed ratio. Therefore, the wind turbine often operates below its optimum performance, and generally does not extract maximum power from the wind [5]. Variable speed turbines are being used to overcome these drawbacks.

1.4.2 Variable speed wind turbines

As the wind speed varies, the speed of the turbine varies accordingly. In typical variable speed applications, a converter unit (connecting the generator to the grid) is controlled to operate at the optimum tip speed ratio, thereby achieving an optimum operation of the system at different wind speeds [6]. Variable speed wind turbines can present the following advantages:

- Increased Annual Energy Production (AEP) due to the fact that the turbine speed can be adjusted as a function of wind speed to maximize the output power [6];
- Reduced mechanical stresses. Energy stored in the mechanical inertia of the turbine, creates a compliance that reduces torque pulsations [7-8];

- Improved Power quality due to low power pulsations. The reduction of power pulsations decreases the voltage deviations from its rated level at the point of common coupling (PCC), thereby allowing an increased penetration of the wind power in the network [8];
- Reduced acoustic noise.

The main disadvantages of the variable-speed wind systems are the additional cost and the complexity of power converters required to interface the generator and the grid.

1.4.3 Power control in wind energy systems

Wind systems are designed with specific controllers used to control the aerodynamic forces acting on the wind rotor. The following control techniques are typically used.

1.4.3.1 Stall or passive control

In this method, the blades are bolted onto the hub at a fixed angle. The rotor aerodynamics is designed to cause the rotor to lose power (to stall) when the wind speed exceeds a certain level. This is a slow aerodynamic power regulation resulting in low power fluctuations of the wind generator compared to fast–pitch regulation. Some advantages of the passive control method are:

- Simple structure;
- Robust control method;
- Lower cost of the control unit;

The following drawbacks of the passive control can be highlighted:

- Low efficiency at low wind speeds;
- No assisted start up;

- High steady-state power variations due to the air density and grid frequency variations.

1.4.3.2 Pitch or active control

In this method, the blades are allowed to turn out or into the wind as the output power becomes too high or too low. Active control method can present the following advantages:

- Good power control. At high wind speeds, the output power is kept close to the rated power of the generator;
- Assisted start up;
- Emergency stop;

Some disadvantages of the active control method are:

- Extra complexity (due to the pitch mechanism);
- Limited speed of the pitch mechanism. Thus, the instantaneous power fluctuates around the rated mean power due to the gusts components of the wind speed;

1.4.3.3 Active stall control

In this method, the stall of the blade is actively controlled by pitching the blades. At low wind speeds, the blades are pitched (similar to the pitch-control method) in order to achieve maximum efficiency. At high wind speeds the blades are kept into a deeper stall by being pitched slightly into the opposite direction to that of the pitch-control. Active stall wind turbines can generate power with limited fluctuations compared to pitch-controlled wind turbines. This control method has the advantage of being able to compensate variations in the air density. The combination with the pitch mechanism makes it easier to carry out emergency stops and start up assistance.

1.4.4 Main characteristics of hybrid wind-diesel systems

Hybrid diesel systems are systems designed to increase the capacity and to reduce the cost and environmental impact of the electricity generation in remote communities and facilities that are not linked to a power grid. The following aspects represent some of the features related to these systems.

- Reduced consumption of the fuel;
- Reduced environmental impact, fuel transportation and emission issues;
- Can be used for larger power demands up to MW ranges;
- Batteries, if used, store power to cover short lulls in the renewable sources;
- Reduced diesel storage needs;
- However, it requires a good renewable resource to be economical;

Hybrid wind-diesel systems owe their sustainable operation to the amount of wind resource available where they operate. In general, low, medium and high wind penetration hybrid diesel systems are being used [9-13].

1.4.4.1 Low penetration Wind-diesel systems

Wind-diesel systems with low wind penetration can present the following characteristics:

- Easy integration in existing diesel system with little or no diesel modifications required;
- Diesel engines provide all the frequency, voltage and reactive power control;
- Switch gear would have to be modified to add wind turbines in the system;
- Modest fuel savings up to approximately 20% is possible;
- Require limited operating staff.

1.4.4.2 Medium penetration Wind-diesel systems

Medium penetration systems present the following characteristics:

- Diesels are expected to operate all the time and provide main system stability control;
- Additional components are required to control the system frequency, to eliminate the excess energy and to provide VAR support;
- Secondary diesels may be shut off when not needed, reducing diesel operating hours and fuel used;
- In high wind periods, primary diesel runs at low loading. Therefore, Diesels may operate outside of their standard operating region and may require more maintenance;
- Thermal loads could be used to set minimum loading;
- A limited supervisory control is required to assist diesels in maintaining the power quality.

1.4.4.3 High penetration Wind-diesel systems

In high penetration systems the following observations can be made:

- All diesel engines are allowed to shut down during high wind periods, reducing fuel consumption and operation hours;
- Require hardware to maintain voltage, frequency and reactive power control;
- High technology dependency with system architecture that requires automated operation;
- A safe operation strategy is required so that if some components are not working, diesel engines can be operated to supply the load;

- There is a limited required operating staff.

Table 1.1 summarizes the main features related to the individual hybrid system configurations.

Table 1. 1 Summary of the hybrid systems characteristics

Level of wind penetration	Operating characteristics
Low	- Wind power reduces negative load on diesel - All wind energy goes to primary load - Does not require complex supervisory control
Medium	- At high wind speeds, secondary loads are dispatched to ensure sufficient diesel loading or wind power curtailment - Requires relatively simple control system
High	- Diesel(s) may be shut down during high wind availability - Auxiliary components are required to regulate voltage and frequency - Requires sophisticated control system

High penetration systems have low operating costs and greater fuel savings. Therefore, these systems are the type assumed in this research work. However, their capital cost can be relatively high.

1.5 Technical issues in high penetration wind-diesel systems

In high penetration systems, the diesel engine (genset) may be shut down during high wind availability. Therefore three modes of operation can be observed: “diesels only (DO)”, “wind only (WO)” and “wind and diesel (WD)”. A sophisticated control system for voltage and frequency regulation and suitable energy storage devices are required. An important issue with hybrid systems based on high wind penetration is the power shedding. When there is excess of the wind power and the storage device is full, part of the power produced by the wind system needs to be shed. One way to achieve this is to use a dump load.

During the “WD” operating mode, the load power is supplied by both generators. However, due to the stochastic nature of the wind and the highly variable load

characteristic (typical in remote communities), the frequency tends to vary widely. Thus, the diesel engine which is the grid forming unit would have to compensate for the power imbalance due to the wind variations. On the other hand, load variations in the system create an output power variation of the individual generators, which could lead to torque pulsations (resulting in high stress on mechanical components), reactive power variations and unbalanced current in the individual generators. This can be especially severe in the genset unit since diesel engines have relatively poor dynamic performance.

Significant research efforts have been made to reduce the fuel consumption and to provide good power quality of diesel power system. In [14], a multivariable frequency domain technique for dynamic analysis of an autonomous wind-diesel power system is discussed. The author demonstrates that it is possible to improve the system performance using simple model based controllers for the diesel engine. In [15], an adaptive fuzzy logic controller for a wind-diesel system using a stall regulated wind turbine equipped with induction generator is presented. In this work the authors use an adaptive network based inference system (ANFIS) to generate fuzzy membership functions and control rules for the diesel engine governor. Authors in [16] deal with the implementation of a distributed control system using the controller area network (CAN) in hybrid wind diesel systems with high wind penetration. In [17], the authors propose a Monte Carlo based method for predicting the economic performance and reliability of autonomous energy systems consisting of diesel generators and wind energy converters (WECs), meanwhile in [18] an algorithm for determining the optimal operation scheduling over a period of hours for an autonomous energy system consisting of diesel units and wind generators is given.

These related works do share a common feature. The approach and contributions suggested by the authors are based on active control systems whereby a converter unit used to interface the wind generator and the grid is required, thereby increasing considerably the cost of the system.

The contribution of the research work presented in this thesis differs from the cited works based on the fact that it is based on passive or reduced active control approach in which no converter is required between the wind generator and the grid. In this case the overall cost of the electrification system can be considerably minimized.

1.6 Research goal and research objectives

The goal of this research is to design a small scale hybrid wind-diesel system that presents suitable power sharing scheme between the generators, while featuring reasonable cost and efficient load demand satisfaction. The research objectives are the following:

- Examine the appropriate generator selection for small scale generation;
- Propose an approach to obtain the power-frequency characteristic of fixed-speed wind turbines;
- Identify key parameters that affect the slope of the power-frequency curve;
- Examine the performance of type 1 wind turbines in the mini-grid;
- Propose an approach to enhance slope of the power-frequency curve using simple variable speed (type 2) wind turbines in the hybrid system.

The research work presented in this thesis involves the following steps:

- Elaborate the background and related work on hybrid wind-diesel systems and define the research goal and objectives (details in chapter 1);

- Generator assessment for small scale generation (details in chapter 2);
- Mathematical modeling and experimental validation (details in chapter 3);
- Fixed-speed wind turbine performance in diesel mini-grids (details in chapter 4);
- Type 2 wind turbine performance in diesel mini-grids (details in chapter 5);

Figure 1.4 summarizes the key steps of the study presented in this thesis.

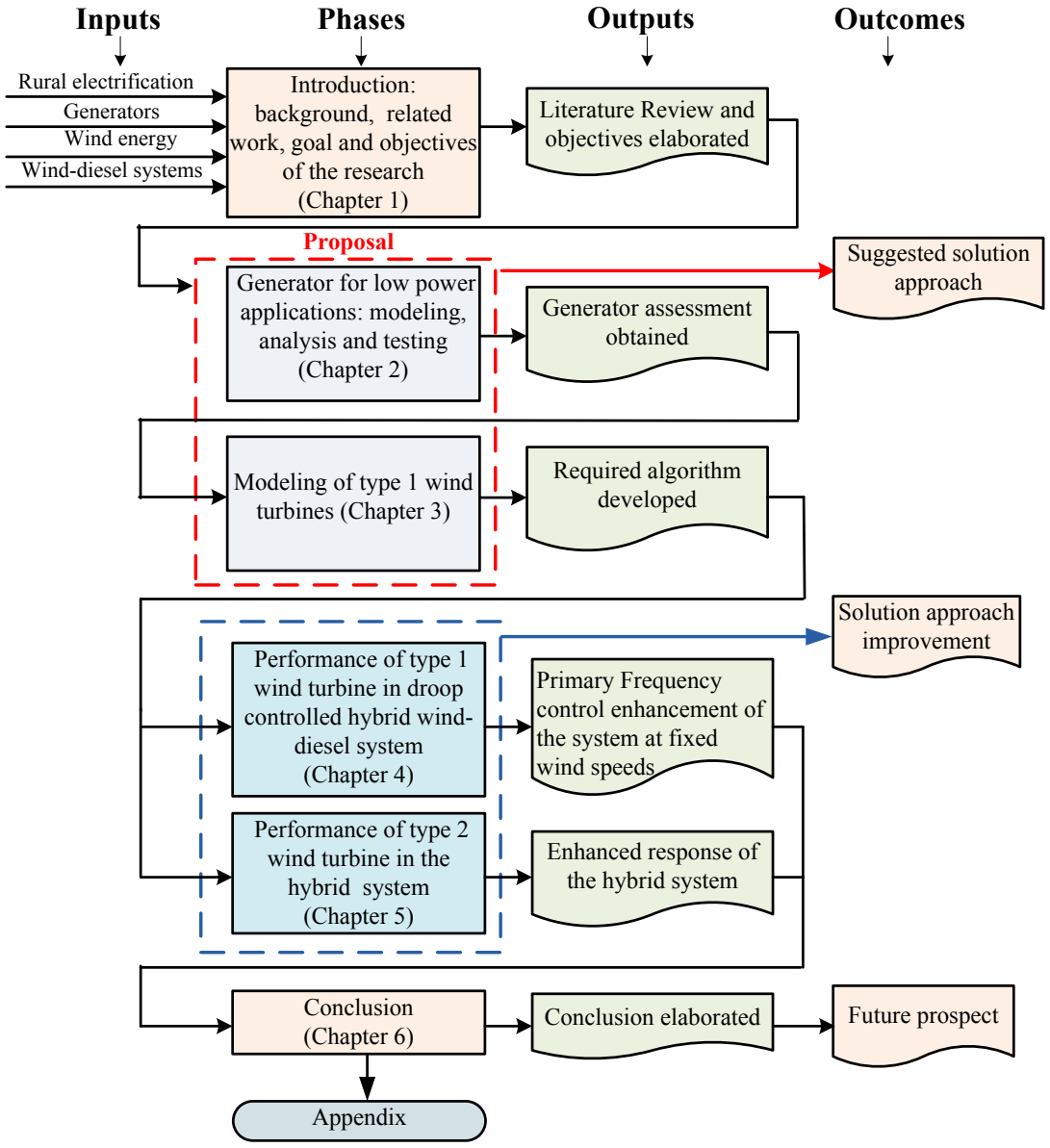

Figure 1. 3 Key steps of the research work

1.7 New contributions of the research

The limitations of the diesel power supply, mainly the electricity cost and environmental concerns have made hybrid wind-diesel generation to be a better alternative for remote communities. For optimum wind energy extraction at all wind speeds the system would typically operate with variable speed turbine. This configuration involves a converter that allows wide speed range operation of the wind turbine. However, the cost of the electrification system using this configuration increases considerably. From this aspect (cost wise), simple wind turbine technologies such as type1 and type 2 wind turbines appear to be cost effective. Droop control is a well-known technique used for parallel operation and power sharing of generators, whereby the relationship between generated power and generator frequency is required.

While a desired droop characteristic can easily be realized in the governor of controllable generators (such as a diesel engine), it is not as obvious for uncontrollable ones like fixed-pitch type 1 and type 2 wind generators. The new contribution of this thesis involve three main aspects: first, an algorithm which can be used to obtain the droop characteristic of type 1 and type 2 wind turbines is proposed and verified experimentally. Next, an identification of key parameters that affect the slope of the wind turbine power-frequency curves is done based on which a design approach to achieve suitable droop-controlled operation of the wind turbine in the hybrid diesel mini-grid has been proposed. Some standards such as the new European grid codes require that renewable energy sources should be able to decrease their output power proportionally to the grid frequency, as the frequency exceeds certain values. In droop controlled systems, this requirement can be achieved if the renewable energy source presents a means to control

the droop factor of the power-frequency characteristic. The third aspect of the contribution of this thesis concerns an approach that has been suggested to achieve this, using controlled type 2 wind turbines. A dynamic model of a storage-less hybrid wind diesel mini-grids has been developed and used to demonstrate the effectiveness of the proposed techniques. Several benefits of these techniques are highlighted.

Although the integration of wind turbines in diesel power plants is aimed at reducing the fuel consumption of the system, while providing good power quality to the mini-grid, the work presented in this thesis does not address the diesel engine fuel optimization, or advanced control strategy for regulating the network frequency. Instead, this research focuses on a simple approach that uses the aerodynamic characteristics of wind turbines to enhance the frequency regulation of the mini-grid through a passive control scheme.

This way, the system does not require any converter or advanced control strategy to interface the wind generator and the mini-grid. Thus, the overall cost of the mini-grid can be substantially reduced.

1.8 Summary of chapter 1

This chapter has provided an overview of the related work and research issues through which the research goal and objectives have been defined. The key steps used to achieve the goal of the research work are presented. The chapter ends with the new contributions of the research and provides the structure of the thesis as well as the list of publications related to this research.

1.9 Structure of the thesis

Chapter 1 discusses the background and related work. Some research issues are discussed and the goal and objectives of the research are defined. This chapter ends with the key steps of the research work.

Chapter 2 presents an assessment of suitable generator types for low power applications. A dynamic model of the individual generator types is derived and used to aid the analysis.

Chapter 3 proposes an approach to obtain the droop characteristic of fixed-speed wind turbines.

Chapter 4 provides the design steps to achieve a droop controlled behavior of the fixed-speed wind turbine in the hybrid mini-grid. The performance of type 1 wind turbines in the hybrid mini-grid is verified in this chapter.

Chapter 5 presents the potential of type 2 wind turbines in the hybrid mini-grid. An approach to implement type 2 wind turbines is proposed in this chapter.

Chapter 6 draws the conclusion and future prospects of the research work.

1.10 List of publications

1.10.1 Journal proceedings

1. O. Dzune Mipoung, P. Pillay and Lopes, L. A. C, "Generator Assessment for Rural Electrification from Renewable Energy" *JEE Electrical machine and drives*, 2012;
2. O. Dzune Mipoung, P. Pillay and Lopes, L. A. C, “Fatigue Failure Estimation of Fixed-Speed Wind Turbines in Droop Controlled Storage-Less Hybrid Diesel Mini-grids", *International Journal of Energy Science, 2012;*

3. O. Dzune Mipoung, Lopes, L. A. C, and P. Pillay, "Potential of Type 1 Wind Turbines for Assisting with Primary Frequency Control in Storage-Less Diesel Hybrid Mini-Grids", (submitted for publications to *IEEE Transaction on Industrial Electronics*);
4. O. Dzune Mipoung, Lopes, L. A. C, and P. Pillay, "Frequency support from a fixed-pitch type 2 wind turbine in a diesel hybrid mini-grid", (submitted for publications to *IEEE Transaction on sustainable energy*).

1.10.2 Refereed conference proceedings

1. O. Dzune Mipoung, L.A.C Lopes and P. Pillay, "Wind-Diesel Emulator for Isolated Grid Applications," *International Council on Large Electric Systems*, Montreal, Canada, Sep. 2012;
2. O. Dzune Mipoung, L.A.C Lopes and P. Pillay, "Power Estimation of Induction Generators fed from Wind Turbines," in Proc. *IEEE Industry Applications Society Annual Meeting*, Orlando, FL, USA, Oct. 9-13, 2011;
3. O. Dzune Mipoung, P. Pillay and L.A.C Lopes, "Generator Selection for Rural Electrification from Renewable Energy," in Proc. *IEEE International Electric Machines and Drives*, Niagara Falls, ON, Canada, May 2011;
4. O. D. Mipoung and P. Pillay, "Generator Requirements for Rural Electrification from Renewable Energy", XII World Energy Congress, Sept 2010, Montreal;
5. O. Mipoung, P. Pillay, "Generators for Rural Electrification from Renewable Energy" *IEEE Electrical Power and Energy Conference*, Montreal, Canada, Oct. 22-23, 2009;

6. O. Dzune Mipoung, L.A.C Lopes and P. Pillay, “Fixed-Pitch Type 1 Wind Turbines with Large Droop Slopes for Diesel Hybrid Mini-Grids” (submitted for publications to *IEEE ICIT 2013, South Africa*).

CHAPTER 2

GENERATORS FOR SMALL SCALE POWER APPLICATIONS

This chapter presents an assessment of generators for small scale power generation. Different generator configurations are analyzed. Some synchronization techniques suitable for the individual generator types are introduced. Detailed models of the individual machine types are developed and used to aid the analysis. The equations representing the dynamic model and the parameters of the machines used are given in the appendix.

Generators represent one of the essential components of the electrification system. There is a scant literature on generators for small scale generation (≤ 100 kW). However, diverse types of electrical machine with different performance characteristics and power rating are available, thereby providing the possibility to design decentralized units at relatively reasonable cost. The following generator configurations are examined in this analysis:

- Three phase grid connected induction generator (TIG);
- Three phase self-excited induction generator (SEIG);
- Single phase capacitor start induction generator (SCIG);
- Permanent magnet synchronous generator (PMSG);
- Single phase split-phase induction generator (SSIG);
- Three phase induction machine excited as single phase generator (TIGES).

2.1 Generator models

2.1.1 Three phase grid connected induction generator

In this mode of operation the generator consumes reactive power from the grid and supplies active power to the grid. The equivalent circuit of the three phase induction

machine where the machine variables are vector quantities can be represented as shown in the figure below. R_s and X_s represent the stator resistance and reactance, R_r and X_r the rotor resistance and reactance referred to the stator side, X_m the magnetizing reactance, and v_s the phase voltage of the machine. p denotes the differential operator d/dt. λ_s, λ_m, and λ_r represent the flux in the stator coil, the flux in the magnetizing inductance and the flux in the rotor coil respectively, meanwhile i_s and i_r represent the stator and rotor current vetors.

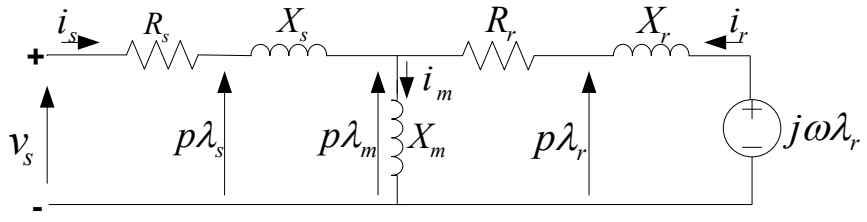

Figure 2. 1 Phase equivalent circuit of the three phase induction machine

Based on this circuit, a dynamic model of the three phase induction machine can be derived as described in the appendix. Some results of the grid connected induction generator obtained using the experimental set-up presented in the figure below are presented in Figure 2.3.

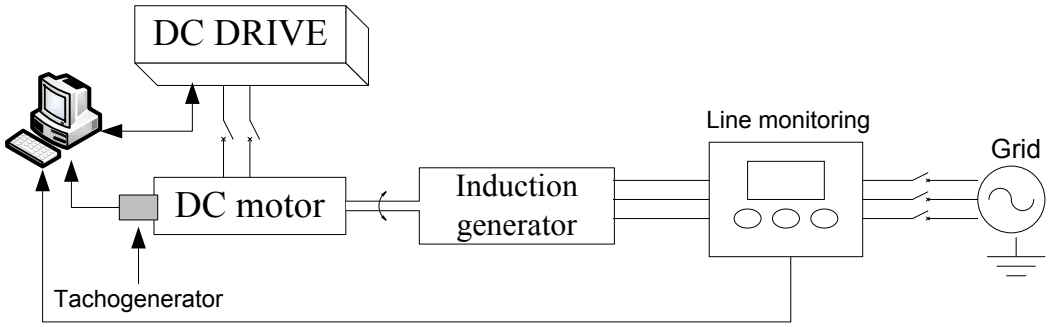

Figure 2. 2 Experimental set-up of the grid connected induction generator

Mechanical power is applied on the shaft at 40s, to drive the machine into generation mode. This explains why at 40s, the shaft speed becomes greater than synchronous speed and the phase current in the machine increases.

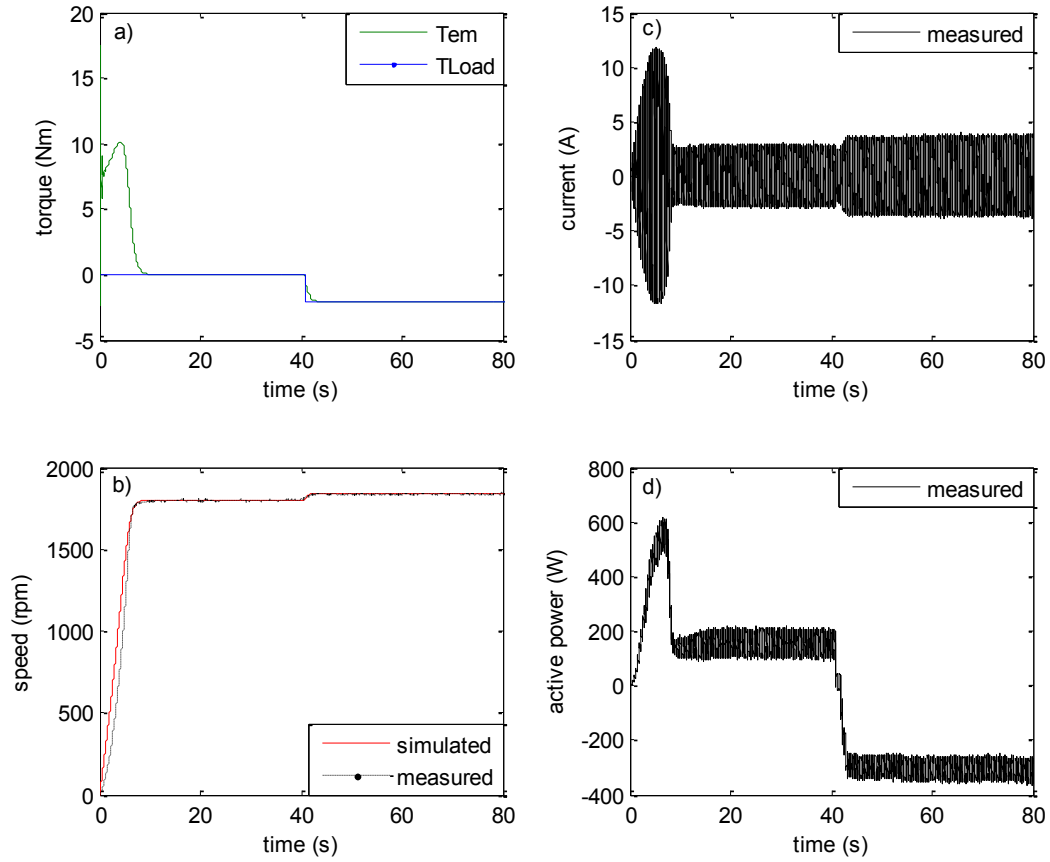

Figure 2. 3 Results of the three phase induction generator: a) torque response b) speed response, c) phase current, d) active power

Figure 2.3.d shows the active power obtained based on the measured phase voltage and phase current of the machine. Notice that at 40s, the active power becomes negative. A negative power means the energy is flowing from the generator to the grid.

Figure 2.4 represents the stator phase voltage along with the instantaneous power of the machine. For proper validation of the model, it is important to verify that the frequency of the power is twice that of the voltage.

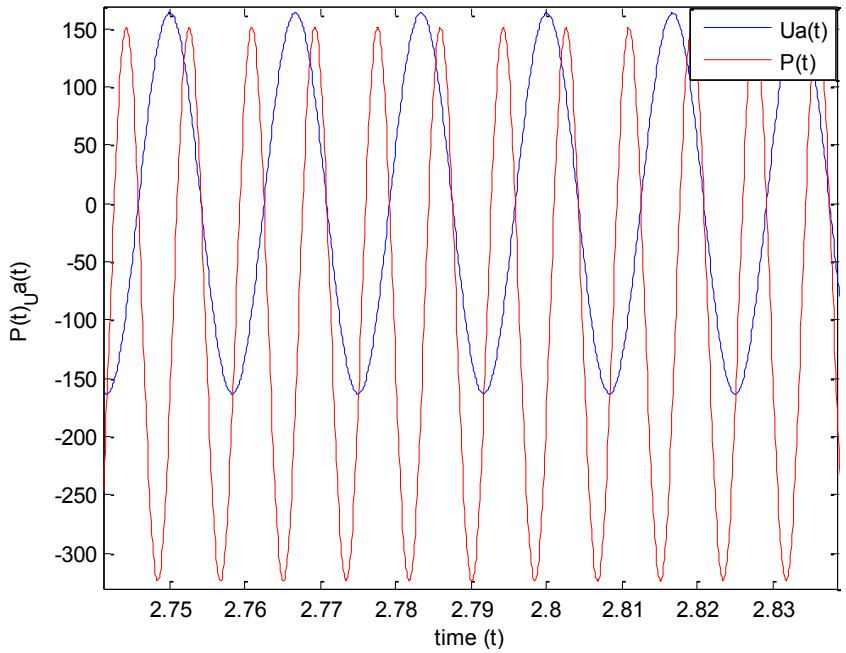

Figure 2. 4 Power and phase voltage

2.1.2 Three phase self-excited induction generator

In this mode of operation, the machine is not connected to the grid and needs to be self-excited. Thus, suitable capacitor bank is used to provide the self-excitation. The generator needs to be loaded after reaching steady state to avoid losing the self-excitation. The equivalent circuit of the SEIG in the stationary reference frame can be represented as shown in the Figures bellow. Based on these figures a dynamic model of the SEIG in the stationary reference frame has been derived. This model is described in detail in the appendix.

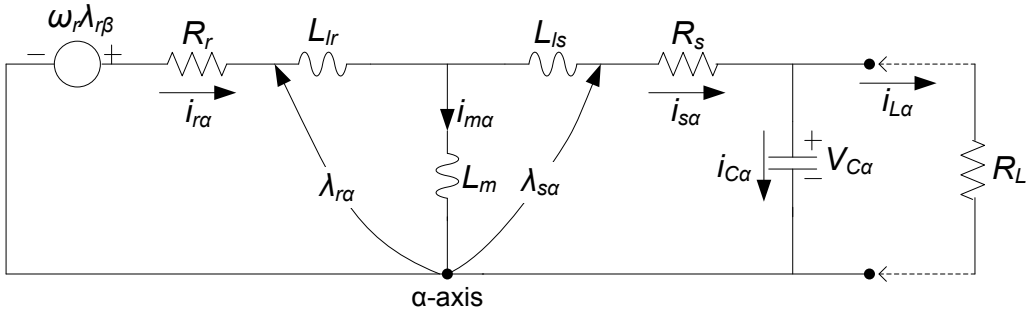

Figure 2. 5 Phase equivalent circuit of the self-excited induction generator alpha-axis

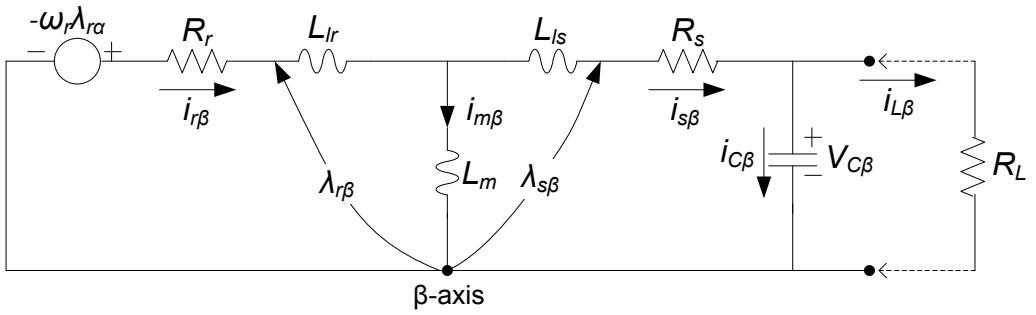

Figure 2. 6 Phase equivalent circuit of the self-excited induction generator beta-axis

2.1.2.1 Magnetizing inductance and capacitance for self-excitation

Unlike the grid connected mode of operation where the magnetizing inductance of the machine is fixed at rated voltage, in self-excited mode, the magnetizing inductance of the machine varies as the voltage builds up. Therefore, for accurate modeling of the SEIG, the relationship between magnetizing inductance and current (or voltage) obtained experimentally from open circuit tests at synchronous speed is required. Then, the minimum capacitor value required for self-excitation can be estimated. The magnetizing inductance characteristic of the machine used in this analysis with the parameters given in the appendix is shown in the figure below.

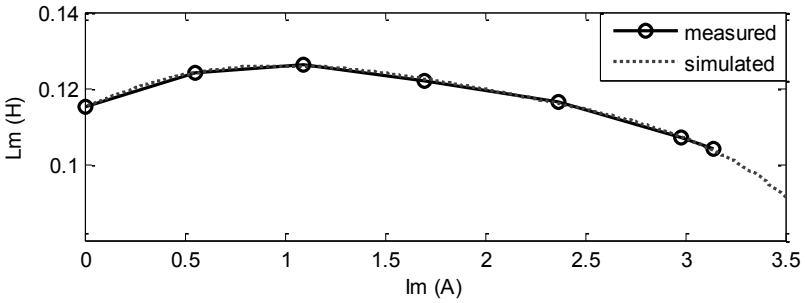

Figure 2. 7 Magnetizing characteristic of the induction machine

This characteristic can be represented by a fifth order polynomial curve fit using the following equations.

$$L_m = -0.0004I_m^5 + 0.0025I_m^4 - 0.0027I_m^3 - 0.0116I_m^2 + 0.0233I_m + 0.115 \quad (2.1)$$

$$I_m = \sqrt{(I_{s\alpha} + I_{r\alpha})^2 + (I_{s\beta} + I_{r\beta})^2} \tag{2.2}$$

where I_m is the measured magnetizing current of the machine, $I_{s\alpha}$, $I_{s\beta}$, $I_{r\alpha}$ and $I_{r\beta}$ the stator and rotor currents in the stationary reference frame. The minimum capacitance required for self-excitation can be estimated using equation (2.3).

$$C_{\min} = \frac{1}{\omega_r^2 L_m} \tag{2.3}$$

Some results of the self excited induction generator obtained using the experimental setup shown in Figure 2.8 are represented in Figures 2.9 and 2.10.

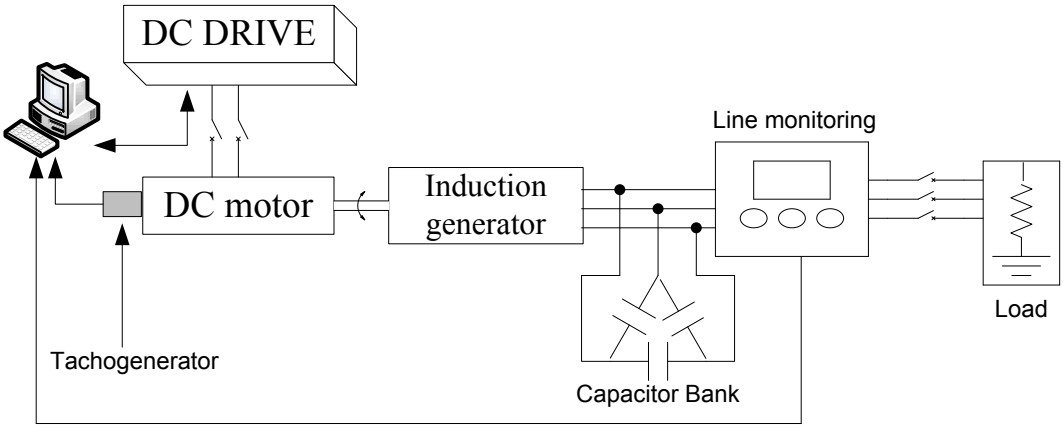

Figure 2. 8 Experimental set-up of the self-excited induction generator

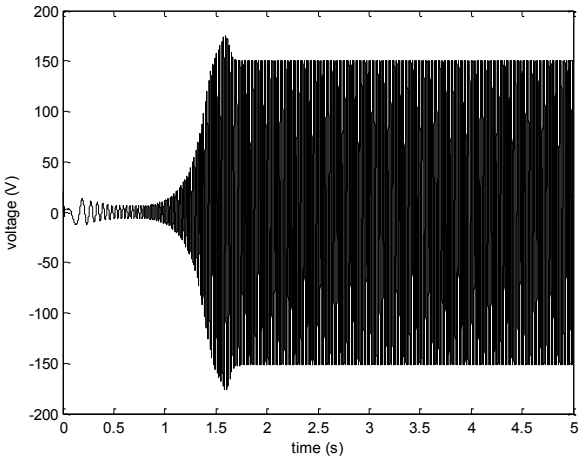

Figure 2. 9 Phase voltage

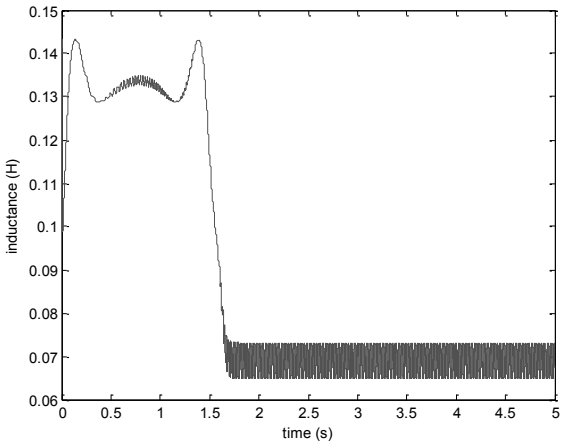

Figure 2. 10 Magnetizing inductance

Figure 2.9 represents the phase voltage of the generator at no load. The variation of the magnetizing inductance as the voltage builds up till steady state where the inductance reaches its saturated value can clearly be seen from Figure 2.10.

2.1.3 Capacitor start induction generator

The configuration of the single phase capacitor start induction machine is represented in Figure 2.11. This circuit comprises two coils, a centrifugal switch and a capacitor. The capacitor and the auxiliary winding are about 90^o ahead of the main winding. The capacitor is used to achieve maximum starting torque. When the switch is closed, the auxiliary winding current leads the main winding current for about 90^o.

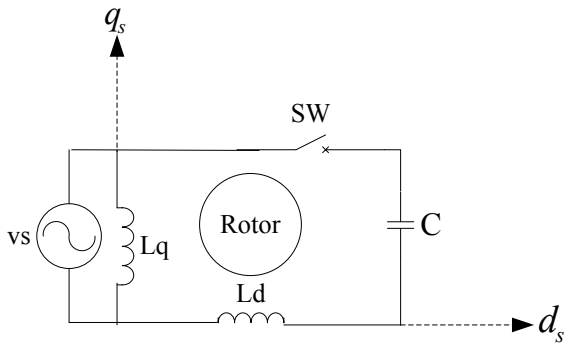

Figure 2. 11 single phase capacitor start induction machine configuration

Based on Figure 2.11, the following observations and modelling steps can be highlighted:

- The axes of the main and auxiliary windings are orthogonal;
- Therefore, for simplification purposes, the stationary dq axes may be aligned with the orthogonal axes of the physical windings;
- The rotor cage may be represented by a pair of equivalent dq symmetrical rotor windings;
- The rotor dq windings and variables need to be transformed to the stationary dq reference frame;

- The transformed variables and rotor winding parameters have to be referred to the input side (relative to the main winding);
- For asymmetrical stator windings, the d-axis winding and the capacitor will also have to be referred to the main winding side.

Based on these assumptions, the equivalent circuits (per phase) of the single phase capacitor start induction generator in the dq reference frame can be represented as follows:

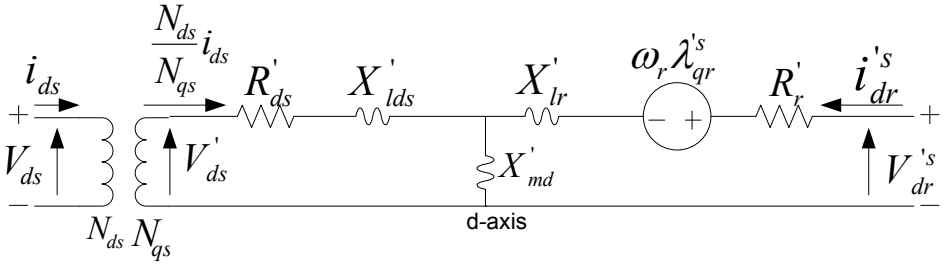

Figure 2. 12 Phase equivalent circuit of the single phase CSIG-d axis

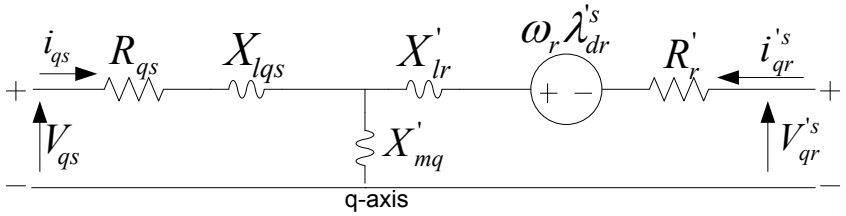

Figure 2. 13 Phase equivalent circuit of the single phase CSIG-q axis

A dynamic model of the single phase capacitor start induction generator has been derived and given in the appendix. Figure 2.14 represents the experimental setup used to validate the model of the capacitor start induction generator while Figures 2.15 represents some results of the model.

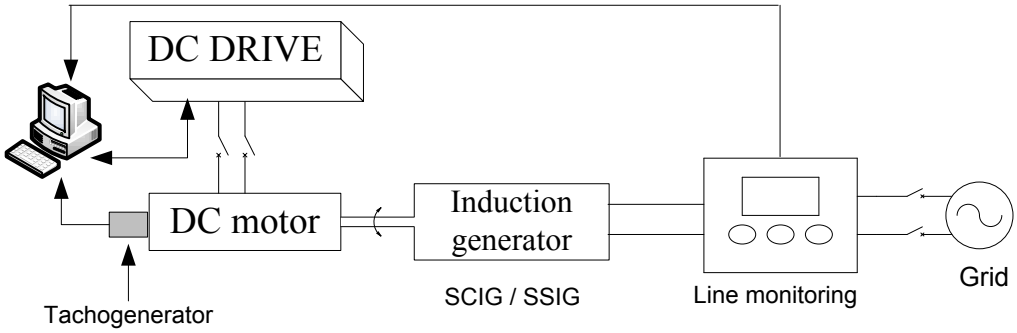

Figure 2. 14 Experimental set-up of the capacitor start induction generator

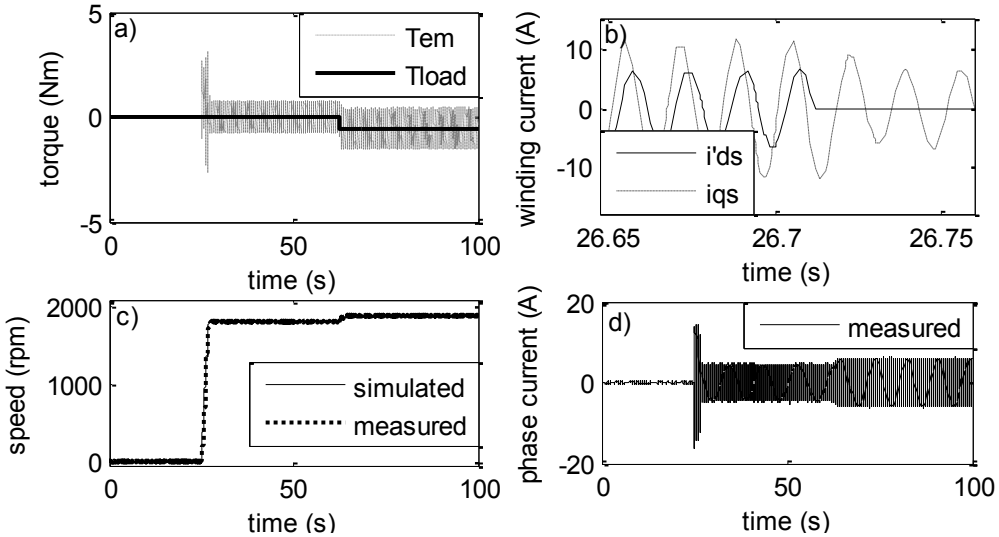

Figure 2. 15 Simulated and experimental results of the SCIG: a) torque response, b) currents in the windings, c) speed response, d) measured phase current

An increase in the current at 55s (Figure 2.15.d) is due to the applied mechanical power on the generator shaft. This explained why at 55s, the shaft speed increases above synchronous speed (Figure 2.15.c). The open circuit condition is shown in Figure 2.15.b where the auxiliary winding current becomes zero.

2.1.4 Permanent magnet synchronous generator

Permanent magnet synchronous generators are often used in renewable energy systems for fixed and variable speed applications [19]. A typical configuration of such a system is illustrated in the figure below.

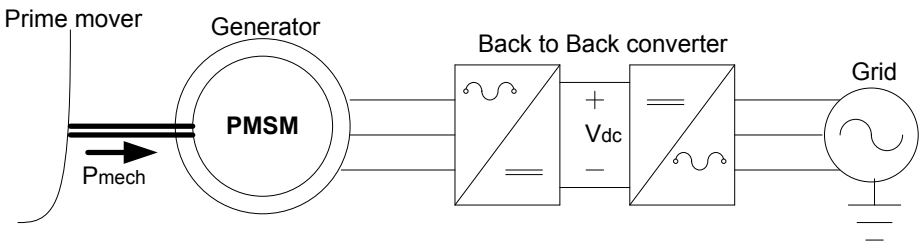

Figure 2. 16 Typical permanent magnet synchronous generator application

The generator is connected to the grid through a converter which is used to control the generator frequency. An important issue when a permanent magnet generator is connected to the grid is the flow of reactive power. In typical applications, the generator can be controlled to provide no reactive power to the grid. A dynamic model of the system represented in Figure 2.16 is derived in the appendix. To simplify the analysis, the prime mover and the grid side converter models are left beyond the scope of this analysis. Some results of the permanent magnet generator are represented in the figures below, showing how the torque (or mechanical power) variations affect the generated currents.

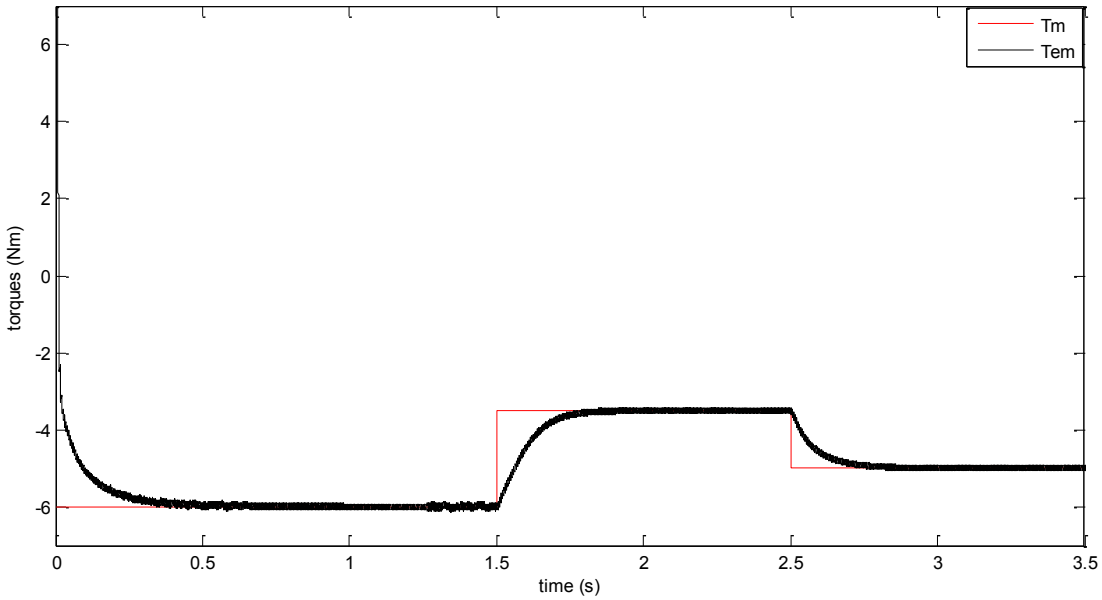

Figure 2. 17 Generator torque response

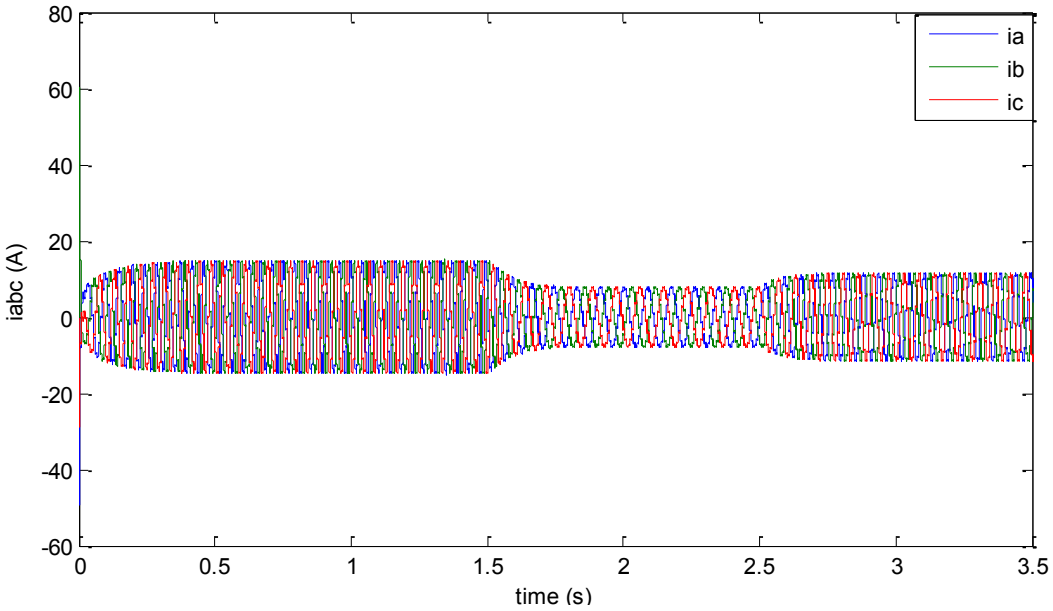

Figure 2. 18 Generator output currents

2.1.5 Split phase induction generator

The electric circuit of the split phase induction machine is represented in the figure below.

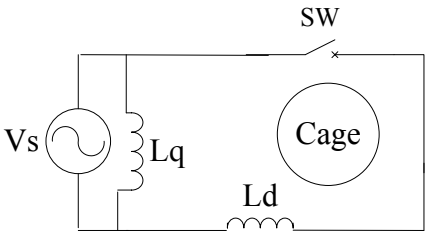

Figure 2. 19 Single phase split phase induction machine configuration

The auxiliary winding is made of smaller conductor size, requiring fewer turns than the main winding. Therefore, the auxiliary winding has a higher resistance to inductance ratio than the main winding. Similar to the capacitor start machine, a dq model of the single phase split phase induction machine can be derived as given in the appendix. Some results of this model are represented in the figures below.

Figures 2.24 and 2.25 represent the voltages and currents waveforms of the main and auxiliary windings respectively. The open circuit condition can clearly be seen from the current waveforms. The switch is open at 2s. Thus, the auxiliary winding current becomes zero.

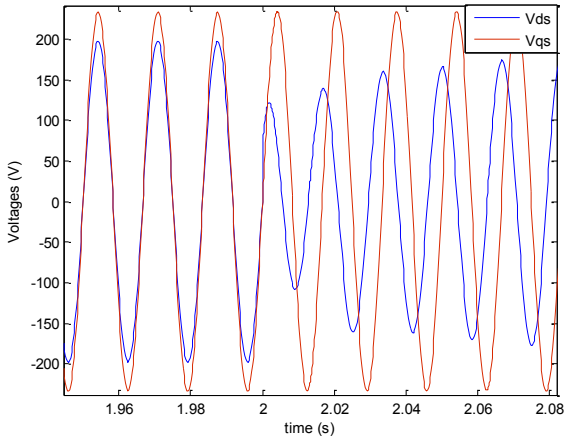

Figure 2. 20 Main and auxiliary winding Voltages

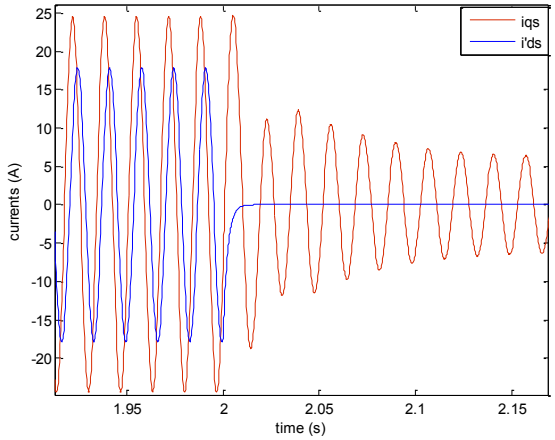

Figure 2. 21 Main and auxiliary windings currents

Figure 2.26 is used to verify that the frequency of the instantaneous power is twice that of the applied voltage.

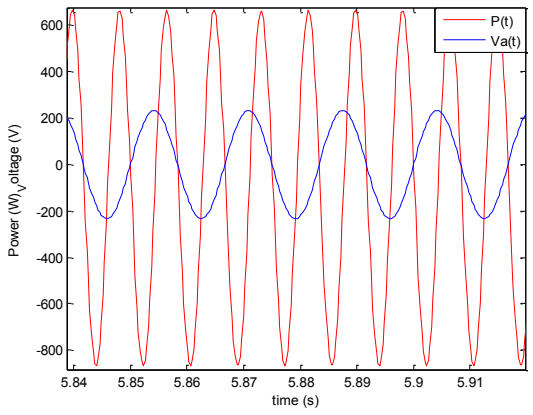

Figure 2. 22 Stator voltage and instantaneous power

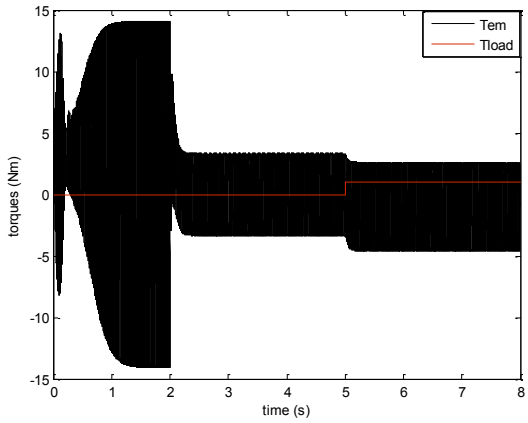

Figure 2. 23 Electromagnetic torque and load torque

Figure 2.27 represents the torque response. Mechanical power is applied on the shaft at 5s. Thus, the slip becomes negative while the shaft speed increases.

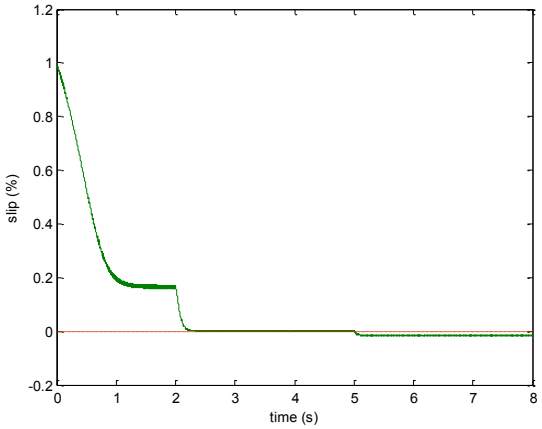

Figure 2. 24 Slip response

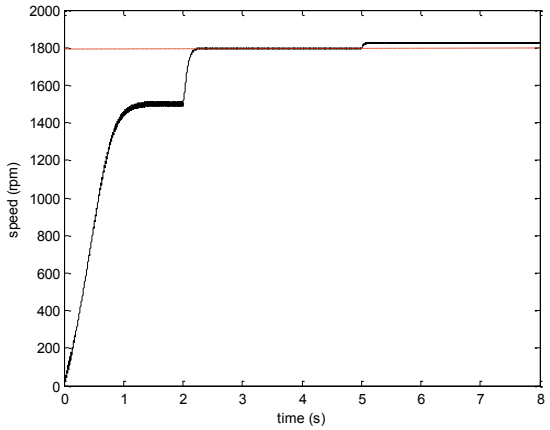

Figure 2. 25 Speed response of the single phase SPIG

At start up, the slip is 1 since the shaft speed is zero. The speed of the machine increases as the slip decreases. At 5s, mechanical power is applied on the shaft and the machine runs into generation mode, therefore, the shaft speed becomes greater than synchronous speed, resulting in negative slip.

2.1.6 Three phase induction machine excited as single phase generator

Three phase induction machines can be used to supply single phase loads [20]. This configuration is illustrated in the figure below.

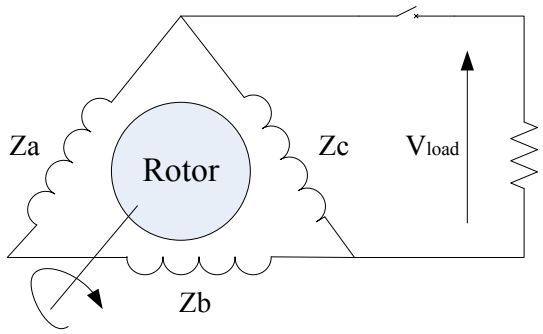

Figure 2. 26 of the three phase induction machine excited as single phase generator

The use of a three phase induction generator to supply single phase loads results from the fact that single phase machines are available up to 15 hp only. Thus, it becomes expensive to meet certain load requirements using single phase generators. The cost per

kW of a single phase generator is generally higher than that of the three phase generator. In order to minimize the investment cost of the electrification system, three phase machines can be excited as single phase generators while connecting the stator windings in delta. However, this operating condition results in an output power lower than the nominal power of the machine. Approximately 80 % of the rated power can be achieved. Single phase operation of three phase machines might lead to torque pulsations, resulting in lower output power quality of the system. Figure 2.27 represents the conventional approximated single phase equivalent circuit referred to the stator side, of a three phase induction machine.

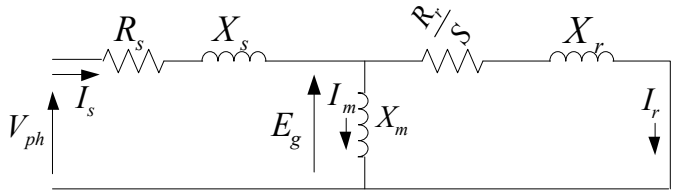

Figure 2. 27 Induction machine phase equivalent circuit

In the generating mode, the slip is negative. Thus, the real part of the equivalent circuit terminal impedance will be negative if the generating requirements are to be satisfied. This means that $\lceil R_s+R_r/s \rceil < 0$. Thus, the slip range providing the operation in generating mode is $-R_r/R_s < s < 0$. However, it is possible to increase this range using higher rotor resistance at the expense of reduced efficiency. The experimental setup used to validate the model of the three phase induction machine excited as single phase generator is represented in the figure below.

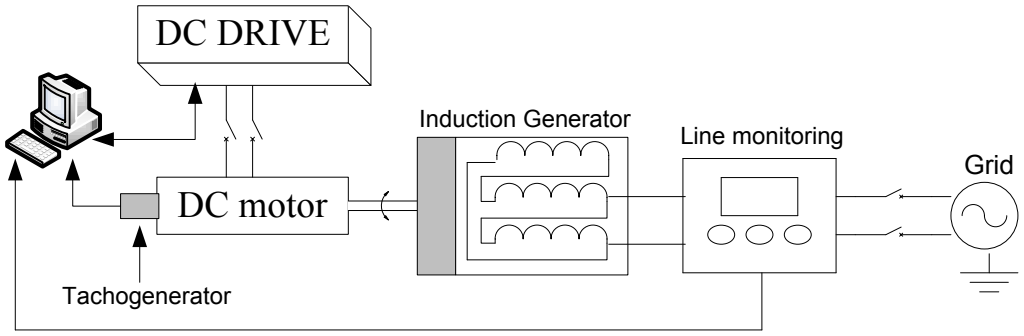

Figure 2. 28 Experimental set-up of the three phase machine excited as single phase generator

Figure 2.29 represents some results of the three phase induction machine operating as a single phase generator.

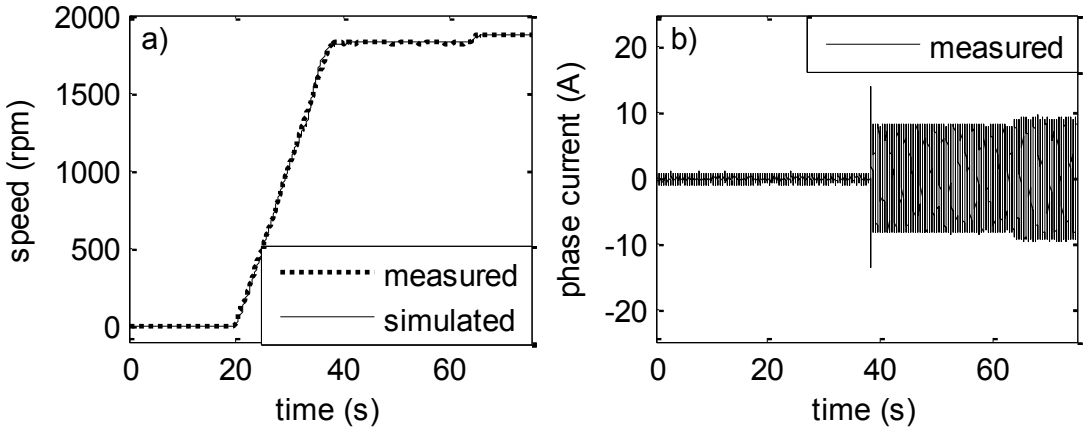

Figure 2. 29 Results of the three phase induction machine excited as a single phase generator

At 62 s, mechanical power is applied on the shaft, thereby driving the machine into generation mode. Thus, the current in the machine winding increases as shown in Figure 2.29.b. One issue with three phase machines running as single phase generators is that the current in the generator windings might not be balanced.

2.2. Synchronization schemes of the generator types

Synchronization is an essential requirement to be met when a generator needs to be connected to the utility or in parallel with other generators. This requires having the same amplitude and phase angle of the generator output variables before closing the breaker, to

avoid damaging the protection system and the load. This Section introduces suitable synchronization (or soft grid connection) techniques for the generator types discussed in the previous Sections. Basic grid synchronization (or interconnection) schemes can be classified as follows:

- Soft starter based connection scheme (SST)
- Zero crossing detection based connection scheme (ZCD)
- Phase lock loop based connection scheme (PLL)
- Inverter interface based connection scheme (IVT)

2.2.1 Soft-Starter based Connection Scheme

Soft starters are being widely used in industrial applications to reduce mechanical stress on mechanical components and electrical stress on supply systems. Other applications of soft starters can be found in direct grid connected wind systems equipped with three phase squirrel cage induction generators. Figure 2.30 represents a typical application of soft starters in wind systems.

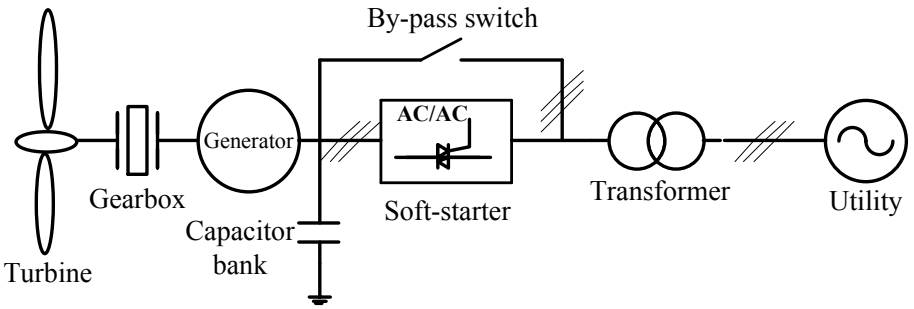

Figure 2. 30 Typical application of the soft starter in direct grid connected wind system

In such applications, a control system is required to assure proper operation of the wind system under all conditions. The soft starter is made of two antiparallel thyristors per phase. A capacitor bank is used to control the generator output power factor. The soft

starter is used only during the generator start-up sequence, in order to limit the inrush currents and the starting torque transients in the drive train.

2.2.2 Zero-crossing detection based connection scheme

The ZCD is another type of soft connection scheme suitable for single phase induction machines. This scheme can be used to synchronize a generator with the grid or to synchronize generators operating in parallel to form a mini-grid. A typical application of the ZCD scheme is represented in Figure 2.31. In this scheme, the generator and grid signals are compared in order to connect the incoming generator to the grid at the instant of perfect phase matching. The grid and generator voltages are stepped-down and converted into square waves (using the ZCD modules). Phase angles of the grid and generator voltages are compared using a phase matcher.

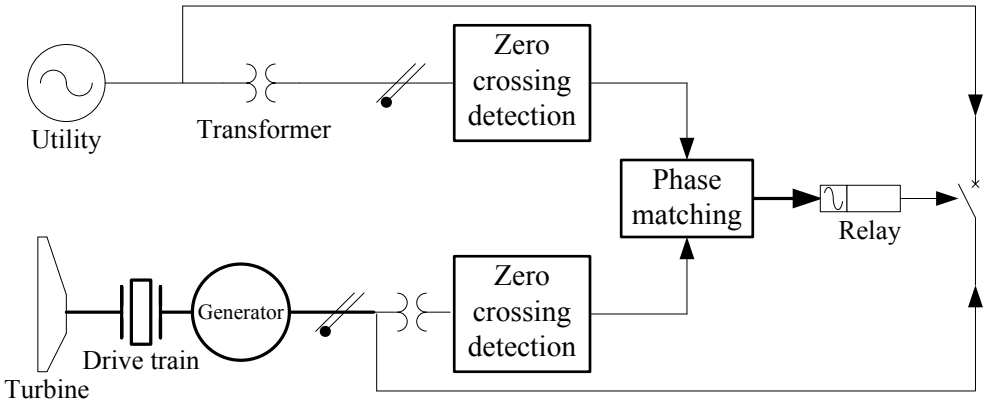

Figure 2. 31 Typical application of the ZCD scheme

2.2.3 Phase Lock Loop based Connection Scheme

Phase lock loop schemes are being used in industrial applications and power generation systems. This scheme is often used for three phase machines. Figure 2.32 represents the general concept of the phase lock loop.

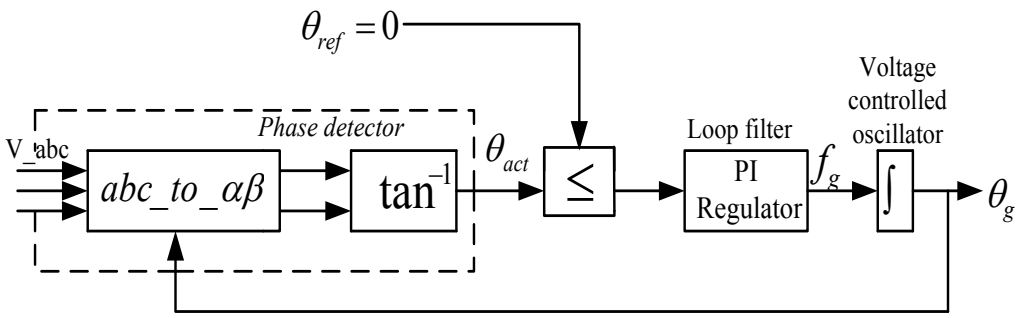

Figure 2. 32 General concept of the PLL

The PLL estimates the grid angle used to generate the control signals for a converter intended to be connected to the grid. Input voltages are transformed into components referred to the grid voltage phasor. These components provide sufficient information concerning the phase angle of the system. A low pass filter (loop filter) is used to suppress the noise and high frequency terms in the signal (from the phase detector), which can be due to the asymmetry in the three phase voltages. The performance of the PLL would depend on the phase detector and the bandwidth of the loop filter. With a slow dynamic response of the PLL loop, a higher rejection of disturbances can be achieved at the expense of poor tracking of the grid angle. Table 2.1 summarizes the features related to the individual generator types.

Table 2. 1 Summary of the generator characteristics

Generator types	Cost, power range & maintenance	Synchronization scheme			
		SST	ZCD	PLL	IVT
TIG	+ + +	+	-	+	+
SCIG	+ - -	-	+	-	-
PMSG	- + -	-	-	+	+
SSIG	+ - +	-	+	-	-
TIGES	+ + -	-	+	-	-

2.3 Summary of chapter 2

In this chapter, an assessment of generator types for small scale power generation is presented. Suitable generator selection (based on cost and required maintenance) can

enhance the design of the electrification system. Induction machines have simple and rugged construction, low maintenance with possible direct connection on AC power. Therefore they have relatively low costs. In single phase applications requiring high starting and accelerating torques, single phase capacitor start induction machines will be suitable. These machines can present high starting torque, due to the capacitor used in the electric circuit. For low power single phase applications, capacitor start and split phase induction machines can be used. However split phase machines present low or moderate starting torque. Induction machines can be limited in applications where high efficiency is required. Permanent magnet machines have high power density, high efficiency due to the elimination of magnetizing current and copper losses in the rotor and they can provide high performance. The main disadvantage of these machines is the cost of magnets and converter required for their application.

CHAPTER 3

MATHEMATICAL MODELS AND EXPERIMENTAL VALIDATION OF FIXED-SPEED WIND TURBINES

In this chapter, an algorithm to obtain the power-frequency characteristic of fixed-speed wind turbines is proposed. The research work presented in this thesis is based on the parallel operation of a wind turbine and a diesel engine generator set. Droop control is a well known technique for parallel operation of generators; however, it requires having the power-frequency characteristic of the individual generators. While this characteristic is usually available for diesel gensets, it might not be easy to be obtained for uncontrolled wind turbines. In this chapter a simple approach to obtain this characteristic for fixed speed wind turbines is developed and verified experimentally.

Parallel operation of diesel gensets and wind turbines can provide several benefits including reduced fuel consumption and reduced environmental impact. These benefits are high when the wind turbine is a variable speed wind turbine, due to the possibility provided by variable speed wind turbines to achieve maximum wind energy extraction at all wind speeds. However, in these configurations, the wind turbine is equipped with a power converter that increases considerably the cost of the electrification system. Therefore, fixed-speed wind turbines appear to be cost effective. Figure 3.1 illustrates a typical wind-diesel system configuration using fixed-speed wind turbine. The wind system is equipped with a squirrel-cage induction generator (SCIG). Squirrel-cage induction machines are robust and widely manufactured with relatively low cost [21-23]. In high penetration systems, three modes of operation can be observed: “diesels only (DO)”, “wind only (WO)” and “wind and diesel (WD)”. A sophisticated control system for voltage and frequency regulation and suitable energy storage devices are required.

When the load cannot absorb the power produced by the wind turbine, a dump load is added to the system to prevent reverse power flow and consequently tripping of the grid forming diesel unit(s). During the "WD" mode, the load is supplied by both sources. As the wind is characterised by an intermittent and stochastic nature, the power produced by the wind turbine can vary significantly and the genset (master unit) is responsible for balancing power generation and demand. This is not an easy task, especially in remote communities due to their highly variable load characteristic.

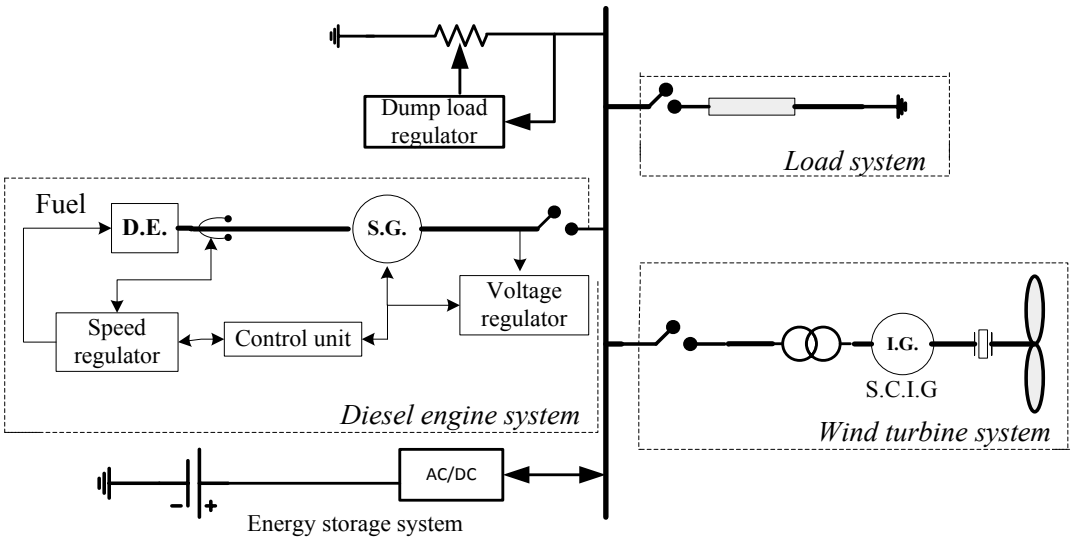

Figure 3. 1 Typical hybrid wind-diesel system configuration

3.1 Problem statement

There have been significant research efforts to optimize the design and operation of hybrid wind-diesel mini-grids so as to meet the load demand with reduced fuel consumption and cost, while providing good power quality and system reliability [24-28]. This is usually achieved by means of power electronic interfaces for the renewable energy sources and energy storage devices employing sophisticated control algorithms. This research work investigates the impact of simple fixed-pitch wind turbines (type 1

and type 2) on steady state and transient state frequency regulation of storage-less wind-diesel hybrid mini-grids.

Figure 3.2 illustrates a simple hybrid wind-diesel power system, where both sources present a droop characteristic. Usually, the droop characteristics of the gensets are known while those of wind turbines are not. It is assumed in this analysis that wind turbine droop characteristics have smaller slopes compare to genset droop characteristics. In systems such as the one represented in figure 3.2, load variations (Δ_{PLoad}) resulting in frequency variations (Δ_f), will be shared by the genset (Δ_{PGen}) and the turbine (Δ_{Pwt}).

It appears from Figure 3.2 that for a given frequency variation (Δ_f), the genset due to its larger slope will experience higher power variation compared to the wind turbine ($\Delta_{PGen} > \Delta_{Pwt}$). In order to identify how much load variations will be shared by the individual generators, the power-frequency characteristic of the wind turbine should be known.

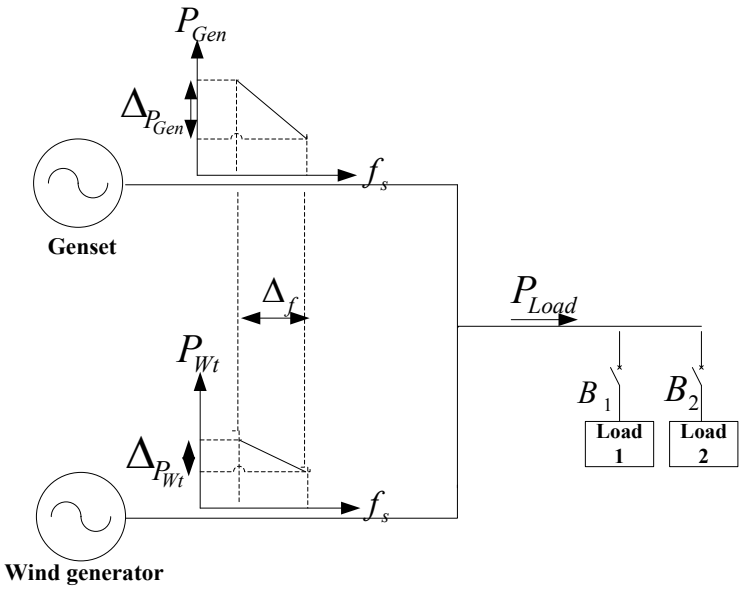

Figure 3. 2 Parallel operation of the wind and diesel generators

In this chapter, a simple approach to estimate the power injected into the grid by fixed-speed wind turbines at different grid frequencies and wind speeds based on the torque-speed characteristic of the induction generator and the aerodynamic characteristic of the wind turbine is proposed and verified experimentally.

3.2 Wind system modeling

The speed loop of a fixed-speed wind turbine can be represented as shown in figure 3.3, where $T_{wt}(\omega_m)$ represents the wind turbine torque, K_{gb} the gear box ratio, J_{eq} the equivalent moment of inertia of the system, $T_{em}(\omega_m)$ the torque developed by the generator and ω_m the shaft speed of the generator. The torque-speed curves of the assumed wind turbine are represented in Figure 3.4.

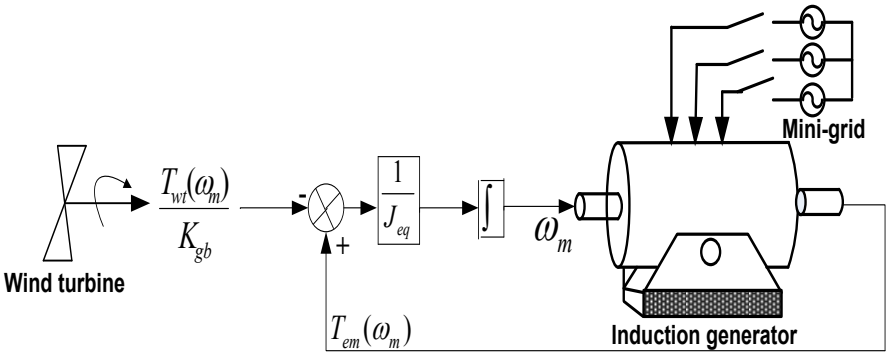

Figure 3. 3 Speed loop of a fixed-speed wind turbine

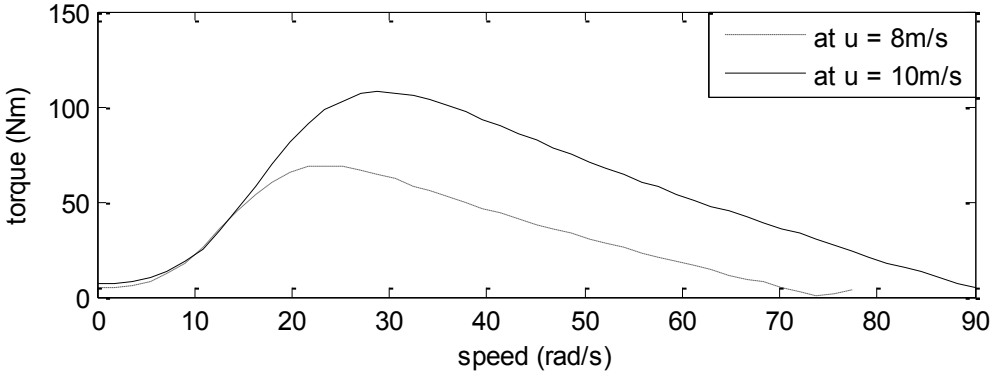

Figure 3. 4 wind turbine torque speed characteristic

3.2.1 Wind turbine torque model

A simple model of the wind turbine rotor aerodynamic characteristic can be represented using the following equations [29-32],

$$T_{wr} = \frac{\rho}{2}\pi R^3 u^2 C_t(\lambda, \beta) \tag{3.1}$$

$$\lambda = \frac{\omega_r}{u} R \tag{3.2}$$

$$P_{wr} = \frac{\rho}{2}\pi R^2 u^3 C_P(\lambda, \beta) \tag{3.3}$$

where λ is the tip speed ratio, β the pitch angle, R the rotor radius, ω_t the turbine shaft speed, u the wind speed, T_{wt} the turbine torque and P_{wt} the turbine power. C_t (λ,β) and C_P(λ,β) represent the torque and power coefficient characteristics of the turbine, which are functions of the tip speed ratio and pitch angle. The torque-speed characteristic of the wind turbine can be obtained by substituting equation (3.2) in equation (3.1), as given in the following equation (for $\beta=0$).

$$T_{wr} = \frac{\rho}{2}\pi R^3 u^2 C_T(\frac{\omega_r}{u} R) \tag{3.4}$$

3.2.2 Induction generator torque model

The phase equivalent circuit of the induction machine is illustrated in Figure 3.5, where R_s and X_s are the stator resistance and reactance, R_r and X_r the rotor resistance and reactance referred to the stator side, X_m the magnetizing reactance, s the slip and V_{ph} the phase voltage of the machine.

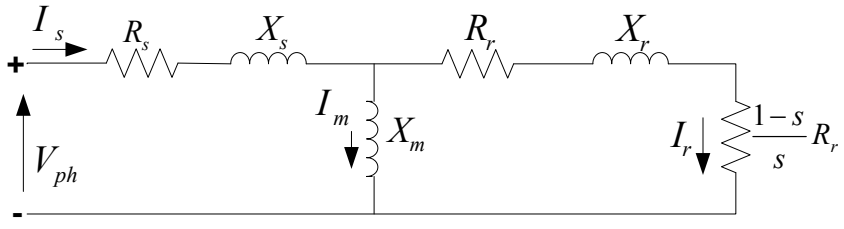

Figure 3. 5 Phase equivalent circuit of the induction machine

The following equations can be derived based on Figure 3. 5.

$$V_{th} = \frac{X_m}{\sqrt{R_s^2 + (X_s + X_m)^2}} V_{ph} \tag{3.7}$$

$$Z_{th} = R_{th} + jX_{th} = \frac{R_s + jX_s}{R_s + j(X_s + jX_m)} jX_m \tag{3.8}$$

$$\omega_{syn} = \frac{4\pi}{P} f_s \tag{3.9}$$

$$T_{em} = \frac{3V_{th}^2 \dfrac{R_r}{\omega_{syn} - \omega_{shaft}}}{\left[\left(R_{th} + \dfrac{R_r \omega_{syn}}{\omega_{syn} - \omega_{shaft}}\right)^2 + (X_{th} + X_r)^2\right]} \tag{3.10}$$

ω_{syn} represents the synchronous speed of the machine and f_s the stator frequency. Equation (3.10) represents the induction generator torque-speed characteristic.

3.3 Power estimation algorithm

The approach to obtain the power-frequency characteristics of a type 1 wind turbine is presented in this Section and validated by means of a laboratory prototype. In order to calculate the power injected into the grid by the wind turbine in steady state at different wind speeds and grid frequencies, the value of the shaft speed (ω_r) should be known. This can be done assuming that in steady state, the torque developed by the wind rotor

reflected to the high speed side of the gear box (T_{wr}^{*}) is equal to the electromagnetic torque of the induction generator (T_{em}).

The curves of T_{wr}^{*} and T_{em}, using the parameters given in Table H of the appendix, are represented in Figure 3.6 at different wind speeds and grid frequencies. An ideal gear box with a gain K_{gb} (>1) has been assumed. The point of intersection between both curves provides the shaft speed on the high speed side (ω_r^{*}) that satisfies the steady state condition. At this point, the slip of the generator and the generator losses should be known, since the grid frequency is known.

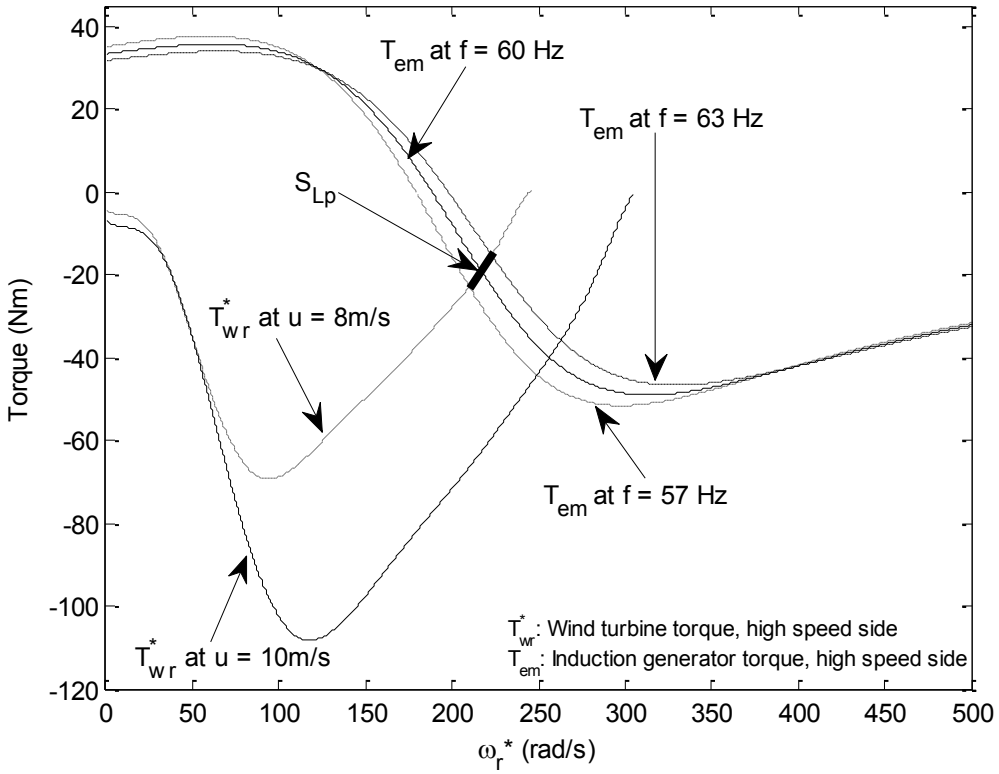

Figure 3. 6 Torque-speed curves of the wind rotor and induction generator on the generator side

Then, the mechanical power and the power injected into the grid by the wind generator at the point of intersection can be predicted. An algorithm for calculating the shaft speed and the power injected into the grid by the wind turbine is developed as illustrated in

Figure. 3. 7. The shaft speed is calculated iteratively by comparing the error between T_{wr}^{*} and T_{em} for candidate shaft speeds. A good initial guess ($\omega_{r\text{-}0}^{*}$) is the shaft speed at which the generator operates with zero slip (s = 0). This is then increased by a small factor ($\Delta\omega_r^{*}$) until the error between T_{wr}^{*} and T_{em} is smaller than $\varepsilon_{\max}$. Once the shaft speed is known, the mechanical power developed by the wind rotor (P_{wr}) can be calculated. Then, the power injected into the grid by the wind turbine for a given wind speed and grid frequency is obtained by subtracting the induction generator losses from P_{wr}. The induction generator losses are calculated using the approach described in the IEEE Standard Test Procedure for Polyphase Induction Motors and Generators (IEEE Std 112-1991). The mechanical losses are assumed to be 1.8% of the rated power, as recommended for machines under 125 HP. The following equations have been used to calculate the generator losses.

$$P_{rot}(\omega_r) = 3R_r[I_2(\omega_r)]^2 \tag{3.11}$$

$$I_2(\omega_r) = \frac{V_{th}}{[(R_{th} + \frac{R_r}{s(\omega_r)}) + j(X_{th} + X_r)]} \tag{3.12}$$

$$P_{stat}(\omega_r) = 3R_1[I_1(\omega_r)]^2 \tag{3.13}$$

$$I_1(\omega_r) = \frac{V_{th}}{R_s + jX_s + \dfrac{1}{\dfrac{1}{jX_m} + \dfrac{1}{\dfrac{R_r}{s(\omega_r)} + jX_r}}} \tag{3.14}$$

$$P_{losses}(\omega_r) = P_{rot}(\omega_r) + P_{stat}(\omega_r) + P_{we+fricct} \tag{3.15}$$

where I_2 (ω_r) represents the steady state rotor current, I_1 (ω_r) the steady state stator current, P_{rot} (ω_r) the steady state rotor losses, P_{stat} (ω_r) the steady state stator losses and $P_{we+frict}$ the mechanical losses of the generator.

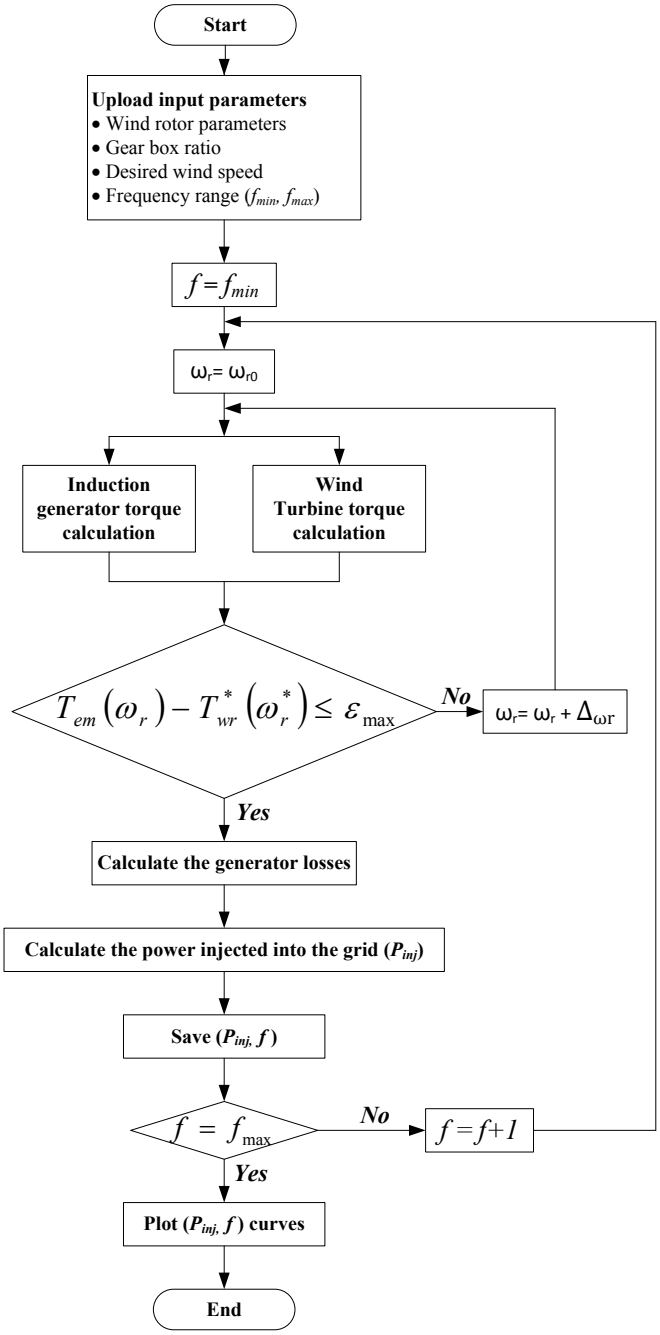

Figure 3. 7 Flow chart of the proposed algorithm

The proposed approach has been validated experimentally using a laboratory prototype hybrid system. The prototype system is made of a hybrid wind-diesel emulator developed and used to aid the analysis. The concept and development of the assumed emulator is described in detail in the following Section.

3.4 Experimental set-up development

Figure 3.8 represents the configuration of the experimental set-up. This set-up consists of two DC drive systems (DCS 800 and buck converter), controlled using DSP controllers (dSpace DS1103 PPC) plugged in a host PC.

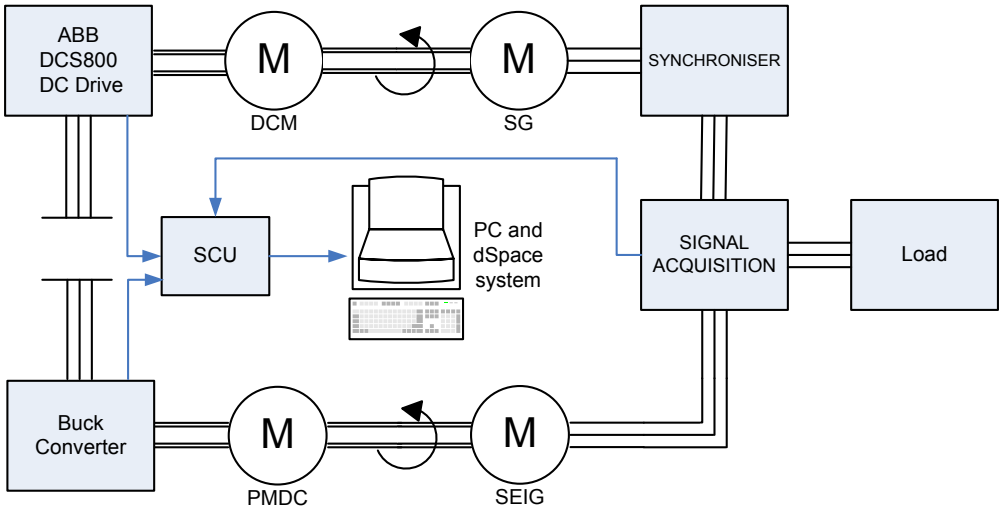

Figure 3. 8 Hardware configuration of the experimental setup

The DC motor (DCM) is used to emulate the diesel engine prime mover torque, while a wound rotor induction machine is excited to operate as a synchronous generator (SG). The wind turbine unit consists of a permanent magnet DC motor (PMDC) that emulates the torque characteristic of the wind turbine, and a squirrel cage induction generator excited externally using a capacitor bank (not shown in the figure). A synchronizer is used to match the phases of the individual generators before connecting them in parallel.

Signals from the set-up are used to feed a Signal Conditioning Unit (SCU), which serves to ensure the galvanic isolation between the PC and the dSpace hardware. The developed system supports the C code extension and Matlab files. Models crated in Simulink are transformed in to C code and used as program to control the setup. Visualization and control parameters are available on a dSpace control desk where layouts that fit specific requirements have been developed.

3.4.1 Wind turbine model used in the set-up

The implementation of the wind turbine torque characteristic is achieved using the aerodynamic characteristic equations given in Section 3.2.1. The induction generator used in the wind system is externally excited. It is therefore necessary to estimate the capacitor value that will provide the required reactive power to the generator. To achieve this, a critical case study where the generator supplies a resistive-inductive (RL) load will be assumed.

3.4.1.1 Capacitor required for the self-excitation

The steady state circuit of a self-excited induction generator per phase feeding an RL load can be represented as shown in Figure 3.9 [33], where the core losses of the machine have been neglected. In this figure, all the parameters except X_m are assumed to be constant and unaffected by the saturation effect. The loop equation for the current shown in Figure 3.9 can be expressed as follows.

$$IZ = 0 \tag{3.16}$$

where Z is the net loop impedance given by:

$$Z = A_Z + B_Z \tag{3.17}$$

$$A_Z = \left(\frac{R_r}{F - v} + jX_{lr} \right) \text{II} \left(jX_m \right) + \frac{R_s}{F} + jX_{ls} \tag{3.18}$$

$$B_Z = -j \frac{X_c}{F^2} \text{II} \left(\frac{R_L}{F} + jX_L \right) \tag{3.19}$$

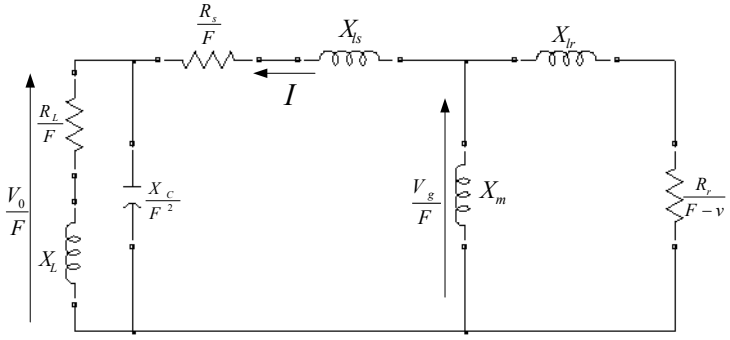

Figure 3. 9 Steady state equivalent circuit of self-excited induction generator with RL load

Under steady state excitation $I \neq 0$, it follows from equation (3.16) that Z = 0 (or both real and imaginary parts of Z are zero). The real part yields,

$$-a_1 F^3 + a_2 F^2 + \left(a_3 X_c + a_4 \right) F - a_5 X_c = 0 \tag{3.20}$$

and the imaginary part yields,

$$-b_1 F^4 + b_2 F^3 + \left(b_3 X_c + b_4 \right) F^2 - \left(b_5 X_c + b_6 \right) F - b_7 X_c = 0 \tag{3.21}$$

where a_i , i =*1,....5* and b_j , j=*1,....7* are positive real constants given in [34] Equations (3.20) and (3.21) can be solved for X_c as shown in the following equations.

$$X_c = \frac{A_1 F^3 - A_2 F^2 - A_4 F}{A_3 F - A_5} \tag{3.22}$$

$$X_c = \frac{B_1 F^4 - B_2 F^3 - B_4 F^2 + B_6 F}{B_3 F^2 - B_5 F - B_7} \tag{3.23}$$

where A_i=a_i and B_j= b_j are evaluated at X_m = X_{smax}, which is the maximum reactance obtained from the no load test characteristic of the induction machine. Figure 3.10 represents the magnetizing characteristic of the induction generator used in this analysis

with the machine parameters given in the appendix. It appears from this figure that X_{smax} is the reactance value that corresponds to $L_m \approx 0.11H$.

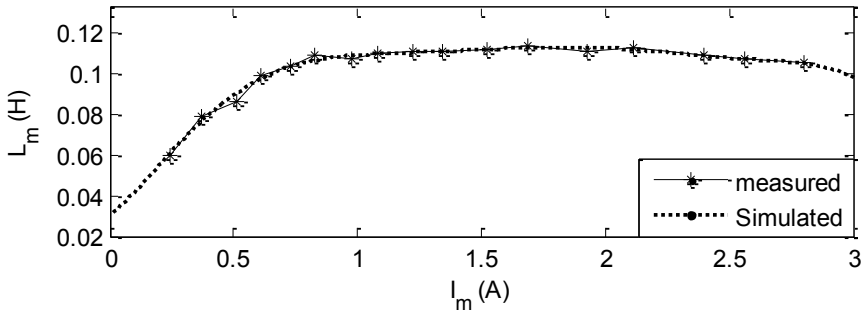

Figure 3. 10 Magnetizing characteristic of the induction generator

Equations (3.22) and (3.23) can be rearranged as follows:

$$\frac{A_1F^3 - A_2F^2 - A_4F}{A_3F - A_5} = \frac{B_1F^4 - B_2F^3 - B_4F^2 + B_6F}{B_3F^2 - B_5F - B_7} \tag{3.24}$$

This simplifies after a tedious elaboration into the following equation.

$$\alpha_4F^4 - \alpha_3F^3 + \alpha_2F^2 - \alpha_1F + \alpha_0 = 0 \tag{3.25}$$

where α_i, i = 0,….4 are positive constants given in [34]. Equation (3.25) has 4 positives real roots. Substituting these roots in equation (3.22) or (3.23) and solving for the capacitor will results in C_i, $i \leq 4$. It follows that the minimum capacitor required for self-excitation is:

$$C_{\min} = \min(C_i, i \leq 4) \tag{3.26}$$

The minimum capacitor required for self-excitation under resistive and no load conditions can be estimated by setting X_L and (or) R_L in equation (3.19) equal to zero accordingly, and solving for X_c. The frequency corresponding to C_{min} can be used to estimate the minimum speed below which the self-excitation fails to take place. If equation (3.25) has no real roots, no excitation is possible.

3.4.2 Diesel engine model used in the set-up

The diesel engine model used in the experimental set-up is a simplified model of diesel prime mover. This model is illustrated in the figure below.

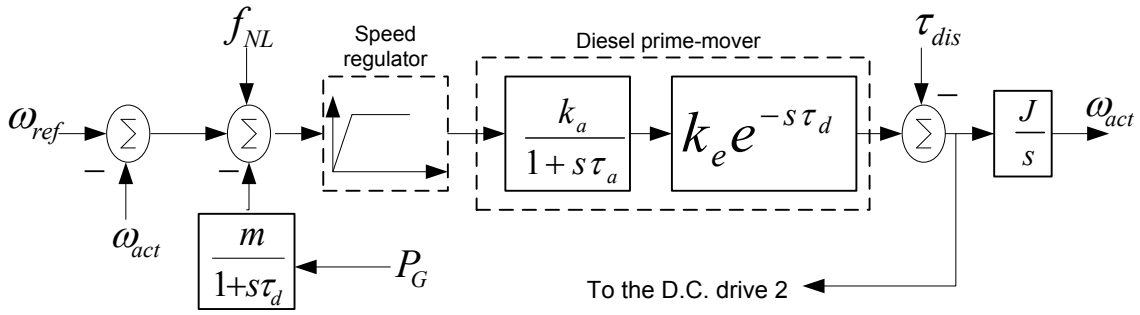

Figure 3. 11 Simplified Diesel engine model

The model represented in Figure 3.11 can be used to achieve two operating conditions of the diesel engine. The fixed-speed mode and the droop controlled mode of operation. f_{NL}, m, P_G represent the no load frequency, the slope of the droop characteristic and the power of the synchronous generator respectively. ω_{ref} represents the reference speed of the governor and ω_{act} the shaft speed. k_a, and k_e are the actuator constant, and the engine torque constant respectively while τ_a, τ_{dis} and τ_d represent the actuator time constant, the load disturbance on the engine shaft and the engine dead time respectively. In fixed-speed mode, f_{NL} and m are set to zero. Table 3.1 provides the parameters of the genset used in the experimental set-up [35].

Table 3. 1 Diesel engine parameters

Woodward governor EG-3P and EA500 actuators	
Parameters	Value (p.u., s)
Engine torque constant (k_e)	0.8-1.5
Actuator constant (k_a)	1.0
Engine inertia (J)	0.5
Actuator time constant (τ_a)	0.05-0.2
Engine dead time (τ_e)	0.0-0.25

3.4.3 Wind-Diesel emulator model

The wind-diesel emulator model implemented in the experimental set-up is illustrated in the figure below. Motors DCM1 and DCM2 are D.C. motors coupled mechanically to the self excited induction generator and synchronous generator (SG) respectively. A synchronizer unit serves to match the phase angle and voltage amplitude of the individual generators.

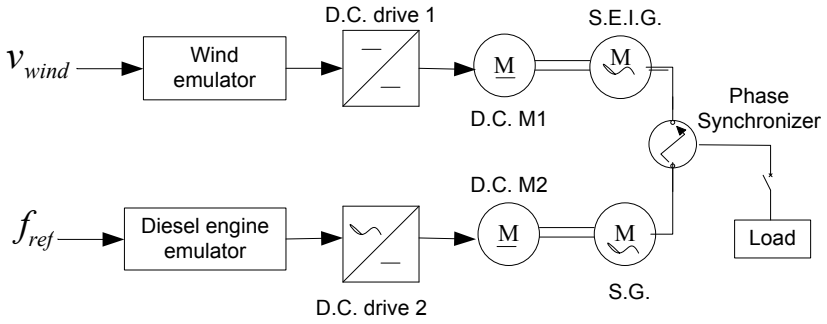

Figure 3. 12 Wind-diesel emulator model

The wind emulator model consists of the aerodynamic characteristic of the turbine, a speed controller and a current controller as illustrated in Figure 3.13.

The output of the aerodynamic block provides the speed command to the speed controller. The speed controller is used to provide the reference current signal for the hysteresis current controller and the output of the current controller block is used to control the switch of the DC drive 1, which is a buck converter. The speed and current controller derivation of the wind emulator is left beyond the scope of this thesis.

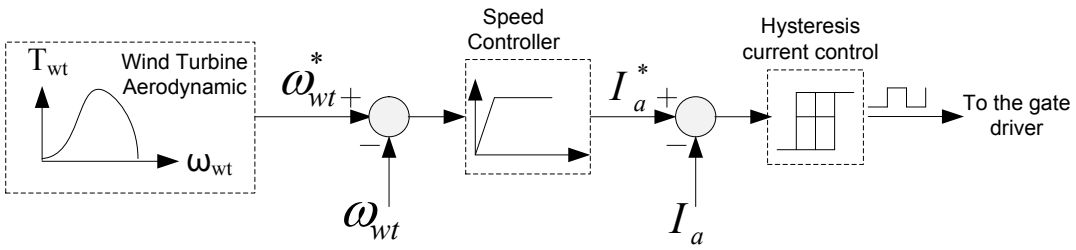

Figure 3. 13 Wind emulator concept

The diesel engine emulator consists of the governor actuator and diesel engine torque model as represented in Figure 3.14. The output of the torque model provides the reference torque (τ_c^*) used to control a D.C. drive (DCS800) that operates in torque control mode. The D.C. drive is used to controls the D.C. motor connected to the synchronous generator. τ_{dis} ($\approx P_{load}/\omega_{act}$) represents the torque disturbance due to the loading of the diesel genset. P_{load} represents the load power demanded from the genset and ω_{act} the shaft speed of the genset.

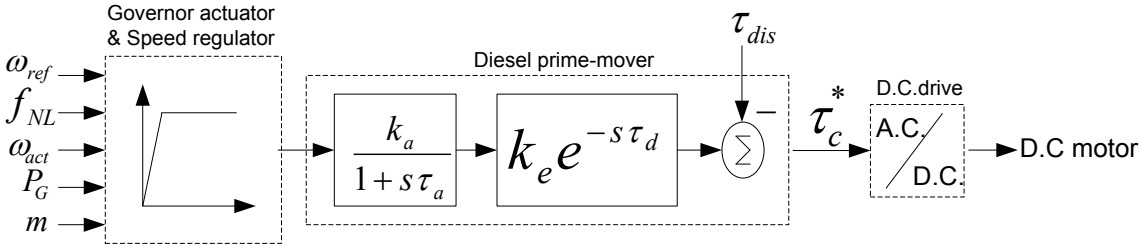

Figure 3. 14 Diesel genset emulator concept

3.4.4 Diesel engine speed controller design

In order to design the genset speed controller shown in Figure 3.14, the direct loop of the system represented in the figure below is needed.

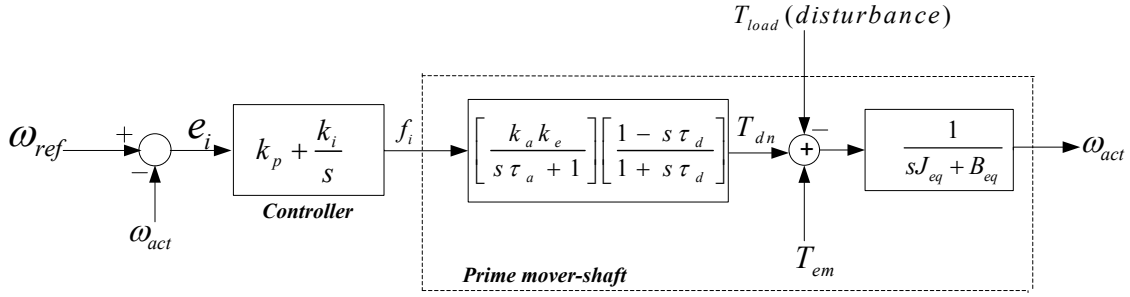

Figure 3. 15 Direct loop model of the coupling shaft

The controller parameters are tunned based on the second order standard system. In Figure 3.15, the time delay of the engine has been expressed using the first order Padé approximation as given in the following equation:

$$e^{-s\tau_d} \approx \frac{1-s\frac{t_d}{2}}{1+s\frac{t_d}{2}} \approx \frac{1-s\tau_d}{1+s\tau_d} \tag{3.27}$$

where,

$$\tau_d = \frac{t_d}{2} \tag{3.28}$$

In order to obtain a closed loop second order system including the PI controller transfer function, the prime mover-shaft part of Figure 3.15 can be approximated to a lower order model, based upon the assumption that $\tau_d < \tau_a < J_{eq}/B_{eq}$, where J_{eq} and B_{eq} are the equivalent moment of inertia and friction coefficient of the diesel genset respectively.

Thus, the transfer function of the direct loop system can be derived as follows:

$$D(s) = \frac{\omega_{act}(s)}{e_i(s)} = \left(\frac{sk_p + k_i}{s}\right)\left(\frac{1-s\tau_d}{sJ_{eq} + B_{eq}}\right) \tag{3.29}$$

The characteristic equation of the closed loop system is obtained by solving the equation $1+D(s) = 0$.

$$s^2 + \left(\frac{k_p + B_{eq} - k_i\tau_d}{J_{eq} - \tau_d k_p}\right)s + \left(\frac{k_i}{J_{eq} - \tau_d k_p}\right) = 0 \tag{3.30}$$

Based on equation (3.30), the following standard parameters for the second order transient response can be derived:

$$\omega_n = \frac{k_i}{\sqrt{k_i(J_{eq} - \tau_d k_p)}} \tag{3.31}$$

$$\xi = \frac{\frac{B_{eq}}{2} + \frac{k_p - \tau_d k_i}{2}}{\sqrt{k_i(J_{eq} - \tau_d k_p)}} \tag{3.32}$$

$$P.O. = e^{\frac{-\pi\xi}{\sqrt{1-\xi}}} \tag{3.33}$$

$$t_s \cong \frac{4}{\xi\omega_n} \tag{3.34}$$

ω_n and ξ represent the natural frequency and the damping ratio of the control system respectively. $P.O.$ and t_s represent the percentage overshoot and the settling time of the system. Parameters k_i and k_p of the controller are obtained by setting the percentage overshoot and settling time and solving equations (3.31) to (3.34).

3.4.5 Experimental Set-up configuration

The implemented experimental set-up of the hybrid wind-diesel emulator is shown in the figure below.

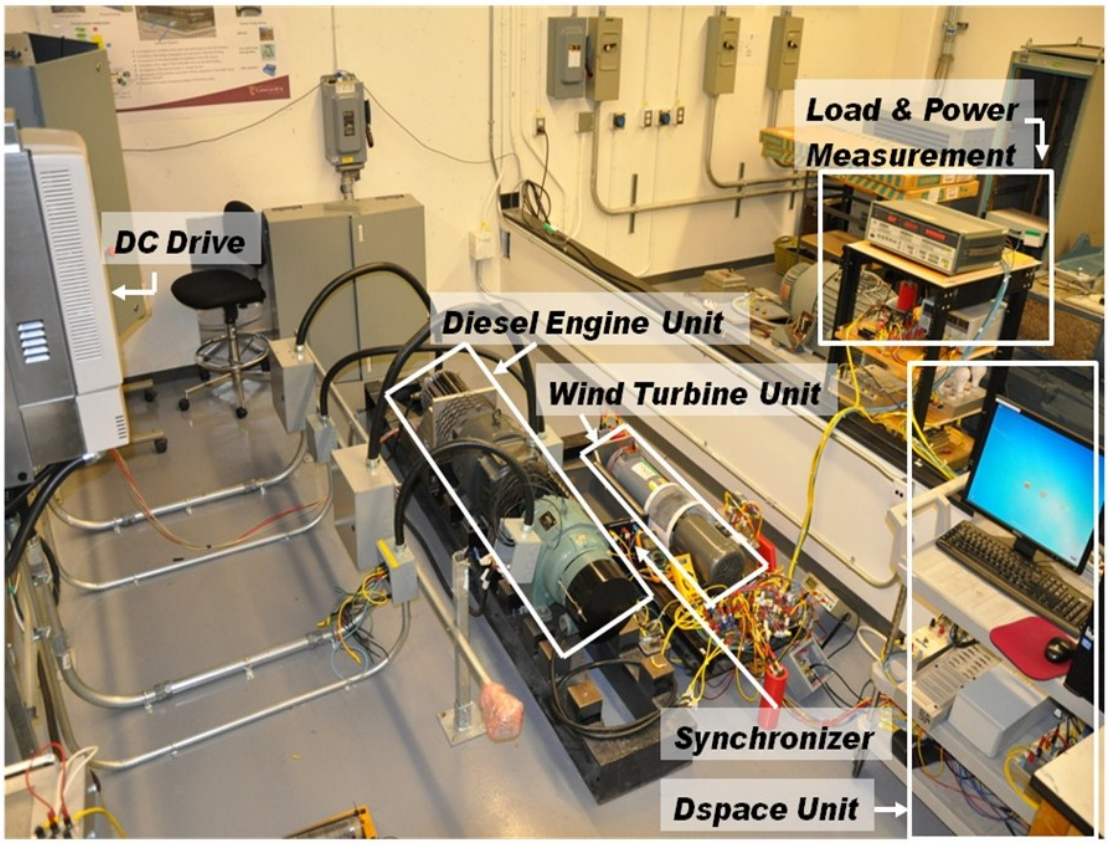

Figure 3. 16 Experimental set-up of the wind-diesel emulator

3.4.6 Results of the wind-diesel emulator

3.4.6.1 Operation in the fixed-speed mode

Figure 3.17 shows some results of the emulator when the diesel engine operates in fixed-speed mode.

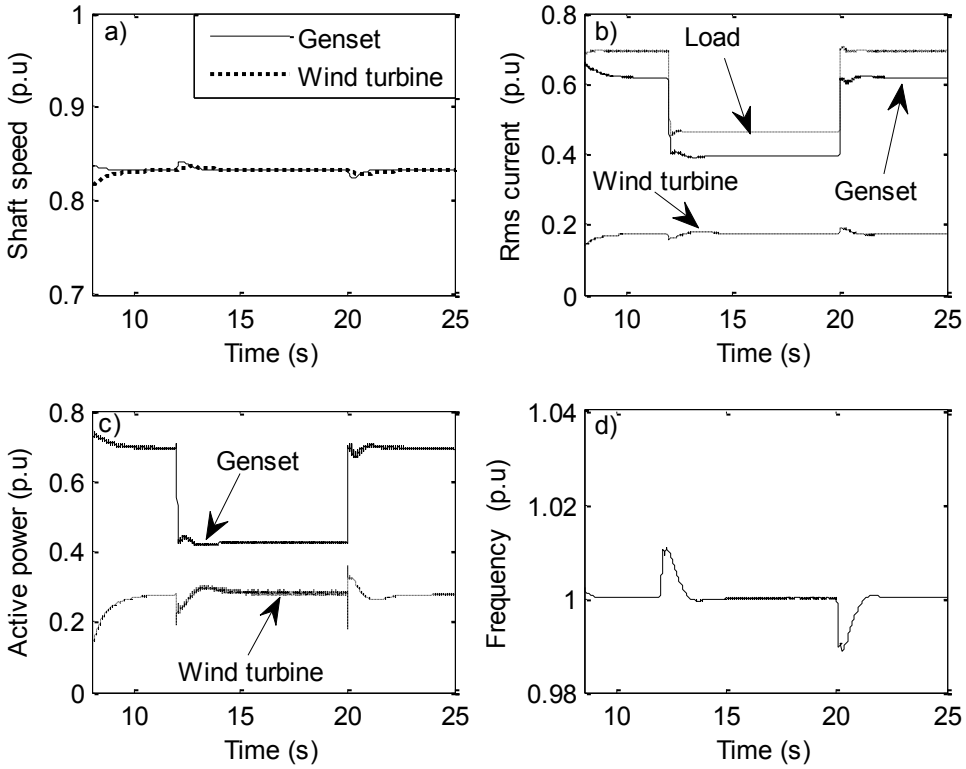

Figure 3. 17 Results of the emulator at constant wind speed and variable load: a) speed response, b) rms phase currents, c) active power of the individual generators, d) grid frequency

A decrease in the load is applied at 12s and brought back to its initial value at 20s. It appears from Figure 3.17.c that the genset power decreases while the wind turbine power remains constant since the wind speed is constant. Figure 3.17.d represents the grid frequency. The genset frequency returns to its initial value after load disturbances. This observation results from the fact that the diesel prime mover operates in fixed speed mode.

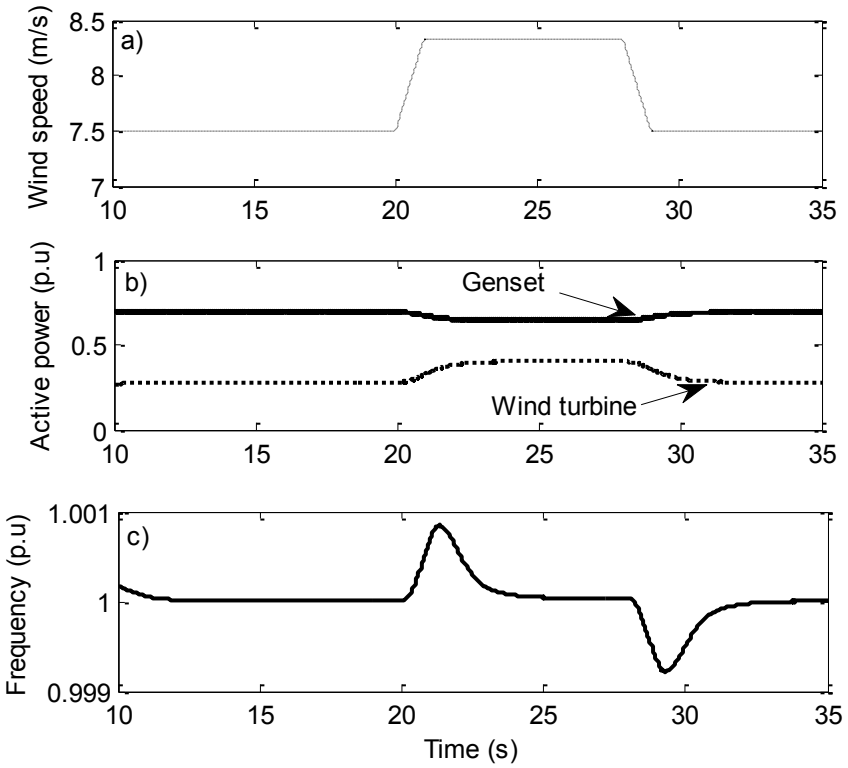

Figure 3. 18 Result of the emulator at constant load and variable wind speed: a) wind speed, b) active power, c) frequency response

Figure 3.18 represents the case where the load is kept constant while the wind speed varies as shown in this figure. As the power generated by the wind system increases, the genset power decreases (Figure 3.18.b). The resulting frequency response is shown in Figure 3.18.c. Since the genset operates in fixed-speed mode, the frequency returns to its steady state value after a step variation in the wind speed has been applied.

3.4.6.2 Operation in the droop control mode

Figure 3.19 represents the system frequency when the genset operates in droop control mode. The genset unit has a rated power of 5 HP meanwhile the wind turbine unit is rated at 2 Hp. The no-load frequency of the genset is set to 52.5 Hz with a minimum frequency at rated power of 50 Hz. Thus, the droop factor of the gen-set is 1.492 kW/Hz. Two cases

are illustrated in Figure 3.19.The case where the genset supplies the load alone and the case where both the wind turbine and the genset share the same load.

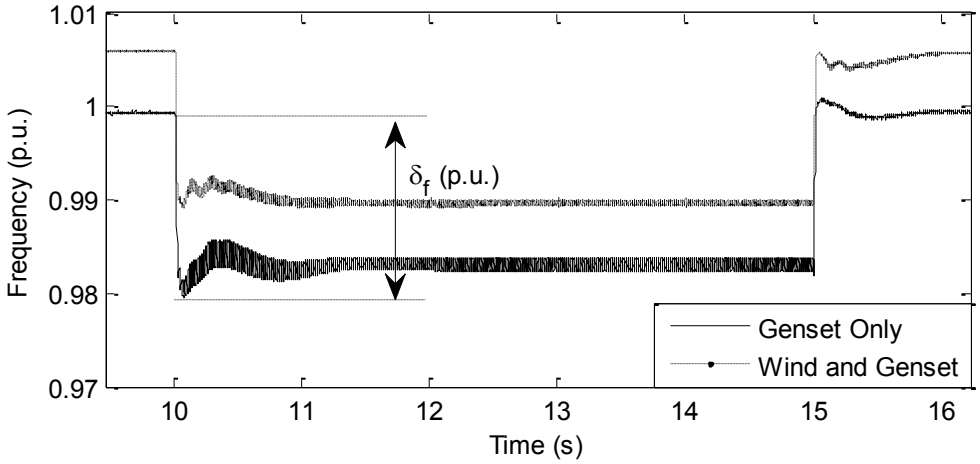

Figure 3. 19 Frequency variations when the system operates in droop controlled mode

The load is increased at 10s and brought back to its initial value at 15s while the wind turbine operates at constant wind speed. It appears from Figure 3.19 that a step change in the load changes the frequency operating point, relatively to the droop operation of the diesel engine (in both cases). Furthermore, when both generators supply the same load the grid frequency is lower than the case where only the genset supplies the load. This characterises the droop controlled behaviour of the system whereby, as the power supplied by the genset (grid forming unit) increases, the system frequency at which it operates must decrease and vice versa.

3.5 Wind turbine droop characteristic validation

The power estimation algorithm illustrated using the flowchart of Figure 3.7 is verified experimentally in this Section. Since this aspect concerns the wind turbine only, the wind turbine unit of the experimental set-up described in the previous Section has been configured as illustrated in the figure below and used to validate the proposed algorithm.

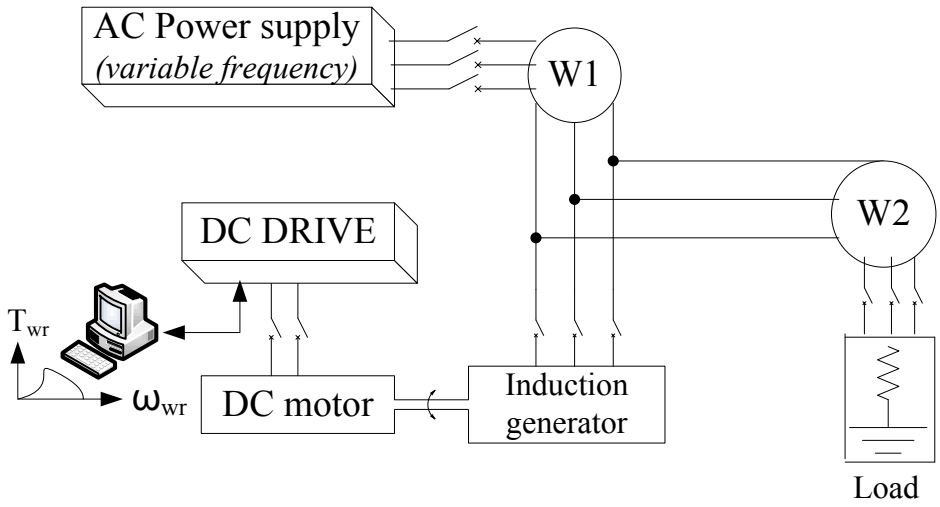

Figure 3. 20 Experimental set-up used to verify the power estimation algorithm

The variable grid frequency is achieved using a 4.5 kVA variable frequency power supply from California Instruments. A resistive load, calculated to consume more power than the power supplied by the wind turbine is used to prevent reverse power flow in the unidirectional power supply. The active power injected into the grid by the type 1 wind turbine is obtained by subtracting the power generated by the AC supply (W1) from the load power (W2). Tables 3.2 and 3.3 summarize the estimated and measured results at different wind speeds.

Table 3. 2 Estimated and measured injected power at 8 m/s

f_s *(Hz)*	ω_m *(rad/s)*	Estimated (W)	Measured (W)
47	154.6	1035	1015.3
48	157.5	979.4	965.29
49	160.4	921	903.40
50	163.2	858	847.36
51	166	796.4	774.89
52	168.8	730.1	717.17
53	171.6	661.8	651.74
Δ_f (Hz)	6		
Δ_P (W)		-62.20	-60.59
S_{Lp} (W/Hz)		-10.37	-10.10

Table 3. 3 Estimated and measured injected power at 10 m/s

f_s *(Hz)*	ω_m *(rad/s)*	Estimated (W)	Measured (W)
47	167.6	3078	3048.7
48	171	3053	3035.7
49	174.4	3021	2993.9
50	177.7	2983	2963.6
51	180.9	2938	2918.5
52	184.1	2888	2877.6
53	187.2	2830	2812.4
Δ_f (Hz)	6		
Δ_P (W)		-248	-236.3
S_{Lp}(W/Hz)		-41.33	-39.38

Figure 3.21 represents the power-frequency characteristics of the wind turbine plotted using the estimated and measured quantities of Tables 3.2 and 3.3.

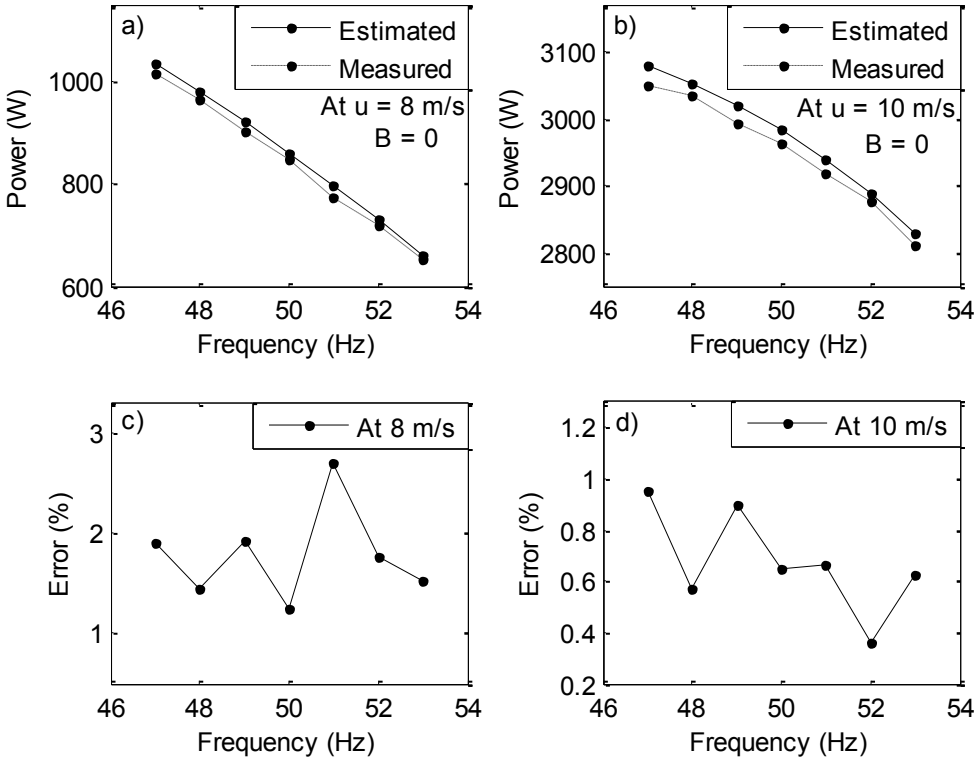

Figure 3. 21 Estimated and measured power-frequency curves at different wind speeds

It appears from Figure 3.21 that both characteristics present similar shapes. However, the estimated quantities are larger than the measured quantities. This is mostly due to the rotational losses of the generator which have been neglected in the estimation part.

The errors depicted in Figures 3.21.c and 3.21.d are relatively small. These errors are good enough to validate the proposed approach to estimate the power-frequency characteristic of type 1 wind turbines.

3.4 Summary of chapter 3

Fixed-pitch fixed-speed wind turbines equipped with induction generators present low capital and maintenance costs which are interesting features for small hybrid diesel mini-

grids. However, the lack of means for controlling the amount of injected power might create some concerns regarding frequency stability. In this chapter, a method for obtaining the injected power vs. grid frequency characteristic of this wind turbine type has been presented. The proposed approach has been validated by means of simulation and experimental results. An experimental set-up involving a diesel genset and a wind turbine emulator was built.

CHAPTER 4

TYPE-1 WIND TURBINES IN DROOP-CONTROLLED DIESEL MINI-GRIDS

This chapter examines the performance of fixed-speed wind turbines in diesel mini-grids. In the previous chapter, it has been shown that this turbine type presents an inherent droop characteristic. A design approach to select the turbine parameters that will results in high slope of the power-frequency curve is first presented in this chapter. High slope is beneficial for the hybrid system, since it will help to assist more with the frequency regulation. Next, the steady state and transient behavior of the hybrid system is analyzed.

The use of renewable energy sources to offset conventional power generation based on diesel fuel in remote communities can present many benefits [36]. Usually the diesel power plant forms the grid and balances the active and reactive powers in autonomous power systems. This is not an easy task in diesel hybrid mini-grids operating with high wind penetration, since the wind speed is highly intermittent. In addition to this, the load profile in remote communities can vary with the peak loads as high as 5 to 10 times the average loads [37]. Thus, the power demanded from the diesel generator sets and the grid frequency tend to vary widely, compared to conventional systems, thereby increasing the mechanical stress of the generators and decreasing the power quality of the system [38]. Energy storage units could be used to assist with power balancing, but the capital cost can become considerable if large amounts of storage are required. Another option could be to use secondary loads with intrinsic energy storage characteristics (such as water heaters, water pumps, water desalination plants and ice making plants), that can be switched on and off for some time without creating major effect on the consumer load. This can be achieved in a centralized way, via a communication channel as presented in [39-40].

However, this can become costly if the controllable loads are far from the mini-grid supervisory controller. Alternatively, a decentralized approach can be used where the controllable loads would react relatively to locally measured quantities such as the grid frequency. This scheme can be implemented by operating the mini-grid with a variable frequency, based on a power-frequency droop characteristic. In this way, the frequency value conveys the information of power availability in the mini-grid and the controllable loads as well as the generation units dispersed in the mini-grid so that they can adjust their power levels to assist with frequency control. Although systems operating with tightly regulated frequencies are customary, some standards such as the European EN50160 only require the frequency in autonomous power systems to be within ± 2% of the rated value (50 Hz) during 95% of the week and within 15% during 100% of the week [41].

As for the renewable energy sources integrated into diesel hybrid mini-grids, it is also desirable that they adjust their output power to assist with power balancing and frequency control. For instance, the new European grid codes require that renewable energy sources decrease their output power proportionally to the grid frequency, when this exceeds certain values [42-43]. In general, this can be achieved using pitch controlled wind turbines where the generator could be squirrel-cage induction generators (SCIG), double-fed induction generators (DFIG) or permanent magnet synchronous generators (PMSM) [44-46]. In the two latter cases, the power electronic interfaces also offer reactive power flow control capabilities. However, these features obviously increase the cost of the wind turbine and the electrification system.

Fixed-speed fixed pitch wind turbine is a configuration that is less expensive but often overlooked. However, this configuration presents some desirable features for practical applications in remote communities such as lower part count, improved reliability, reduced maintenance and lower technician expertise, the latter being extremely difficult to find in remote northern communities. In cases where the technical expertise is available nearby, travel conditions can introduce lengthy delays in repair, thus mandating longest possible times between failures. In addition to this, type 1 turbines have an inherent inertial response that helps to reduce the rate of change of frequency whenever there is an active power imbalance in the system [47-48], which can be an asset for systems with reduced rotating masses. Furthermore, the output power of type 1 turbines is affected by the stator frequency [49-50], which makes it possible to assist with frequency regulation in a passive way.

This Chapter investigates the potential of fixed-pitch type 1 wind turbines for remote communities, to assist with primary frequency control in storage-less wind-diesel hybrid mini-grids. As a passive system, it does not require any wind speed, active power and grid frequency measurements for control purposes. The impact of the number of blades and pitch angle on the power-frequency characteristics of the wind turbine is investigated using the approach described in the previous Chapter. Design parameters that maximize the capacity of this passive low-cost wind turbine technology to share load variations with a droop controlled diesel generator, thereby helping with frequency regulation, are identified. The effectiveness of the suggested designs is demonstrated by means of simulation using a storage-less hybrid wind-diesel mini-grid model.

4.1 System description

A wind-diesel hybrid mini-grid without storage, using type 1 wind turbine and a secondary (controllable) load is represented in Figure 4.1. The diesel gen-set operates with a drooped power-frequency characteristic. In such a case, the grid frequency is high when the output power of the gen-set is low. The controllable load is used to provide a coarse compensation for the consumer load and wind turbine power variations.

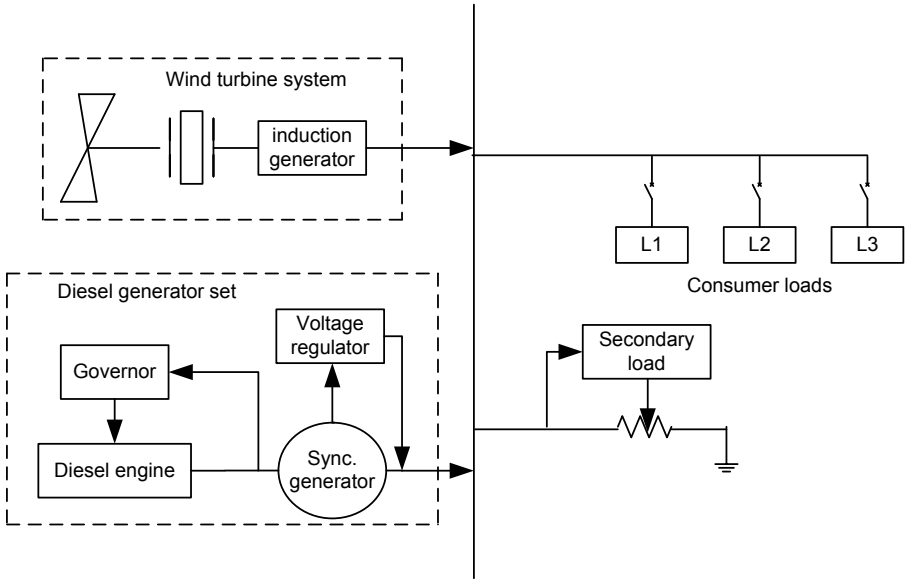

Figure 4. 1 Typical storage-less hybrid wind-diesel system

The power (P_{gen}) vs. frequency (f) characteristic of a generator operating in droop controlled mode can be described using the following equation:

$$P_{gen} = s_p(f_{nl} - f) \tag{4.1}$$

where $f < f_{nl}$. s_P represents the slope of the curve (kW/Hz) and f_{nl} the no-load frequency of the generator (Hz), often used for power dispatching. The impact of load variations on the grid frequency of a system supplied by two droop controlled generators can be calculated using the following equation.

$$\Delta f = -\frac{\Delta P_{load}}{s_{p1} + s_{p2}} \tag{4.2}$$

The output power variations of each generator due to load variations can be calculated as follows.

$$\Delta P_{gen1,2} = \frac{s_{p1,2}}{s_{p1} + s_{p2}} \Delta P_{load} \tag{4.3}$$

In general, all rotating prime movers tend to behave in a similar fashion: As the power drawn from them increases, the speeds at which they turn, and the frequency of the power they produce, decrease. However, if the slope of the droop curve (s_P) of a given generator is much smaller than those of the other generator(s), it will not be able to assist sufficiently with frequency regulation and power balancing.

In the following Sections, the impact of some parameters on the power-frequency characteristic of type 1 wind turbines is investigated. Ideally, this would provide a means for implementing a slope large enough to allow the type 1 wind turbine to share load variations with the grid forming diesel gen-set, thus helping with frequency regulation.

4.2 Wind Rotor Characteristics

In Figure 4.1 the main components of a type 1 wind turbine (wind rotor, gear box and SCIG) are represented. In typical applications, a breaker is used to disconnect the turbine from the grid and a fixed capacitor bank is used to provide the reactive power required by the induction machine. These components do not have any effects on the issues discussed in this analysis and, are therefore omitted from the analysis. The power (P_{wr}) and torque (T_{wr}) developed by a wind rotor can be obtained using the following equations.

$$P_{wr} = \frac{\rho}{2} \pi R^2 u^3 C_P(\lambda, \beta) \tag{4.4}$$

$$T_{wr} = \frac{\rho}{2}\pi R^3 u^2 C_T(\lambda,\beta) \tag{4.5}$$

Where ρ is the air density, R is the rotor radius, u the wind speed, C_P and C_T the power and torque coefficients of the wind rotor. The latter are functions of λ, the tip speed ratio, and β, the pitch angle. The tip speed ratio is defined by:

$$\lambda = \frac{\omega_r}{u} R \tag{4.6}$$

where ω_r is the wind rotor angular velocity.

Manufacturer specific power coefficient curves are typically represented by high order polynomials with dozens of coefficients [51]. This research work assumes only general features of the 2- and 3-blade rotors generic expressions of power coefficients. The power coefficient of a generic 3-blade wind rotor can be represented using the following equation [52].

$$C_{P3}(\lambda,\beta) = 0.5176\left(\frac{116}{z_i} - 0.4\beta - 5\right)^{\frac{-21}{z_i}} - 0.0068\lambda \tag{4.7}$$

where,

$$\frac{1}{z_i} = \frac{1}{\lambda + 0.08\beta} - \frac{0.035}{\beta^3 + 1} \tag{4.8}$$

That of a generic 2-blade wind rotor can be represented by [49]

$$C_{P2}(\lambda,\beta) = 0.5\left(\lambda - 0.022\,\beta^2 - 5.6\right)e^{-0.17\lambda} \tag{4.9}$$

The torque coefficient for both cases can be obtained using equation (4.10).

$$C_T(\lambda,\beta) = \frac{C_P(\lambda,\beta)}{\lambda} \tag{4.10}$$

It is assumed in this analysis that the values of R and β of the wind rotor are fixed and the slip of the induction generator can be neglected. In this case, the impact of grid frequency

variations on the power developed by the wind turbine will depend mostly on the C_P vs. λ curve characteristics.

Figure 4.2 represents the C_P-λ curve for a 3-blade wind rotor at different pitch angles. From equation (4.6), it can be seen that as the grid frequency increases, the shaft speed of the induction machine and wind rotor increase, thus increasing λ. In order to have a decreasing output power of the wind turbine, the system should always operate with $\lambda > \lambda_{CP\text{-}M}$, where $\lambda_{CP\text{-}M}$ is the value of λ at which C_P is maximum. It appears from Figure 4.2 that as the pitch angle increases, the slope of the C_P vs. λ curve decreases. Thus, in principle, the largest slope for the power-frequency characteristic of the wind turbine should be obtained at minimum β. On the other hand, for the wind turbine to produce power, it has to operate with $C_P > 0$ and $\lambda < \lambda_{CP=0}$, where $\lambda_{CP=0}$ is the value of λ at which C_P is equal to zero. As β increases, so does $\lambda_{CP=0}$, which will have an impact on the minimum wind speed at which the wind turbine can generate power.

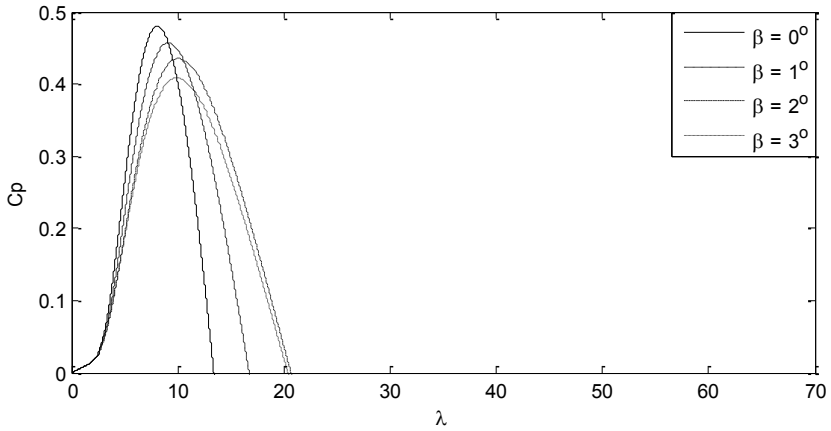

Figure 4. 2 C_P-λ curve of a 3-blade wind rotor at different pitch angles.

Figure 4.3 represents the C_P-λ curve of a 2-blade wind rotor at different pitch angles. The shape of this curve is different from that of the 3-blade wind rotor, featuring large values

of $\lambda_{CP=0}$ with a variable slope in the region where $\lambda > \lambda_{CP\text{-}M}$. However, these curves do not change much with the pitch angle.

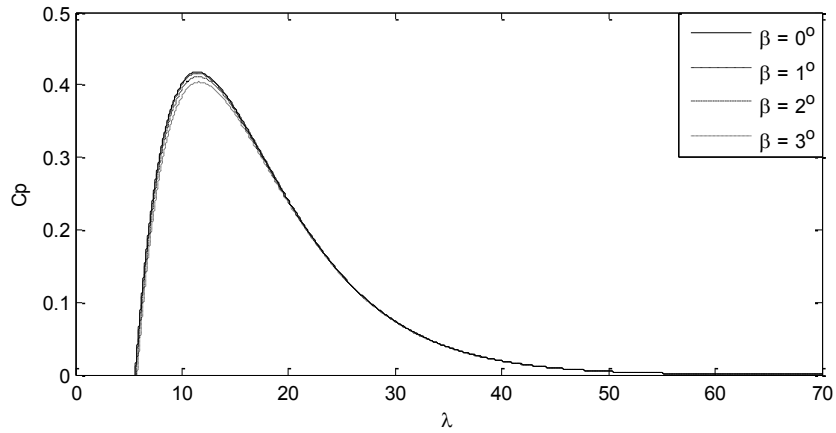

Figure 4. 3 C_P-λ curve of a 2-blade wind rotor at different pitch angles.

4.3 Wind turbine parameter selection

In this Section, the impact of the number of blades and pitch angle on the wind rotor power-frequency droop characteristic of a type 1 wind turbine is used to define the turbine design specifications. Design approaches based on the power-frequency droop characteristics of type 1 wind turbines are not common in literatures. Therefore, a simple methodology for selecting the main parameters of the wind turbine is proposed in this Section. The design specifications used in this analysis can be stated as follows; the turbine should:

- Supply rated power (P_{rat}) to the grid at rated frequency (f_{rat}) and rated wind speed (u_{rat}). Passive stall is assumed as a means for limiting power injection as the wind speed exceeds the rated value.
- Inject power into a variable frequency grid, from f_{min} to f_{max}, for wind speeds above a minimum value ($u_{\min}$).

- Reduce the injected power as the grid frequency increases, thus presenting the desired power-frequency droop characteristics.

To comply with the third criterion, the wind rotor should always operate with $\lambda > \lambda_{CP\max}$. From equation (4.6), it can be seen that the critical case is at minimum shaft speed and rated wind speed ($u = u_{rat}$). Taking into account the gear ratio and neglecting the slip of the induction generator ($\omega_r \approx \omega_{sync\min}/K_{gb}$), the following constraint can be defined based on equation (4.6).

$$\frac{K_{gb}}{R} < \frac{\omega_{sync\min}}{u_{rat}\,\lambda_{CP\max}} \tag{4.12}$$

Concerning the second criterion, it is necessary that the power produced by the wind rotor be larger or equal to the losses in the induction generator at minimum wind speed ($u = u_{\min}$). To simplify the analysis, it is assumed that the induction generator losses are fixed and equal to the no-load losses ($P_{IG\text{-}NL}$) of the generator at rated grid frequency. These losses can easily be obtained from the no load tests of the induction machine. Thus, the wind rotor has to operate with $C_P = C_{P\min}$ for all cases when $u = u_{\min}$. A ratio between $C_{P\min}$ and $C_{P\max}$ can be derived using equation (4.4) based on the assumption that at rated wind speed and operating with $C_{P\max}$, the wind rotor generates rated power injected into the grid plus the generator losses. In addition to this, at minimum wind speed and operating with $C_{P\min}$, the wind rotor should generate a minimum power equal to the mechanical power, so as to match the generator losses. Therefore,

$$C_{P\min} = \left(\frac{u_{rat}}{u_{\min}}\right)^3 \frac{P_{IG-NL}}{P_{rat} + P_{IG-NL}} C_{P\max} \tag{4.13}$$

The worst case related to the second criterion occurs at maximum grid frequency, which results in maximum synchronous speed and maximum shaft speed at the low speed side of the gear box. In this case, taking into account the effect of the gear box, the following design constraint can be derived using equation (4.6).

$$\frac{K_{gb}}{R} > \frac{\omega_{sync\max}}{u_{\min}\lambda_{CP\min}} \tag{4.14}$$

Where $\lambda_{CP\min}$ can be calculated from $C_{P\min}$ and the C_P vs. λ curve of the wind rotor.

Assuming that the number of poles of the induction generator is known, the only missing parameters of the turbine are K_{gb} and R. After selecting a ratio for K_{gb} and R that complies with equations (4.12) and (4.14), the value of R that satisfies the first criterion is calculated iteratively, using the approach developed in chapter 3. If the value obtained from equation (4.14) exceeds the one obtained using equation (4.12), the value of the K_{gb}/R ratio should be selected using equation (4.14). The actual cut-in wind speed is obtained using the following equation.

$$u_{\min} \approx \frac{\omega_{sync\max}}{\omega_{sync\min}} \frac{\lambda_{CP\max}}{\lambda_{CP\min}} u_{rat} \tag{4.15}$$

4.3.1 Case study of the wind turbine parameter selection

The main objective of this Section is to compare different designs of a type 1 wind turbine and identify how their parameters affect their power-frequency characteristics. The general specifications of the wind turbine and the parameters of the induction generator selected for this study are given in the appendix.

4.3.1.1 2-Blade wind turbine parameter selection

As shown in Figure 4.3 the pitch angle (β) has low impact on the C_P-λ curve of the 2-blade wind rotor. However, since this turbine type presents a wider variation of λ and

dC_p/dλ, it will be used for identifying the impact of different regions of the C_P-λ curve on the power-frequency characteristics of the turbine. The numerical values of some parameters required for the design and analysis of the 2-blade wind rotor at β = 0° are given in Table 4.1. The no-load losses of the induction machine are estimated to be 2.2 kW while $C_{P\min}$ = 0.165. As shown in this table, the value of K_{gb}/R min is greater than that of K_{gb}/R max. Thus, one of the two constraints should be ignored. It has been noticed that increasing $u_{\min}$ makes it possible to achieve a relatively high droop factor of the power-frequency characteristics. This appears to be a useful compromise.

Table 4. 1 Parameters of the 2-blade wind rotor

β (°)	$C_{P\max}$	$\lambda_{CP\max}$	$\lambda_{CP\min}$	K_{gb}/R max	K_{gb}/R min
0	0.417	11.2	23.43	1.332	1.689

Two values of K_{gb}/R are considered to compare the behaviour of the wind turbine when operating at two different regions of the C_P vs. λ curve: 0.75 and 1.15. In the following, both cases will be referred to as design #1 and design #2 respectively. The power injected into the grid by the wind turbine at different wind speeds and grid frequencies for both deigns are represented in Figure 4.4, using their respective data given in Tables 4.2 and 4.3.

Table 4. 2 Power-frequency variation of the 2-blade (design 1)

Design #1: K_{gb}/R = 0.75 (R = 10.4 m)						
f (Hz)	u =12 m/s		u=10.5m/s		u = 9 m/s	
	Power (kW)	λ	Power (kW)	λ	Power (kW)	λ
57	81.9	20.1	40.6	22.9	15.6	26.5
58	79.5	20.4	39.0	23.2	14.9	27.1
59	77.1	20.8	37.4	23.6	14.0	27.6
60	74.7	21.1	35.8	24	12.7	28.0
61	72.3	21.4	34.2	24.4	11.7	28.4
62	69.0	21.8	32.2	24.9	10.5	28.9
63	65.3	22.2	30.0	25.3	9.3	29.3
$s_{p\text{-}u}$ (kW/Hz)	2.77	----	1.77	----	1.04	----

It appears from these tables that both designs can supply rated power at 60 Hz and rated wind speed. However, as the grid frequency varies, the output power of design #1 varies more than that of design #2.

Table 4. 3 Power-frequency variation of the 2-blade (design #2)

Design #2: K_{gb}/R = 1.15 (R = 7.68 m)						
f (Hz)	u =12 m/s		u=10.5m/s		u = 9 m/s	
	Power (kW)	λ	Power (kW)	λ	Power (kW)	λ
57	76.8	13.1	46.9	14.9	22.9	17.4
58	76.0	13.3	45.9	15.2	22.5	17.7
59	75.4	13.6	45.0	15.4	22.1	18.0
60	74.6	13.8	44.0	15.7	21.6	18.3
61	73.9	14.0	42.9	16.0	21.0	18.6
62	73.0	14.2	42.0	16.2	20.4	18.8
63	71.9	14.5	41.0	16.5	19.9	19.2
$s_{p\text{-}u}$ (kW/Hz)	0.81	----	0.97	---	0.50	----

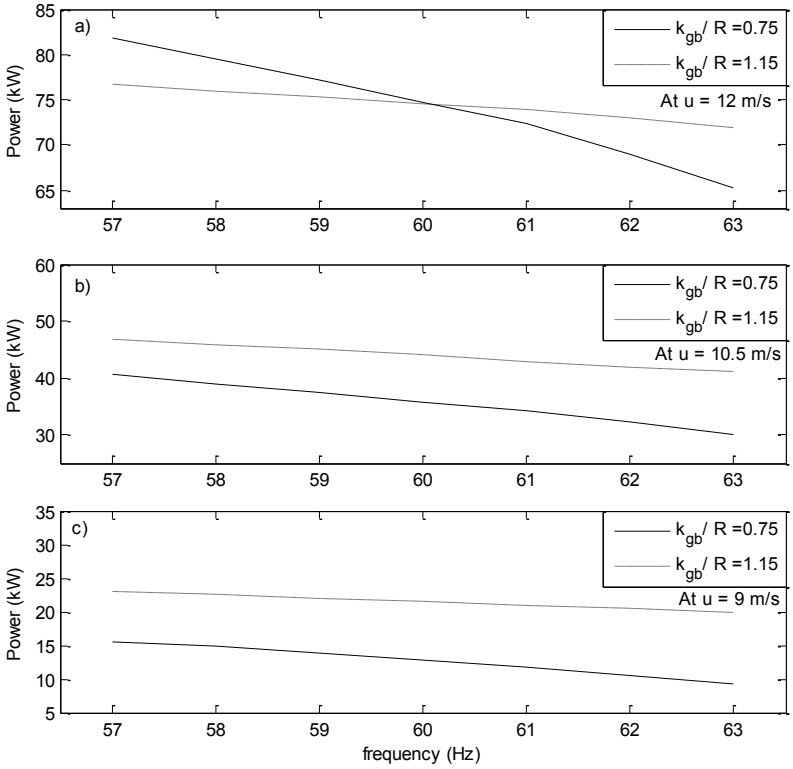

Figure 4. 4 Power-frequency curves of the 2-blade designs at β = 0° and different wind speeds

This is due to the region in the C_P vs. λ curve where both designs operate for the given wind speed and grid frequency values and also on the variation of λ. Furthermore, design

#1 provides a larger power boost at rated wind speed when the grid frequency drops to the minimum value. On the other hand, as the wind speed decreases, the output power of design #1 becomes smaller than that of design #2, for the same wind speed and grid frequencies. This is mainly due to the increased value of λ, resulting in smaller values of C_p. The average slope (s_p) of the power-frequency curves for both designs is 1.86 for design #1 and 0.76 for design #2.

Unlike conventional generators or controllable wind turbines, type 1 wind turbines do not generally operate at "no-load." In this case, a different mathematical representation of the power-frequency variations should be considered. The following equation can be used to represent the type 1 WT power-frequency variations.

$$P_{WT} = P_{u-f_{\max}} + s_{p-u}\left(f_{\max} - f\right) \tag{4.16}$$

where $f_{\min} < f < f_{\max}$. $P_{u\text{-}f\max}$ is the injected power at a given wind speed and maximum grid frequency. $s_{P\text{-}u}$ represents the slope of the curve which varies with the wind speed. Equation (4.16) is compatible with Equation (4.1) since $f_{\max}$ for a conventional generator represents f_{nl} and $P_{u\text{-}f\max}$ is equal to zero. This equation provides the value of the slope for the droop curve ($s_{P\text{-}u}$), required to calculate the variation of the grid frequency and power supplied by the individual generating units, in response to load variations.

4.3.1.2 3-Blade wind turbine parameter selection

As illustrated in Figure 4.2, the pitch angle (β) has a significant impact on the C_P vs. λ curve of 3-blade wind rotors. As β increases, $C_{P\max}$ decreases, $\lambda_{CP\max}$ and $\lambda_{CP=0}$ increase and the slope of the C_P-λ curve in the region where $\lambda > \lambda_{CP\max}$ decreases. In this Section, the cases of a 3-blade wind rotor at $\beta = 0°$ and $\beta = 2°$ will be considered. The numerical values of the parameters required for the design and analysis of these cases are given in

Table 4.4. Values of $C_{P\min}$ at $\beta = 0°$ and $\beta = 2°$ are 0.19 and 0.17 respectively. Since K_{gb}/R max is smaller than K_{gb}/R min for both cases, the selected values of K_{gb}/R should be smaller than K_{gb}/R max, similarly to the 2-blade wind rotor case.

Table 4. 4 Parameters of the 3-blade wind rotor

β (°)	$C_{P\max}$	$\lambda_{CP\max}$	$\lambda_{CP\min}$	K_{gb}/R max	K_{gb}/R min
0	0.48	8.1	12.0	1.833	3.288
2	0.44	10.2	17.5	1.463	2.259

The selected values of K_{gb}/R are 1.75 for $\beta = 0°$ (design #3) and 1.2 for $\beta = 2°$ (design #4) slightly lower than K_{gb}/R max for both cases. R is then calculated for both cases to achieve rated power at rated wind speed and rated grid frequency. The resulting power injected into the grid by the wind turbine at different wind speeds and grid frequencies in these cases is represented in Figure 4.5 using Tables 4.5 and 4.6.

Table 4. 5 Power-frequency variation of the 3-blade (design 3)

Design #3: $\beta = 0^\circ$ $K_{gb}/R = 1.75$ ($R = 7.1$ m)						
f (Hz)	u =12 m/s		u=10.5m/s		u = 9 m/s	
	Power (kW)	λ	Power (kW)	λ	Power (kW)	λ
57	76.5	8.6	44.0	9.8	17.4	11.4
58	76.1	8.8	42.9	10.0	14.8	11.6
59	75.3	8.9	41.6	10.1	13.3	11.8
60	74.8	9.0	40.2	10.3	11.7	12.0
61	74.1	9.2	38.9	10.5	10.0	12.2
62	73.1	9.3	37.4	10.7	8.3	12.4
63	72.4	9.5	35.8	10.8	6.4	12.6
$s_{p\text{-}u}$ (kW/Hz)	0.68	----	1.36	----	1.83	----

Table 4. 6 Power-frequency variation of the 3-blade (design 4)

Design #4: $\beta = 2^\circ$ $K_{gb}/R = 1.2$ ($R = 7.88$ m)						
f (Hz)	u =12 m/s		u=10.5m/s		u = 9 m/s	
	Power (kW)	λ	Power (kW)	λ	Power (kW)	λ
57	76.7	8.6	43.7	14.3	17.5	16.6
58	76.0	8.8	42.5	14.5	16.2	17.0
59	75.3	8.9	41.2	14.8	14.9	17.2
60	74.6	9.0	39.0	15.0	13.1	17.5
61	74.0	9.2	37.5	15.3	11.8	17.8
62	73.2	9.3	36.0	15.6	10.5	18.1
63	72.0	9.5	33.8	15.8	9.2	18.3
$s_{p\text{-}u}$ (kW/Hz)	0.78	----	1.64	----	1.37	----

It appears from these results that while the slope of the power-frequency characteristics of design #3 increases as the wind speed increases, it first increases and then decreases for design #4. The average slope (s_p) of the power-frequency curves for design #3 and design #4 are 1.29 and 1.26, respectively.

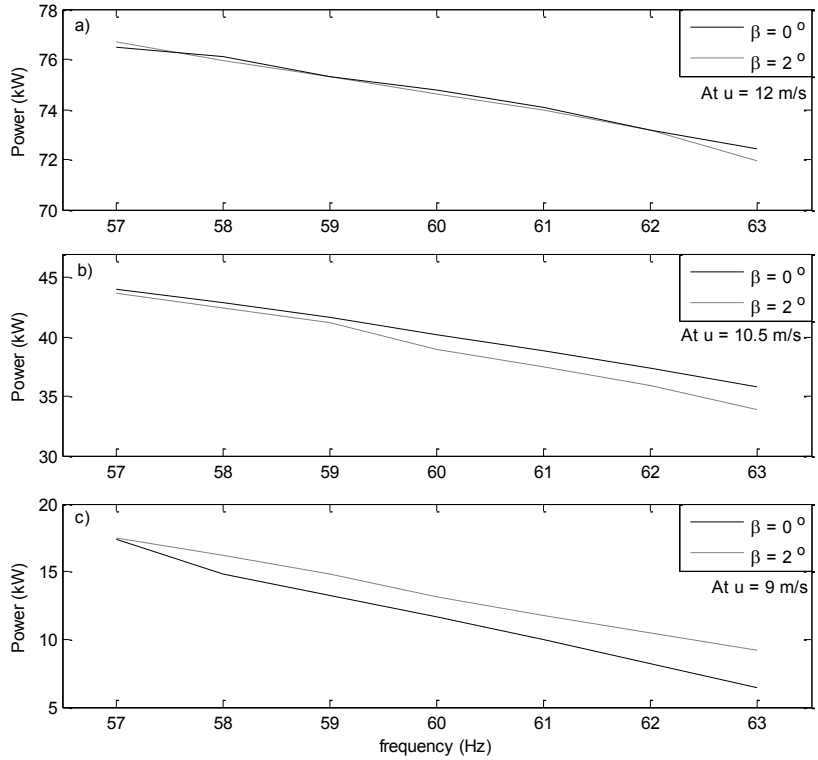

Figure 4. 5 Power-frequency curves of the 3-blade designs at different β and wind speeds

4.4 Steady state performance of type 1 wind turbines in the hybrid diesel mini-grid

The aim of this Section is to verify how the droop factor magnitude of the power-frequency characteristics of type 1 wind turbines affects the variation of the grid frequency and power developed by the gen-set in the wind-diesel mini-grid, during steady state. The dynamics of the wind turbine and gen-set are neglected and the simulation is done using an energy flow model of the hybrid system [53]. The energy flow model of the system is illustrated in Figure 4.6. Designs #1 and #2 presenting the

highest and the lowest droop factors are selected for this analysis. For both designs, the wind turbine presents a nominal power of 100 HP and operates in parallel with a 30 kVA gen-set. The genset no-load frequency is 62 Hz while its minimum frequency at rated power is 58 Hz. Thus, the droop factor of the gen-set is 7.5 kW/Hz. Generally, in similar systems (with high wind penetration), a secondary load is used to assist with power balancing. Figures 4.7 and 4.8 represent the wind speed and load profiles assumed in this analysis.

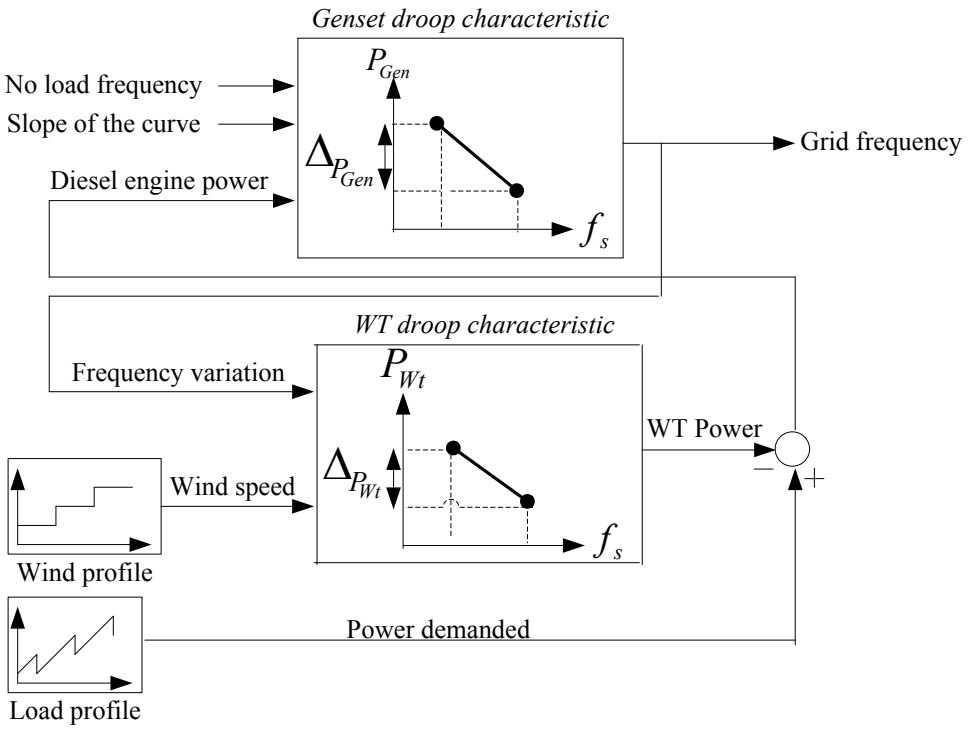

Figure 4. 6 Energy flow model of the hybrid system

The wind speed varies in steps while the load profile varies between minimum and maximum values, estimated such that the individual wind turbines can operate in parallel with the gen-set without exceeding their output power constraints.

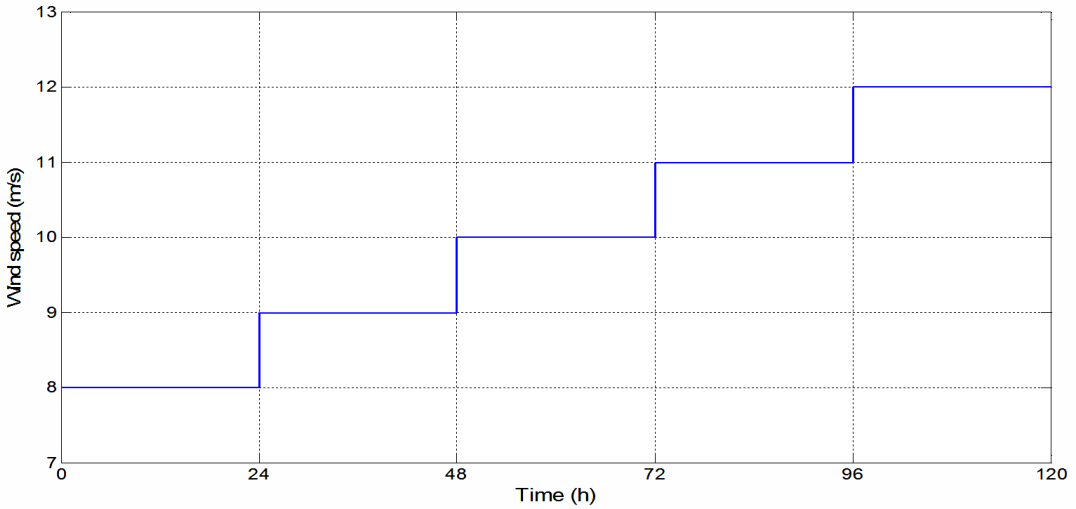

Figure 4. 7 Wind profile

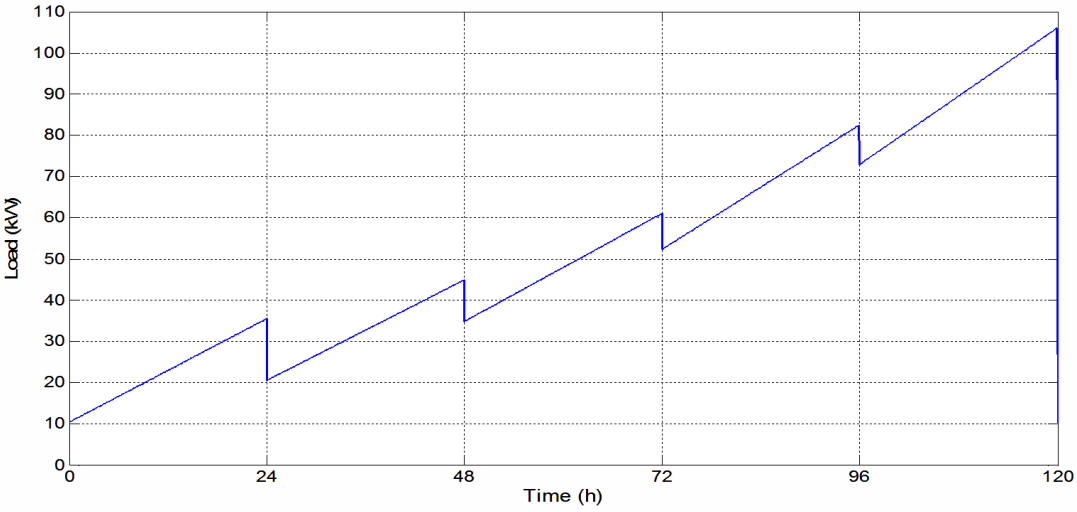

Figure 4. 8 Load profile

Unlike using typical wind and load profiles, this approach allows considering all possible operating points on the assessment of the average frequency and gen-set power variations with respect to both designs. The variations of the gen-set output power and grid frequency are represented in Figures 4.9 and 4.10 for both designs, where the results of Design #1 are represented using the solid line and those of design #2 represented using the dotted line.

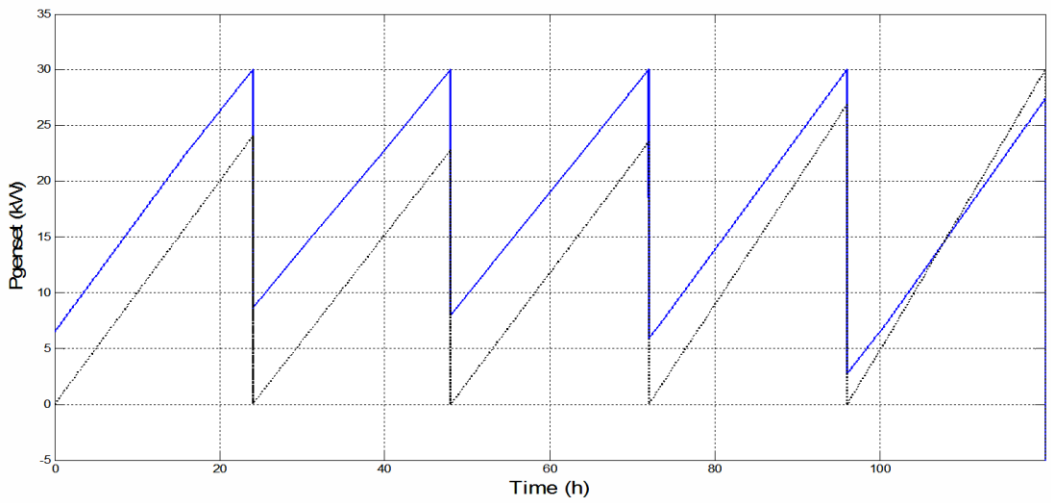

Figure 4. 9 Genset output power: design#1 (solid line); design#2 (dotted line)

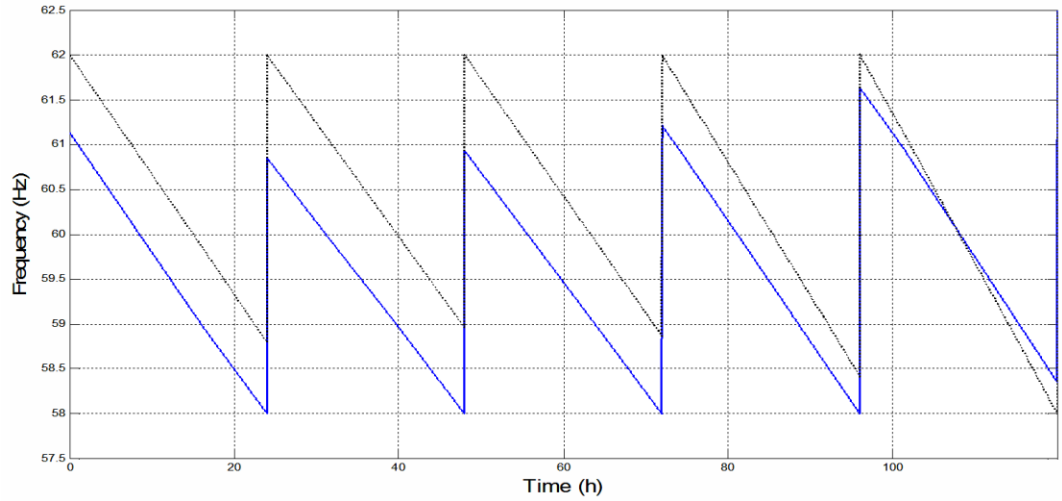

Figure 4. 10 Grid frequency: design#1 (solid line); design#2 (dotted line)

It appears from this result that as the load demand varies, design #1 due to its larger droop factor reduces the frequency and gen-set output power variations more than design #2 which presents lower droop factor. The benefits are the largest at high wind speeds. It also appears from these results that the power from the gen-set increases when the wind turbine with high droop factor is used. The numerical values of these results are given in the Table below.

Table 4. 7 Summary of the simulation results

WIND	P_{load}		Design #1			Design #2		
u (m/s)	Min (kW)	Max (kW)	ΔP_{gen}(kW)	P_{AV} (kW)	Δf (Hz)	ΔP_{gen}(kW)	P_{AV} (kW)	Δf (Hz)
8	10.4	35.5	23.53	18.24	3.13	24.03	12.02	3.12
9	20.5	44.9	21.39	19.3	2.85	22.82	11.41	3.04
10	34.8	61.0	21.99	19.0	2.93	23.52	11.76	3.13
11	52.3	82.5	24.08	17.96	3.21	26.89	13.45	3.58
12	72.9	106	24.65	15.03	3.26	30.0	15.0	4.0
Ave.	----	----	23.13	17.91	3.08	25.45	12.73	3.37

The gen-set output power and frequency variations obtained from the simulation are in good agreement with those obtained using equations (4.1) to (4.3).

One aspect to be further investigated is the impact of the increased droop factor on the diesel engine shaft loading. This requires a dynamic model of the hybrid mini-grid with accurate values of the turbine inertia, compliance of the drive train, and time constants of the gen-set frequency control loop.

4.5 Dynamic model of the hybrid system

The dynamic model of the hybrid system developed in this chapter involves the wind turbine aerodynamic model (see Section 4.2), the drive train model and the diesel gen-set model. The diesel gen-set model consists of two main elements: A synchronous generator (SG) and the prime mover (diesel engine). The SG is implemented with the 37.5 kVA/460 V, 18000 RPM/ 60 Hz "synchronous machine" block available in Simulink. The input field voltage "Vf" is provided by a PI voltage regulator for which the reference voltage is set to be equal to the generator rated voltage. The mechanical input is selected to be the "speed w," thus making the inertia constant H of the block to be disregarded. The mechanical shaft of the gen-set is represented by a first order transfer function with the moment of inertia of the engine and SG lumped together. The fuel injection actuator is represented by a first order transfer function while a delay block models the time

interval between fuel injection and torque developed in the mechanical shaft of the diesel engine. The governor of the gen-set is of the PI type with droop, fed from the no-load speed of the gen-set which can be used by the supervisory controller for frequency regulation and/or power dispatching.

4.5.1 Drive train dynamic model

Figure 4.11 represents the model of the drive train used in this analysis. This figure illustrates a two-mass model of the wind turbine drive train, where an equivalent stiffness and damping factor of the system has been assumed. The moment of inertia for the shafts and gearbox wheels can be neglected since they are small compared to that of the wind turbine or generator. Thus, the resultant model is essentially a two mass model connected by a flexible shaft.

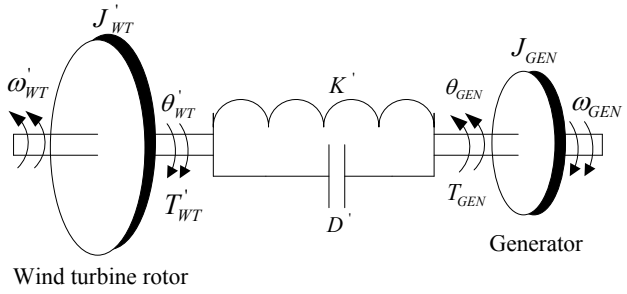

Figure 4. 11 Model of the turbine drive train on the generator side

The dynamic equations of the drive-train written on the generator side can be derived as follows:

$$T'_{WT} = J'_{WT}\frac{d\omega'_{WT}}{dt} + D'\left(\omega'_{WT} - \omega_{GEN}\right) + K'\left(\theta'_{WT} - \theta_{GEN}\right) \tag{4.16}$$

$$-T_{GEN} = J_{GEN}\frac{d\omega_{GEN}}{dt} + D'\left(\omega_{GEN} - \omega'_{WT}\right) + K'\left(\theta_{GEN} - \theta'_{WT}\right) \tag{4.17}$$

$$\frac{d\theta'_{WT}}{dt} = \omega'_{WT} \tag{4.18}$$

$$\frac{d\theta_{GEN}}{dt} = \omega_{GEN} \tag{4.19}$$

where the equivalent moment of inertia of the turbine is

$$J_{WT}^{'} = J_{WT}\frac{1}{k_{gb}^2} \tag{4.20}$$

and the equivalent stiffness and damping coefficient given by,

$$\frac{1}{K^{'}} = \frac{1}{\frac{k_{WT}}{k_{gb}^2}} + \frac{1}{k_{GEN}} \tag{4.21}$$

$$D^{'} = D_{GEN} + \frac{D_{WT}}{k_{gb}^2} \tag{4.22}$$

T_{WT} represents the wind turbine torque, J_{WT} the turbine moment of inertia, ω_{WT} the wind turbine shaft speed, k_{WT} and k_{GEN} the spring constants indicating the torsional stiffness of the shaft on the turbine and generator sides respectively. T_{GEN} represents the generator torque, J_{GEN} the generator moment of inertia, ω_{GEN} the generator shaft speed and K_{gb} the gear ratio. D_{GEN} and D_{WT} represent the damping coefficients on the generator and wind turbine sides respectively. The turbine drive train parameters assumed in this study were obtained from [54], and are given in the appendix.

4.5.2 Diesel engine prime mover model

The diesel engine model used in this study is a simplified model of diesel prime mover. A complete dynamic simulation of the diesel engine would require a very large order model. However, for the purpose of the analysis reported in this work, it is sufficient to use a much lower order model. Figure 4.12 represents the diesel prime mover model assumed in this work.

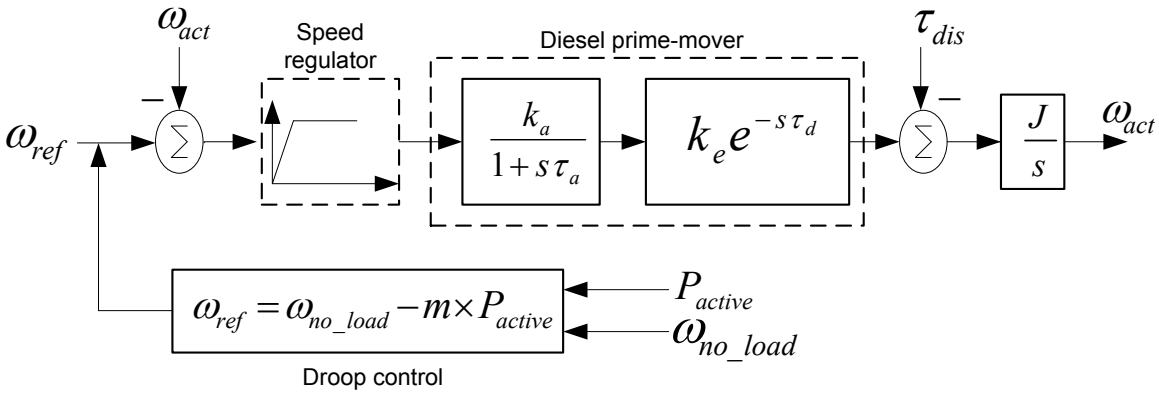

Figure 4. 12 Diesel engine prime-mover model

ω_{NL} represents the no load speed of the diesel generator, m the slope of the power-frequency characteristic of the diesel gen-set and P_{active} the active power of the synchronous generator. ω_{ref} represents the reference speed of the governor and ω_{act} the shaft speed of the prime-mover. k_a, and k_e represent the actuator constant and engine torque constant respectively, while τ_a, τ_{dis} and τ_d represent the actuator time constant, the load disturbance on the engine shaft and the engine dead time. The speed controller and voltage regulator parameters are tuned based on the approach given in [55]. The parameters of the diesel gen-set used are given in the appendix [55].

4.6 Dynamic performance of type 1 wind turbines in the hybrid diesel mini-grid

Three cases have been considered to evaluate the dynamic performance of the hybrid system. The first case follows a step variation in the load; the second case, a step variation in the wind speed and the third case concerns the response of the system due to the gust components in the wind speed. Similar to the steady state analysis, designs #1 and #2 of the 2-blade turbine presenting the largest and the smallest slopes have been selected for this study. In general, the total moment of inertia of the wind turbine depends on the physical dimension and material used in the turbine parts. Designs #1 and #2

present different rotor diameters. Therefore, it is necessary to estimate the moment of inertia corresponding to the individual designs. The total moment of inertia of a wind turbine can be approximated using the following equation [56]:

$$J = N_b m_b \left(\frac{R}{3}\right)^2 = \frac{1}{9} m_r R^2 \tag{4.22}$$

where N_b is the number of blade of the turbine, m_b the mass of the blade, R the blade radius and m_r the mass of the whole rotor including all the blades. In equation (4.22), the ratio *R/3* is based on the assumption that the blade has its mass middle-point at about 1/3 of the radius. The approximated relationship between the rotor mass and diameter is given by [56]:

$$m_r = 0.486 \times (d_r)^{2.6} = 0.486 \times (2R)^{2.6} \tag{4.23}$$

where d_r is the diameter of the rotor.

Based on equations (4.22) and (4.23), the rotor mass and rotor inertia of the individual designs considered in this study have been derived and given in the Table below.

Table 4. 8 Total inertia moment of the individual designs

Parameters	Design #1: K_{gb}/R = 0.75 (R = 10.4 m)	Design #2: K_{gb}/R = 1.15 (R = 7.68 m)
m_r (kg)	1299	590.54
J (kg.m^2)	15611	3870.2

Equation (4.23) is valid for Mega-watt (MW) class wind turbines [56]. Therefore, in the simulation process, the values of the inertia moment obtained in Table 4.8 have been slightly modified to yield reasonable results for a preliminary comparison of the performance of both designs.

4.6.1 Dynamic response of the system due to a step variation in the load

In this case, the hybrid system is subjected to a step variation of 3.3 kW in the load. Three operating conditions have been assumed, representing the case where the genset supplies the load alone and the case where the genset shares the load with the individual

wind turbines (design #1 and design #2). A wind speed of 11 m/s during the short duration of the test has been assumed. The initial loads for the three operating conditions (15 kW, 48.5 kW and 55.4 kW) are selected so that a grid frequency of 60 Hz prior to the load variation is achieved. The genset rating and droop characteristic are similar to those used in the steady state analysis. Figure 4.13 represents the response of the system (grid frequency) to the step variation in the load at 0.15s.

From this figure, one can see the advantage of wind turbines that present droop characteristics. The peak transient ($f_{pk3} < f_{pk2} < f_{pk1}$), and steady state value ($\Delta_{f1} < \Delta_{f2} < \Delta_{f3}$) of the frequency decrease when the genset shares the load with WTs presenting droop characteristics. The benefit is the largest with WT presenting the larger droop factor. The results obtained by simulation are in good agreement with those estimated using equation (4.2).

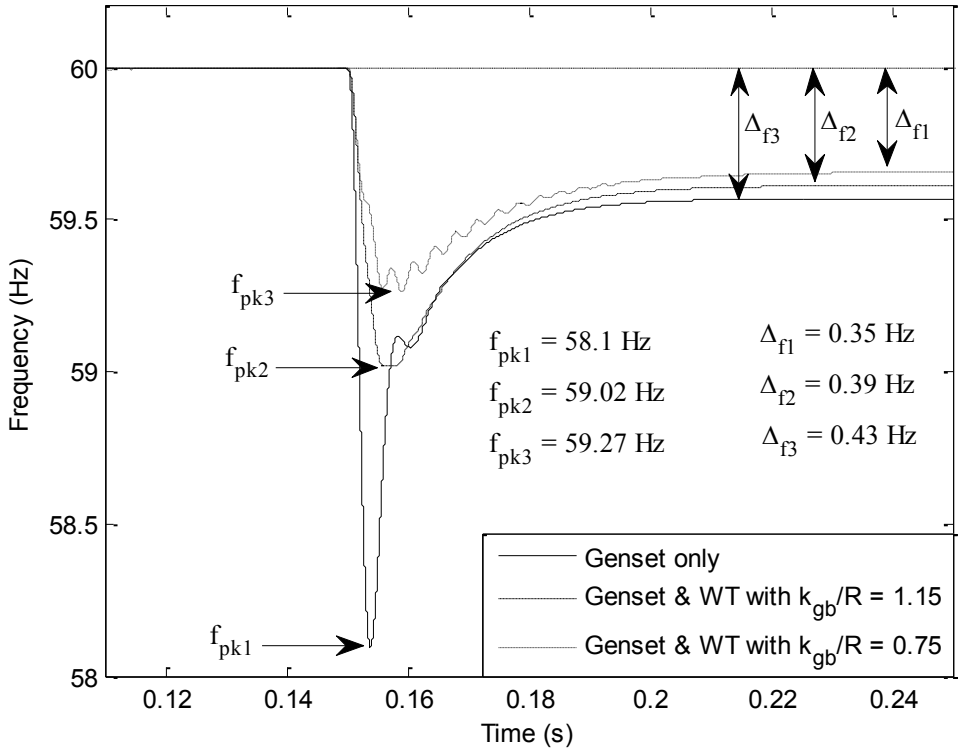

Figure 4. 13 Frequency response of the system subjected to load variation

Figure 4.14 represents some additional responses of the system subjected to the load variation.

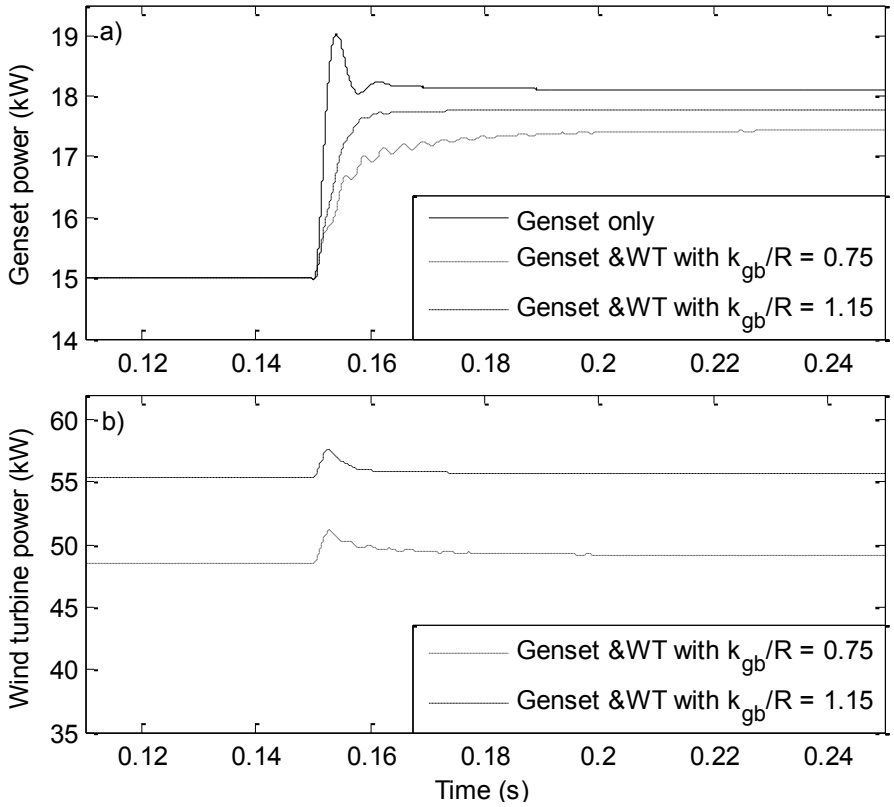

Figure 4. 14 System response to a step load increase. a) Active power of the genset; b) Active power of the WT

The rate of rise, peak and steady-state values of the power supplied by the gen-set decrease when a wind turbine is placed in parallel with the gen-set as shown in Figure 4.14.a. The reductions are bigger with the WT that presents a larger slope of the droop characteristic. The main drawback using WTs with larger droop slope can be highlighted in Figure 4.14.b: The amount of power provided by the WT, at a given wind speed and grid frequency decreases since the droop slope tends to be high.

4.6.2 Dynamic response of the system due to a step variation in the wind speed

Figures 4.15 and 4.16 represent the response of the system as the average wind speed varies from 11 m/s to 11.3 m/s at 0.15s. One can see from Figure 4.15-a, that the peak transient of the network frequency is lower when the wind turbine with the largest droop factor is used. However, little frequency difference can be observed for both designs. This is due to the fact that the inherent droop characteristic of the WT presents a relatively small droop factor compared to that of the diesel engine.

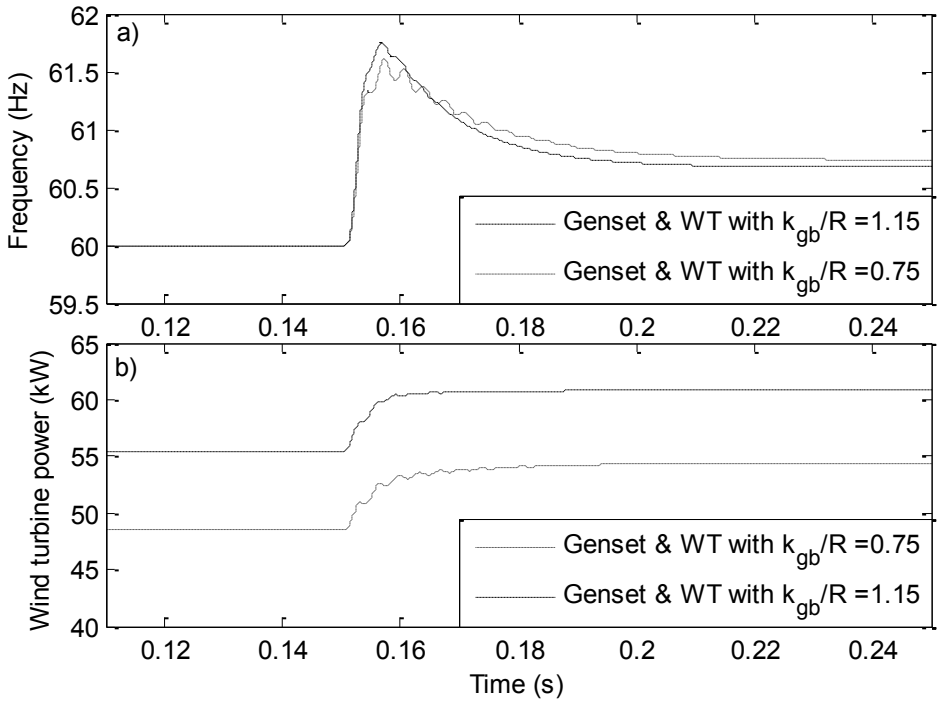

Figure 4. 15 a) Grid frequency; b) Active power of the wind turbine

Figures 4.16.a and 4.16.b represent the genset active power and torque respectively, due to the average wind speed variation. As it can be seen from the first graph of this figure, the genset power variation tends to be lower when the wind turbine that presents larger slope of the droop characteristic is used ($\Delta_{P1} < \Delta_{P2}$). However, these power variations

appear to be relatively small, due to the inherent characteristic of the turbine which presents a limited droop factor.

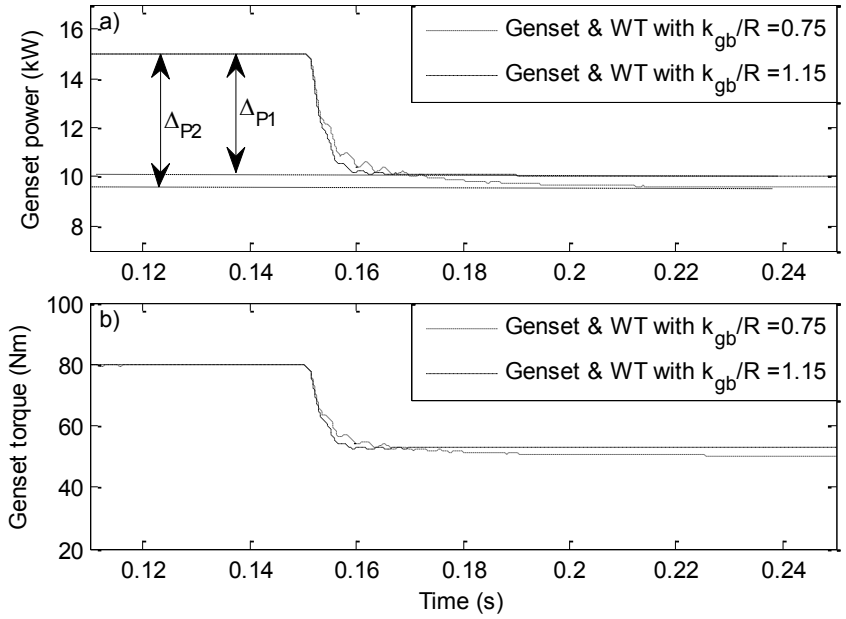

Figure 4. 16 System response: a) Genset Active power; b) Genset torque

4.6.3 Dynamic response of the system due to gust components in the wind speed

This Section examines the response of the system when the wind turbine is subjected to a wind speed variation that includes gust components. The wind profile used for this analysis is represented in Figure 4.17.a. This profile was obtained by adding an average wind speed of 11m/s to a white noise generator output with 5% turbulence and feeding a low pass filter used to minimise the frequency of the turbulence components. The parameters of the low pass filter are left beyond the scope of this thesis.

Figure 4.17.b represents the grid frequency response. The load is kept constant during this interval of time. It can be seen from this figure that the frequency of the system tends to vary less when the genset shares the load with the WT that presents a larger droop factor. Similar effect can be noticed from Figures 4.18.a and 4.18.b, where the genset and

WT power variations tend to be lower when the load is being shared with the WT that presents a larger slope.

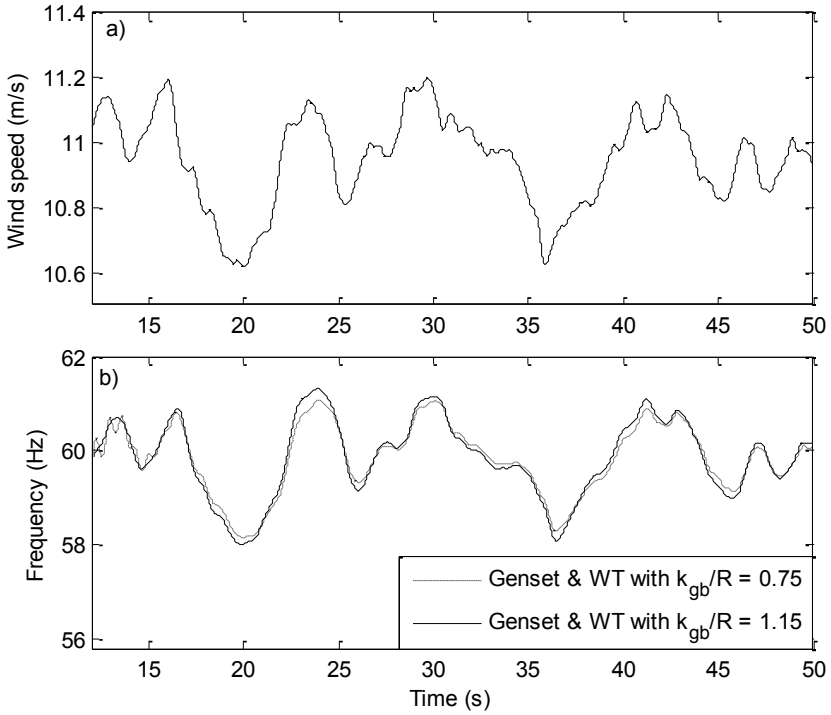

Figure 4. 17 System response to wind speed variation: a) Wind profile; b) Grid frequency

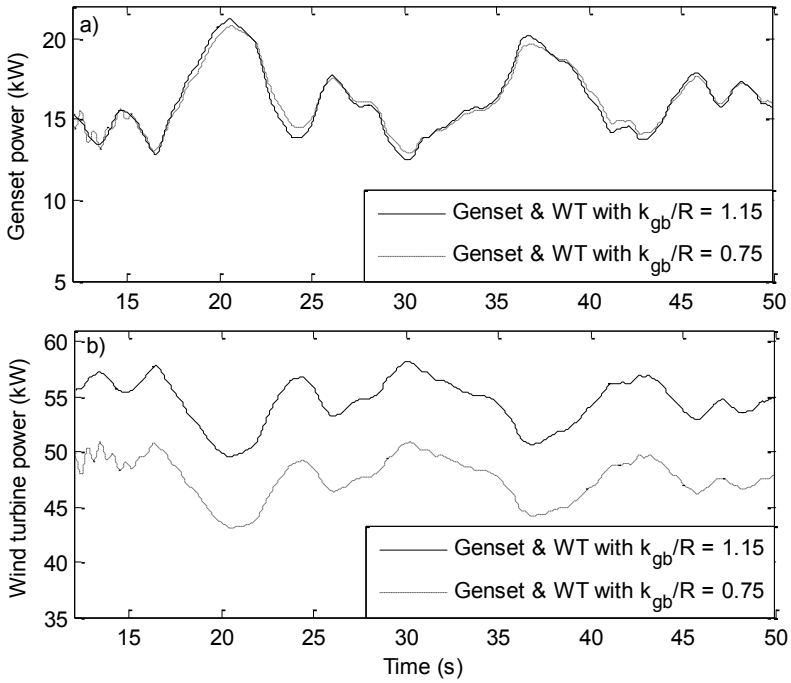

Figure 4. 18 System response to wind speed variation: a) Active power of the genset; b) Active power of the WT

Figure 4.19 represents the shaft loading of the diesel engine due to wind speed variations.

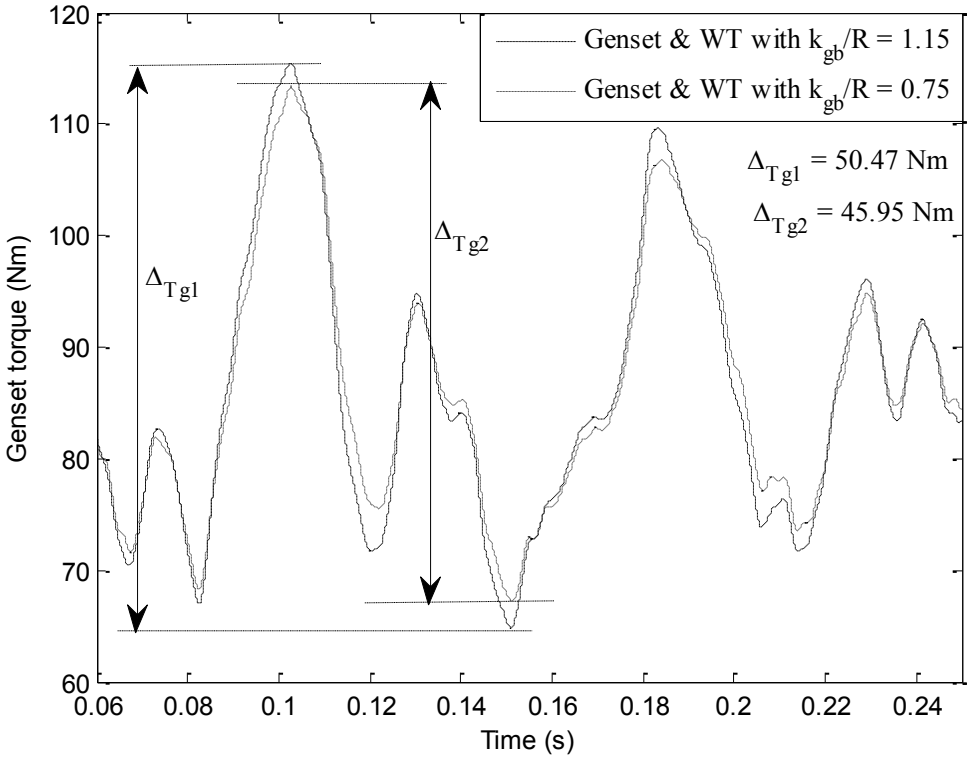

Figure 4. 19 Diesel engine torque response due to wind speed variation

It appears from this figure that genset torque variations tend to be lower ($\Delta_{Tg2} < \Delta_{Tg1}$) with the wind turbine that presents a larger slope of the power-frequency characteristic. This in turn will result in reduced mechanical stress transmitted into the diesel engine shaft as the wind speed varies. One important aspect to be mentioned based on these results is that, while WTs with droop characteristic are being used to assist the genset , their torque and power variations also tend to be improved.

4.5 Summary of chapter 4

This chapter has examined the impact of some parameters of the wind rotor on the power-frequency (droop) characteristics of fixed-pitch type 1 wind turbines. The main objective was to investigate the potential of this turbine type for assisting with primary frequency control in hybrid diesel mini-grids in a passive way for low cost remote

applications. Based on wind turbine generic C_P-λ curves, it has been shown that although the value of the pitch angle (β) has an impact on $C_{P\text{-}Max}$ and $\lambda_{CP\text{-}M}$ for a 3-blade rotor, it does not result in wind turbines with significantly different power-frequency characteristics. Conversely, the value of β has a negligible impact on the C_P-λ curves of 2-blade rotors. However, due to the fact that this curve presents a wider range of possible values for λ, the wind turbine can be designed to operate with either low or high values of λ, producing different power-frequency characteristics. A case study of storage-less diesel hybrid mini-grid operating with variable frequency, high penetration of wind energy and large load variations has been simulated, using an energy flow model and based on models that were experimentally verified. The results show that 2-blade wind turbines with large droop characteristics can be used to reduce the grid frequency and gen-set output power variations of the hybrid system by approximately 10% during steady state. A dynamic model of the hybrid system has been developed and used to analyze the performance of the proposed designs when the hybrid system is subjected to different transient operating conditions. The overall dynamic response of the system shows that implementing a droop characteristic in fixed-speed wind turbines could reduce the frequency variations due to load and wind speed disturbances, as well as the mechanical stress transmitted into the diesel engine shaft. However, the inherent droop characteristic of type 1 wind turbines presents a relatively low droop factor. Therefore, the impact of the droop characteristic implemented in these turbines is found to be relatively low.

CHAPTER 5

TYPE-2 WIND TURBINES IN DROOP-CONTROLLED DIESEL MINI-GRIDS

This chapter examines the performance of fixed-pitch type 2 wind turbines in hybrid wind diesel mini-grids. In the previous chapter, it has been shown that due to the limitation of the wind turbine droop characteristic resulting from its low droop factor, the type 1 wind turbine cannot assist to a high extent with the mini-grid frequency regulation. Thus, the type 2 WT is proposed to overcome this limitation. In this chapter, an approach to implement a type 2 WT that presents a high droop factor in the hybrid system is proposed.

Wind energy integration in diesel power plants is aimed to reduce the fuel consumption and consequently the operating costs of the system. An elementary storage-less hybrid wind-diesel mini-grid is represented in Figure 5.1. The diesel power plant can operate with one or several diesel engine generator sets in parallel, using droop control. In systems with high penetration of fluctuating wind power and large load demand variations (typically in small remote communities), active and reactive power balancing might be difficult to achieve. Therefore, the grid frequency can vary widely and the mechanical stress on the gen-sets and unit cycling can increase, leading to higher operating and maintenance costs of the system.

The output power of pitch controlled WTs associated with power electronics interfaces can be remotely controlled using a supervisory controller via a dedicated communication channel to overcome these problems, and also to assist with primary frequency control. However, this solution might not be economically viable for small mini-grids. In order to achieve an overall cost minimization of the power system (mini-grid), the use of sophisticated wind turbines and supervisory control systems is usually avoided.

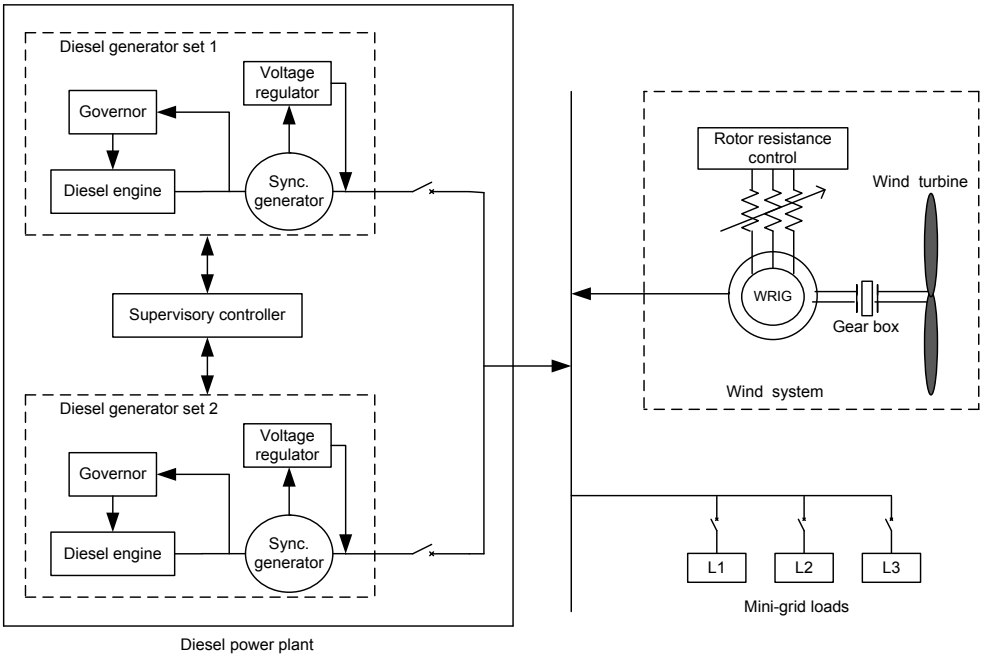

Figure 5. 1 Generic storage-less wind-diesel hybrid system

From the previous chapter, it has been shown that fixed-pitch type 1 wind turbines can assist with frequency regulation while providing reduced genset torque variations. However, this turbine type presents an inherent droop characteristic with relatively small droop factor. On the other hand, as requested by some standards (such as the new European grid codes) renewable energy sources should be able to decrease their output power proportionally to the grid frequency, as this exceeds certain values. Obviously, this requirement cannot be achieved using fixed pitch type 1 WTs. In this case, the use of simple fixed-pitch type 2 WTs, which are equipped with wound rotor induction generators (WRIG) and variable external rotor resistances for adjusting the injected power, might be cost effective. A typical configuration of type 2 WTs is integrated in Figure 5.1. These turbines can provide several advantages, including a relatively low cost, a better power quality compared to type 1 WTs and a possibility to achieve a variable speed operation up to 10 %. The concept of type 2 WTs assumed in this analysis

consists of three external rotor resistances, a diode-bridge rectifier, and an IGBT power switch. The IGBT controls the rotor currents by short circuiting the external rotor resistances.

For wind systems to be able to react to locally measured parameters such as the mini-grid frequency while adjusting their output power accordingly to help the diesel power plant balancing active power in the system without dedicated means of communication, WTs should present a suitable power-frequency droop characteristic with a slope (Δ_P/Δ_f) comparable to that of the gen-set(s).

This chapter discusses the benefits of incorporating a suitable power-frequency droop characteristic in a fixed-pitch type 2 WT operating in hybrid wind-diesel mini-grids with high wind penetration. By allowing the wind turbine to participate in the mini-grid active power balancing, one should be able to reduce substantially the torque variations (mechanical stresses) on the diesel engine shafts, the grid frequency variations and also the unit cycling.

5.1 Hybrid system model including external rotor resistance

A dynamic model of the hybrid system has been described in detail in the previous chapter. However, this model was based on a squirrel cage induction generator. In this chapter, the wind system is based on a wound rotor induction generator, equipped with external rotor resistance and rotor control circuit. Therefore the model of the wind system developed in the previous chapter (mainly the induction generator model) needs to be modified to meet the requirements of the type 2 wind turbine.

5.1.1 Modified induction generator model

Figure 5.2 represents the phase equivalent circuit of the wound rotor induction machine, where V_{ph} is the phase voltage of the stator, R_s and X_s are the stator resistance and reactance, X_m is the magnetizing reactance, R_r and X_r are the rotor resistance and reactance referred to the stator side, R_x is the variable external resistance connected to the rotor circuit by means of slip rings and s is the slip of the machine.

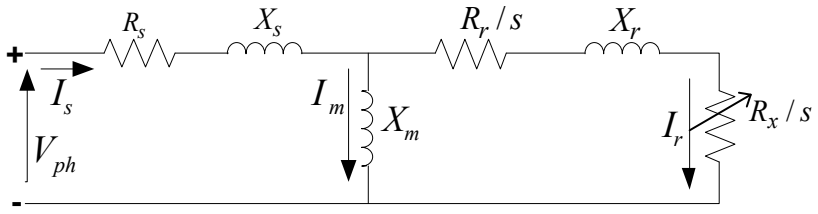

Figure 5. 2 Phase equivalent circuit of the wound rotor induction generator

Based on this figure, the torque-speed characteristic of the wound rotor induction generator can be derived as follows:

$$T_{em} = \frac{3V_{th}^2 \dfrac{R_{rt}}{\omega_{syn} - \omega_{shaft}}}{\left[\left(R_{th} + \dfrac{R_{rt}\,\omega_{syn}}{\omega_{syn} - \omega_{shaft}}\right)^2 + \left(X_{th} + X_r\right)^2\right]} \tag{5.1}$$

Where $R_{rt} = R_r + R_x$, R_{rt} representing the total rotor resistance of the generator.

5.1.2 Rotor resistance control

Several configurations can be used to control the rotor resistance of a WRIG. The configuration type assumed in this analysis is represented in Figure 5.3. The control system is connected to the rotor circuit through slip rings. The equivalent resistance (R_x) is varied by controlling the duty cycle (D) of the IGBT. The operating frequency of the

IGBT can be up to several kHz. The duty cycle is controlled based on the following relation,

$$R_x = (1 - D)R_{\max} \tag{5.2}$$

where R_{max} is the resistance of the external resistors.

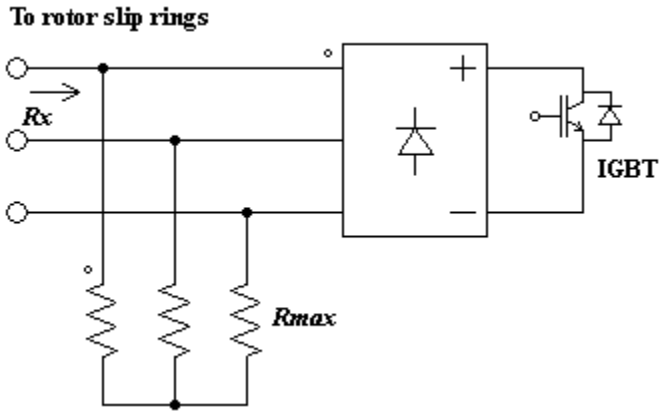

Figure 5. 3 Rotor resistance control circuit

5.2 Droop characteristic of the fixed-pitch type 2 wind turbine

The power generated by the WT during steady-state can be calculated using the approach derived in chapter 3, based on the assumption that in steady-state, the torque developed by the wind rotor is equal to the electromagnetic torque of the induction generator. In this Section, the effect of the rotor resistance, grid frequency and wind speed variations on the active power injected into the mini-grid by the WT is discussed. It is assumed that the voltage at the WT terminals is kept constant at rated value. The wind system used for this analysis is a 100 HP 2-blade fixed-pitch type 2 WT with the parameters given in the appendix. The variation of the power injected by the WT with the grid frequency at different rotor resistances and wind speeds is given in Tables 5.1 and 5.2, and represented in Figure 5.4.

Table 5. 1 Power-frequency variation of the type 2 WT with Rrt = Rr

f(Hz)	u = 8 m/s	u = 9 m/s	u = 10 m/s	u = 11 m/s	u = 12 m/s
	P_{inj}(kW)	P_{inj}(kW)	P_{inj}(kW)	P_{inj}(kW)	P_{inj}(kW)
58	5.45	14.33	28.81	49.71	77.83
59	4.92	13.44	27.38	47.67	75.142
60	4.47	12.59	25.86	45.68	72.49
61	4.05	11.71	24.55	43.74	69.89
62	3.62	10.95	23.28	41.86	67.35
s_{LP} (kW/Hz)	0.45	0.84	1.38	1.96	2.62

Table 5. 2 Power-frequency variation of the type 2 WT with Rr ≤ Rrt ≤ 15 Rr

f(Hz)	u = 8 m/s			u = 9 m/s			u = 10 m/s			u = 11 m/s			u = 12 m/s		
	$5R_r$	$10R_r$	$15R_r$	$5R_r$	$10R_r$	$15R_r$	$5R_r$	$10R_r$	$15R_r$	$5R_r$	$10R_r$	$15R_r$	$5R_r$	$10R_r$	$15R_r$
58	5.26	5.03	4.84	26.66	24.49	22.76	26.66	24.49	22.76	44.84	40.17	36.59	67.74	59.24	52.90
59	4.78	4.59	4.41	25.38	23.36	21.75	25.38	23.36	21.75	43.04	38.61	35.12	65.62	57.28	51.23
60	4.33	4.15	4.00	24.14	22.26	20.70	24.14	22.26	20.70	41.28	37.09	33.80	63.35	55.35	49.58
61	3.91	3.76	3.62	22.87	21.20	19.75	22.87	21.20	19.75	39.58	35.60	32.50	61.11	53.61	48.09
62	3.51	3.39	3.25	21.72	20.11	18.78	21.72	20.11	18.78	37.92	34.16	31.24	59.10	51.75	46.5
s_{LP} (kW/Hz)	0.43	0.41	0.39	1.23	1.09	0.99	1.23	1.09	0.99	1.73	1.50	1.33	2.16	1.87	1.60

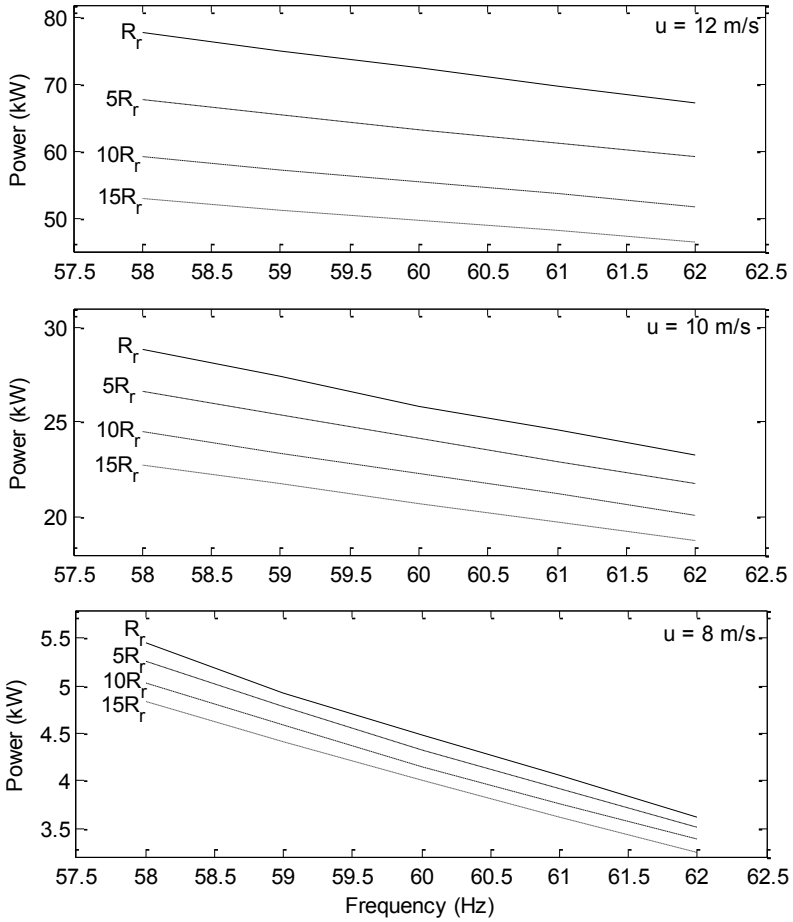

Figure 5. 4 Power-frequency variation at different rotor resistances and wind speeds

It results from Table 5.1 that, at minimum rotor resistance (R_r), the WT injects rated power at rated wind speed and rated grid frequency. The injected power decreases as the

wind speed decreases and also slightly as the grid frequency increases. The relationship between power and frequency can be described using the following equation.

$$P_{WT} = P_{u-f\max} + s_{p-u}\left(f_{\max} - f\right) \tag{5.3}$$

where $f_{\min} < f < f_{\max}$. $P_{u\text{-}f\max}$ is the power injected at a given wind speed for maximum grid frequency and $s_{P\text{-}u}$ is the slope of the curve, which varies with the wind speed. Table 5.2 shows the impact of increasing the value of the rotor resistance to 5, 10 and 15 times the base value on the WT power at different wind speeds and grid frequencies. As expected, the injected power decreases with the rotor resistance and grid frequency while the slope does not change much for a given wind speed.

5.2.1 Droop factor adjustment using external resistance control

In this Section, the approach to adjust the droop characteristics of a fixed-pitch type 2 WT using external rotor resistance control is discussed. Figure 5.5 shows in blue, with thicker trace, how the values of $P_{u\text{-}f\max}$ and $s_{P\text{-}u}$ can be changed by continuously varying the rotor resistance with the grid frequency for fixed wind speeds.

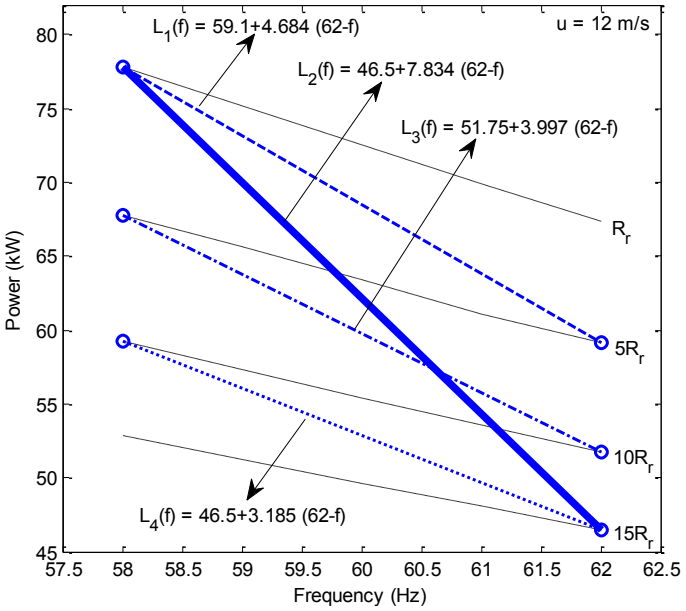

Figure 5. 5 Variation of the WT droop characteristics at 12m/s

In this case, the wind speed is 12 m/s. A case study that takes into account variable wind speeds is presented in the appendix. The value of $P_{u\text{-}f\max}$ can be decreased as much as the rotor resistance used at f_{max} can be increased. Conversely, the value of $s_{P\text{-}u}$ is limited by the selected value of $P_{u\text{-}f\max}$ and the difference between the corresponding rotor resistance and the rated rotor resistance. In order words, larger values of $P_{u\text{-}f\max}$ will limit the maximum value of $s_{P\text{-}u}$ one can achieve in order to take into account the entire frequency range ($58\ Hz \leq f \leq 62\ Hz$).

The derivation of R_x required at a given grid frequency to implement a droop curve given $P_{u\text{-}f\max}$ and $s_{P\text{-}u}$ is not a simple task, mostly because the maximum value of $P_{u\text{-}f\max}$, which occurs for minimum rotor resistance depends on the wind speed, which can vary very fast. A simple approach to achieve maximum droop slope as shown in Figure 5.5 is to use maximum rotor resistance at f_{max} (62 Hz) and minimum rotor resistance at f_{min} (58 Hz). In this case, a linear relation between the injected power and the grid frequency at 12 m/s is obtained and the values of the grid frequency at which the desired droop curves intersect the droop curves at $5R_r$ and $10R_r$, can be calculated. Thus, the relationship between f and R_{rt} can be obtained by curve fitting. Equation (5.4) represents the relation obtained for the case represented in Figure 5.5.

$$R_{rt} = 0.5956 f^2 - 68.004 f + 1941.7 \qquad (5.4)$$

Using this approach for all wind speeds, the parameters of the power-frequency droop curve vary with the wind speed as given in Table 5.3.

Table 5. 3 Droop parameters obtained at different wind speeds using the proposed approach

u (m/s)	8	9	10	11	12
$P_{u\text{-}f\max}$ (kW)	2.59	12.81	25.4	40.25	56.8
s_{LP} (kW/Hz)	0.5625	1.24	2.125	3.225	4.5

The impact of the proposed approach on the WT shaft speed, point of intersection of the wind rotor and generator torque-speed curves, at different wind speeds and grid frequencies is illustrated in Figure 5.6. From this figure, it appears that the slip of the generator increases with the grid frequency and rotor resistance. In this particular case, the maximum slip achieved is 12% at f = 62 Hz and u = 12 m/s, slightly larger than the typical value of 10% usually found in the OPTSLIP systems [57].

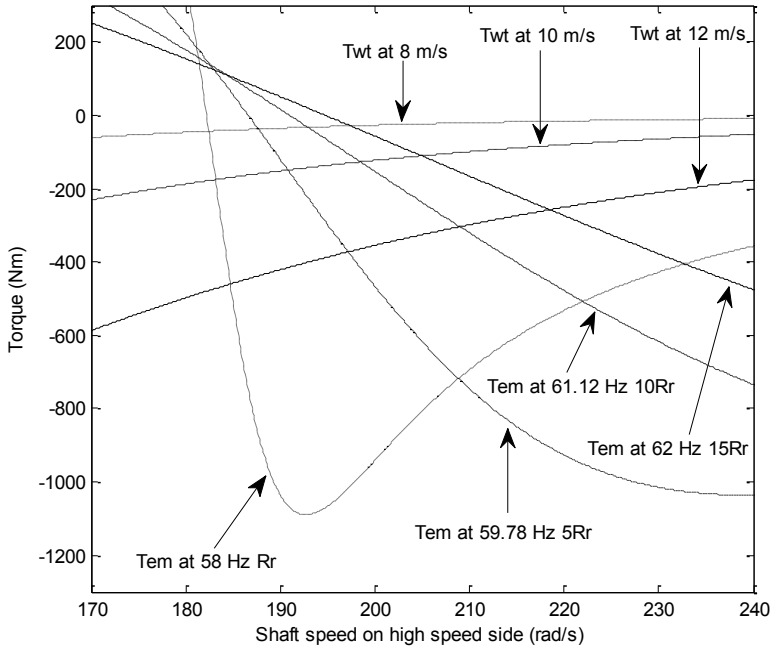

Figure 5. 6 Torque-speed curves of the type 2 WT with the proposed approach for varying the rotor resistance

5.2.2 Mechanical power and losses dissipated in the rotor resistance

The impact of the proposed droop control strategy on the mechanical power drawn from the wind rotor and the power dissipated across the rotor resistance, as the wind speed and grid frequency vary is investigated in this Section. If the goal is to reduce the amount of power injected into the grid by the WT when the frequency is high, it would be desirable to achieve this not only by dissipating power in the external rotor resistance, but also to

reduce the amount of mechanical power drawn from the prime mover. Tables 5.4 and 5.5 show the mechanical power drawn from the WT and the power dissipated in the rotor resistance at the points of intersection represented in Figure 5.5. It appears from these tables that the power injected by the WT mostly decreases in the wind rotor.

Table 5. 4 Mechanical power variation with fixed and variable rotor resistance

P_{mec}(kW)	u = 8 m/s	u = 10 m/s	u = 12 m/s
62Hz/15R_r	5.527	22.213	55.48
61.12Hz/10R_r	5.9728	24.3121	61.8505
59.78Hz/5R_r	6.6818	27.3994	71.3948
58Hz/R_r	7.6799	31.4843	83.6155
62Hz/R_r	5.8292	25.8172	72.2636
61.12Hz/R_r	6.2011	27.0073	74.7342
59.78Hz/R_r	6.7997	28.8318	78.4512
58Hz/R_r	7.6799	31.4843	83.6155

Table 5. 5 Rotor power loss variation with fixed and variable rotor resistance

P_{rot}(kW)	u = 8 m/s	u = 10 m/s	u = 12 m/s
62Hz/15R_r	0.0742	1.0905	5.9521
61.12Hz/10R_r	0.0593	0.8903	5.2293
59.78Hz/5R_r	0.0346	0.5886	3.6920
58Hz/R_r	0.0065	0.1470	1.1363
62Hz/R_r	0.0079	0.1100	0.8665
61.12Hz/R_r	0.0058	0.1036	0.8659
59.78Hz/R_r	0.0067	0.1408	0.9927
58Hz/R_r	0.0065	0.1470	1.1363

5.3 Performance of type 2 wind turbines in the hybrid system

The behavior of the hybrid wind-diesel mini-grid consisting of the diesel genset used in the previous chapter and the 100 HP fixed pitch type 2 WT discussed in the previous Sections is verified by means of simulation in this Section. The control scheme used to generate the switching states of the IGBT switch shown in Figure 5.3 has been implemented as represented in the figure below, based on equation (5.5).

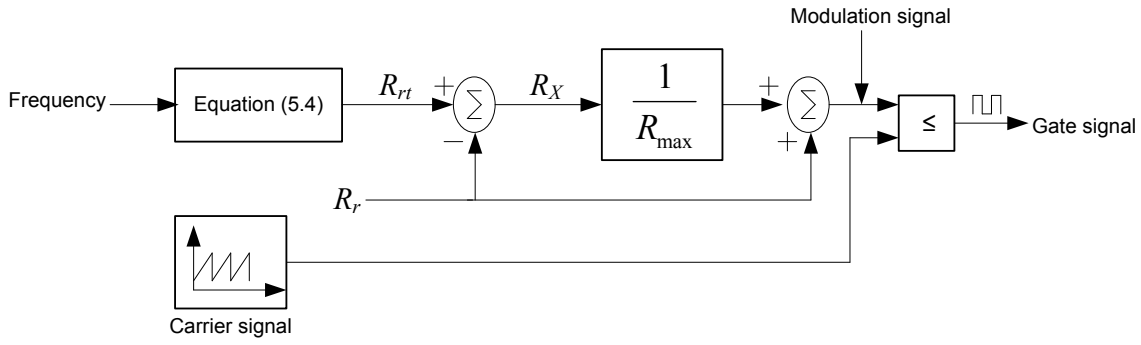

Figure 5. 7 Control scheme for the IGBT switching states

$$\begin{cases} R_{rt} = R_x + R_r \\ 0 \le R_x \le R_{\max} \\ R_{\max} = 14R_r \end{cases} \quad (5.5)$$

where R_r is the nominal rotor resistance of the induction generator, R_x the external rotor resistance and R_{rt} the total rotor resistance of the generator.

5.3.1 Steady state performance

The aim of this Section is to verify how the droop factor magnitude of the power-frequency characteristic of type 2 wind turbines affects the variation of the grid frequency and gen-set power during steady state. The energy flow model shown in Figure 4.6 is used to aid the analysis. This requires having the power-frequency variations of the type 2 WT at different wind speeds. Table 5.6 provides these variations, obtained using equation (5.3) and Table 5.3.

Table 5. 6 Power-frequency variations of the type 2 WT at different wind speeds

f (Hz)	P_{wt}(kW)				
	8 m/s	9 m/s	10 m/s	11 m/s	12 m/s
58	5.50	14.28	28.84	49.68	77.82
59	4.95	13.06	26.33	45.06	69.99
60	4.40	11.84	23.82	40.44	62.16
61	3.85	10.62	21.31	35.82	54.33
62	3.30	9.40	18.80	31.20	46.50

The diesel engine droop characteristic used for this study is similar to the one used in the previous chapter (30 kVA, 7.5 kW/Hz). The load profile is selected to achieve maximum wind power injection into the grid at rated wind speed. The behavior of the hybrid system using the power variations given in Tables 5.1 and 5.6 is analysed to highlight the advantage of the type 2 system during steady state. These variations were obtained using wind turbines with fixed and variable rotor resistance, presenting each a rated power of 100 Hp.

Similarly to the case with the type 1 system, the wind speed varies in steps while the load profile varies between minimum and maximum values, estimated such as to avoid exceeding the wind turbine output power constraints while operating in parallel with the genset. These variations are represented in Figures 5.8 and 5.9 respectively.

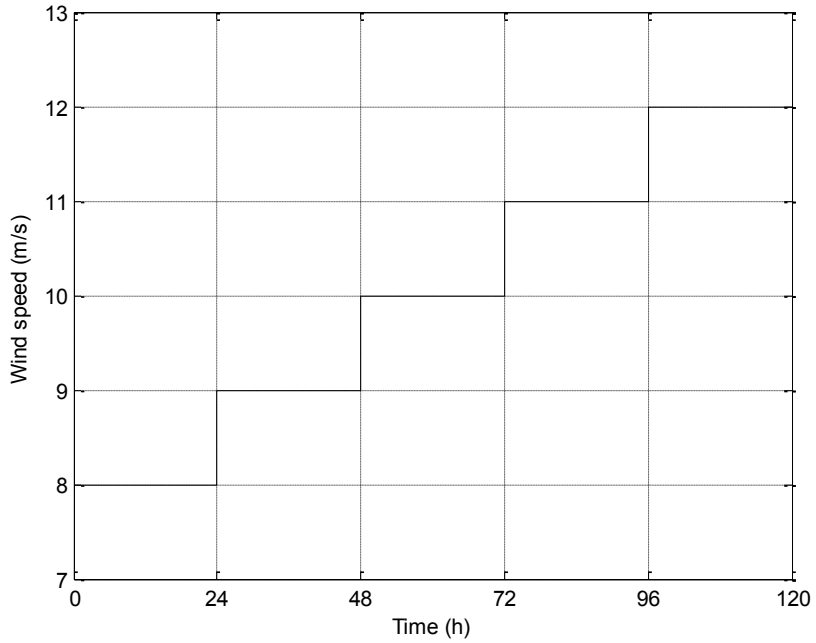

Figure 5. 8 Wind profile

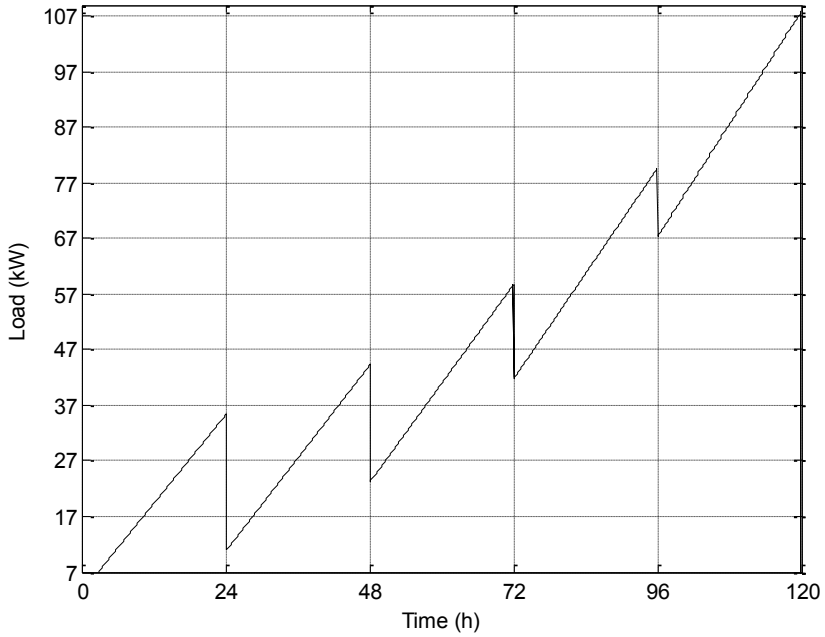

Figure 5. 9 Load profile

The variations of the gen-set output power and grid frequency are represented in Figures 5.10 and 5.11 respectively.

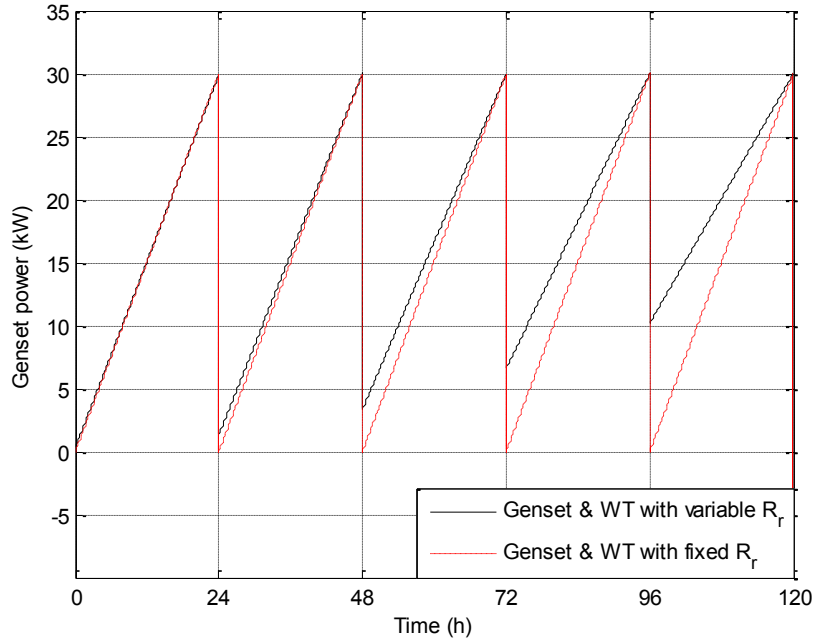

Figure 5. 10 Genset output power for both cases

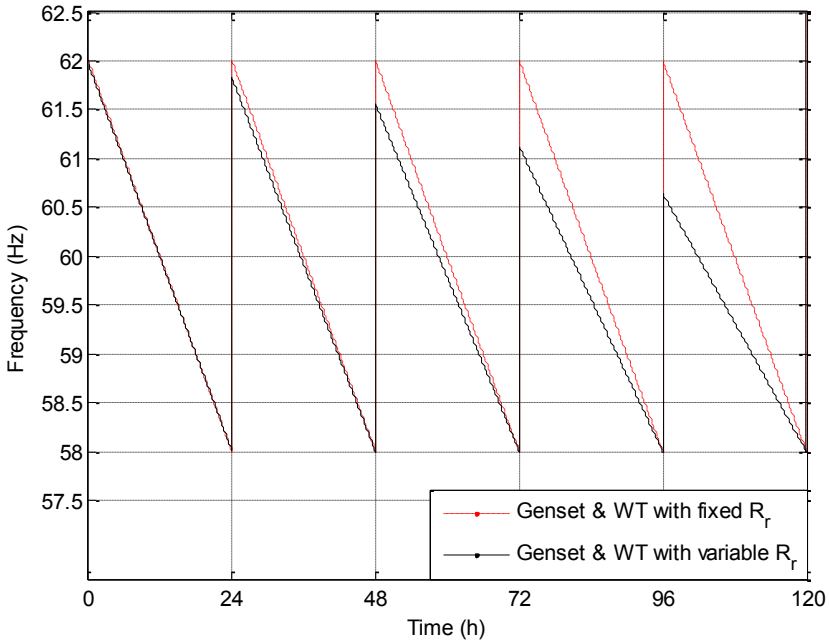

Figure 5. 11 Grid frequency for both cases

It appears from these results that the larger slope of the power-frequency characteristics, corresponding to the WT with variable R_r reduces better the frequency and gen-set output power variations as the load demand varies, compared to the case with lower slope (WT with fixed R_r). The benefits are the largest at high wind speeds. The gen-set output power and frequency variations obtained from the simulation are in good agreement with those obtained using equations (4.1) to (4.3). The numerical values of the simulated results are summarized in the following Table.

Table 5. 7 Summary of the steady state results using type 2 WT

Wind seed	P_{load}		WT with fixed R_r		WT with variable R_r	
u (m/s)	Min (kW)	Max (kW)	ΔP_{gen}(kW)	Δf (Hz)	ΔP_{gen}(kW)	Δf (Hz)
8	3.62	35.45	30	4	29.65	3.96
9	10.95	44.33	30	4	28.70	3.82
10	23.28	58.81	30	4	26.59	3.55
11	41.86	79.71	30	4	23.42	3.12
12	67.35	107.8	30	4	19.81	2.64
Ave.	----	----	30	4	25.63	3.41

5.3.2 Dynamic performance

This Section analyses the dynamic performance of the hybrid system when the diesel genset operates with the type 2 WT using the suggested control approach for the external rotor resistance. Three tests have been performed to observe the performance of the type 2 WT in the hybrid system: Step increase in the load, step increase in the wind speed and system behaviour due to random wind speed variations.

5.3.2.1 System response due to a step variation in the load

This test is used to obtain the response of the system to a 3.3 kW step variation in the load. Three different cases have been assumed: the genset supplying the load alone, the genset supplying the load along with the WT with fixed rotor resistance (R_r kept constant at base value), and the genset operating in parallel with the WT controlled using the

proposed technique (type 2 turbine). A wind speed of 11 m/s during the short duration of the test has been selected. The initial loads for the three cases (15 kW, 68kW and 61.9 kW) have been selected to achieve a grid frequency of 60 Hz prior to the load variation. The increments in the initial loads are due to the power injected by the WT at 11 m/s and 60 Hz. Figure 5.12 represents the variation of the grid frequency for the three cases as the load increases by 3.3 kW at 0.1s. It appears from this figure that the system performance, improves with the use of a WT in parallel with the gen-set. The improvements are bigger with the WT equipped with controlled rotor resistances (increased droop characteristics). The frequency nadir is decreased from 58.09 Hz to 59.35, then to 59.63 Hz while the variation in the grid frequency is decreased from 0.44 Hz to 0.34 Hz and to 0.24 Hz, respectively.

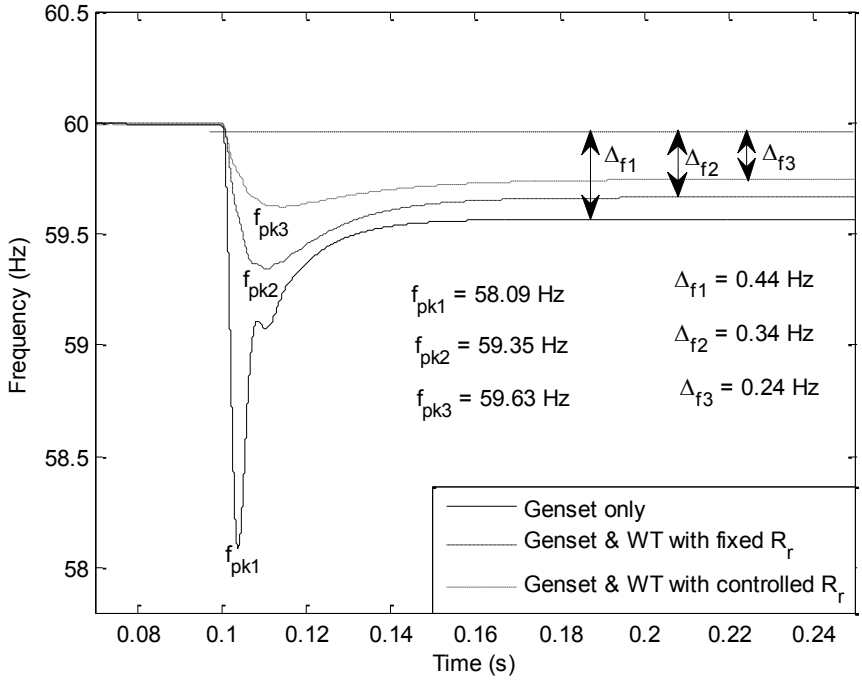

Figure 5. 12 Frequency response of the system subjected to load variation

The measured values are very close to the theoretical values obtained using equation (4.2). These quantities are compared in Table 5.8.

Table 5. 8 Frequency variations of the system subjected to load variation

Frequency variation (Hz)	Estimated values	Simulated values
Δ_{f1}	0.44	0.44
Δ_{f2}	0.35	0.34
Δ_{f3}	0.27	0.24

Figure 5.13 represents other relevant quantities to the study. The rate of rise, peak and steady-state values of the power supplied by the gen-set decrease as shown in Figure 5.13.a, when a WT is used in parallel with the gen-set. The reductions are bigger with the WT controlled with variable rotor resistance. The main drawback of using a WT with a larger droop slope employing the proposed simple strategy for varying the rotor resistance can be seen from Figure 5.13.b: The amount of power provided by the WT, at a given wind speed and grid frequency, decreases since the droop slope is increased using large rotor resistance. It should be noted that the implementation of droop characteristics in WTs usually implies in active power curtailment and consequently an increase in the amount of power demanded from other sources in the system.

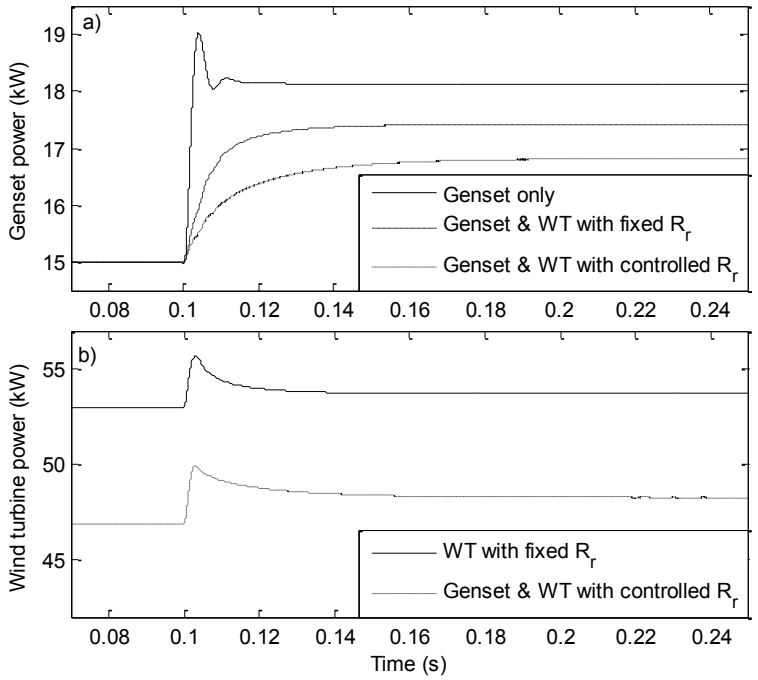

Figure 5. 13 System response to a step load increase. a) Active power of the gen-set; b) Active power of the WT

5.3.2.2 Dynamic response of the system due to a step increase in the wind speed

This Section examines the response of the system to a step increase in the wind speed. The initial conditions for the assumed WTs are the same as in the previous Section.

Figure 5.14 shows the response of the system as the wind speed varies from 11 m/s to 11.4 m/s at 0.1 s. It appears from this figure that the rate of change of frequency (ROCOF), the peak value and also the steady-state value of the frequency are lower using the proposed control strategy that increases the droop slope of the WT. On the other hand, the power demanded from the gen-set increases. In this particular case, this would be appropriate since otherwise, the gen-set would be operating at a low load condition.

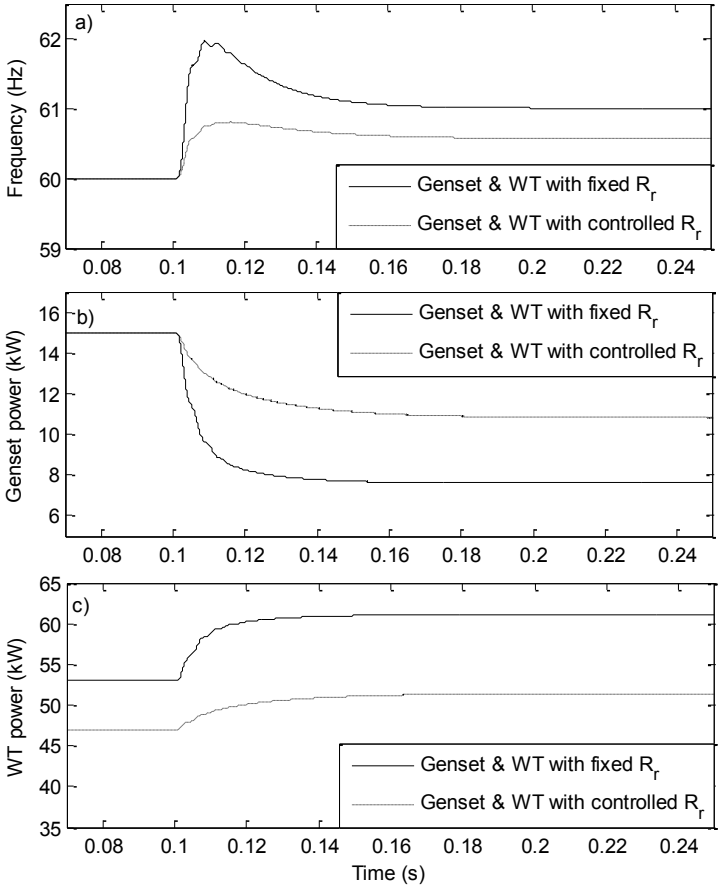

Figure 5. 14 System response to a step increase in wind speed; a) Grid frequency; b) Active power of the gen-set; c) Active power of the WT

5.3.2.3 Dynamic response of the system due to wind speed variations

The response of the system equipped with the controlled type 2 WT, when the wind turbine is subjected to a wind speed variation that includes gust components is examined in this Section. In general, the maximum power developed by WTs tends to vary with the cube of the wind speed. Therefore wind speed variations can affect significantly the variation of the grid frequency and power demanded from the diesel power plant.

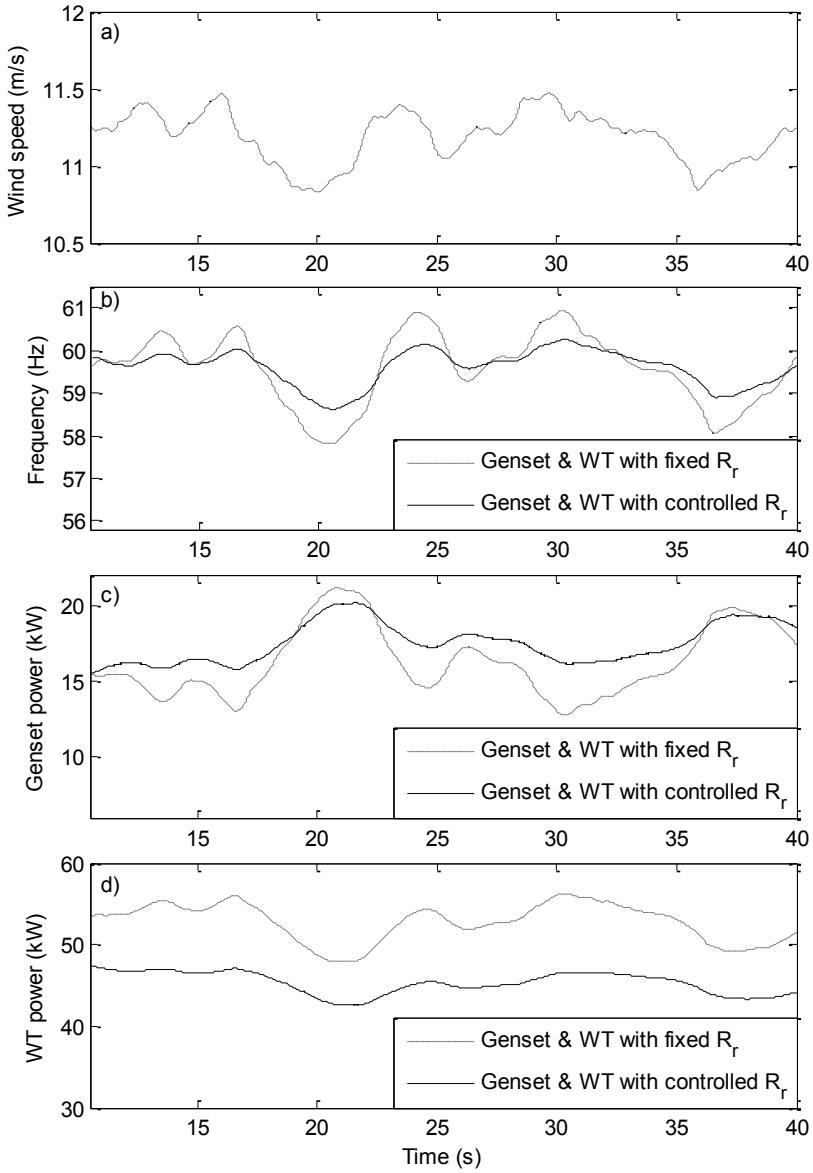

Figure 5. 15 System response to wind speed variation; a) Wind speed profile; b) Grid frequency; c) Active power of the gen-set; d) Active power of the WT

Figure 5.15 shows how these quantities vary with the wind profile shown in Fig. 5.15.a, when the type 2 WT operates with $R_{rt} = R_r$ and with the proposed technique, respectively. It is assumed that the load is kept constant during this short interval. It appears from this figure that when the WT operates with a larger droop slope, the variations in the frequency and power supplied by the gen-set as well as WT, reduce. This is achieved at the expense of reduced average power provided by the WT and, consequently an increase in the amount of power demanded from the diesel genset.

Figure 5.16 represents the shaft loading of the diesel engine when the wind speed varies as represented in Figure 5.15.a. It appears from this figure that the genset torque variations can be substantially reduced ($\Delta_{Tg1} \approx 2\ \Delta_{Tg2}$) when the diesel engine shares the load with the controlled wind turbine. This result shows that the proposed type 2 turbine improves torque variations on the diesel engine shaft, which in turn will result in reduced mechanical stress transmitted into the diesel engine shaft as the wind speed varies.

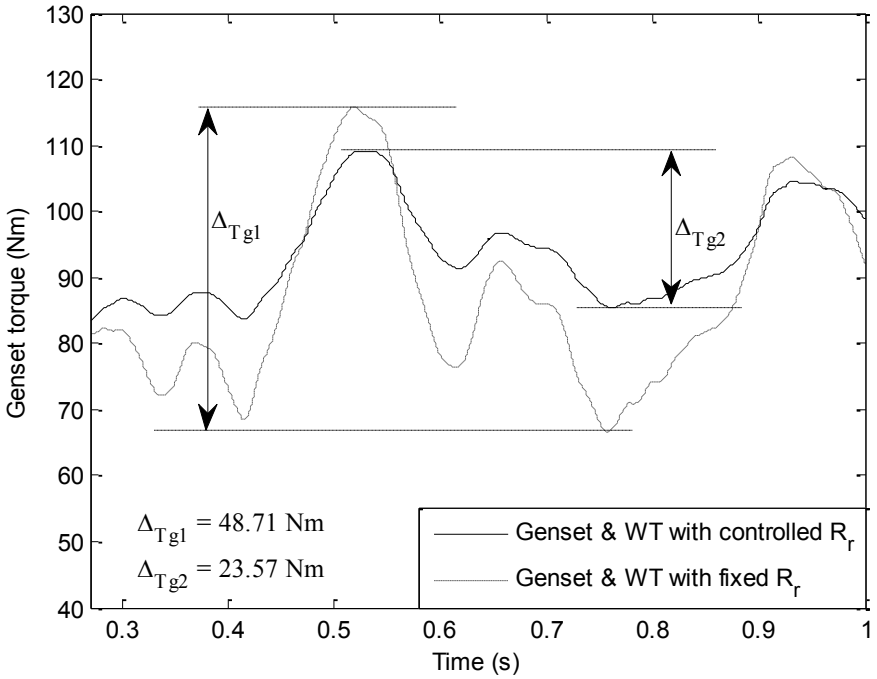

Figure 5. 16 Diesel engine torque response due to the wind speed gust components

5.4 Summary of chapter 5

This chapter discusses an approach for introducing a power-frequency droop characteristic in a fixed-pitch type 2 wind turbine. The basic idea is to increase the rotor resistance as the grid frequency increases, thus reducing the power injected into the mini-grid. A simple method for selecting the value of the rotor resistance, based on the grid frequency only has been proposed. In this case, the slope of the droop curve is not constant, but decreases with the wind speed. This should not present any inconvenient effect on the system, since the power injected by the wind turbine tends to vary less at lower average wind speeds. It should be noted that the reduction in the injected power is not achieved only by dissipating power in the rotor circuit. A considerable part of the reduced injected power is achieved at the wind rotor level, by making it operate at higher speeds and consequently lower values of power coefficients. The steady state results show that the controlled type 2 WT can be used to reduce the grid frequency variations of the hybrid system by approximately 15 %, greater than the one achieved using type 1 WTs. The dynamic simulation results have shown that using this strategy in storage-less wind-diesel hybrid mini-grid, frequency variations due to wind speed and load variations are reduced to a good extend. The variation of the power demanded from the diesel power plant also decreases, which should have a positive impact in reducing unit cycling.

CHAPTER 6

CONCLUSION AND FUTURE PROSPECTS

This chapter addresses the conclusion of the research work presented in this thesis. Based on the observations made through the individual phases of the research, the overall conclusion of the research work is presented, leading to the definition of the future prospects.

6.1 Conclusion

The limitations of diesel power plants are the main reasons why wind energy is being integrated in these systems. However, the intermittent nature of the wind and the highly variable load profile in remote communities lead to small diesel fuel displacement and high frequency variations in the system, especially when the wind turbine operates with high wind penetration. This research work proposes a concept for implementing simple wind energy technologies in droop controlled hybrid diesel mini-grids for remote communities. An assessment of the appropriate generators for small scale power generation is first presented, whereby three phase induction generators appeared to be the appropriate generator type for the application considered in this research, based on some related features such as simple and rugged construction, low maintenance and relatively low cost compared to other generator types.

The research work presented in this thesis is based on fixed-pitch type 1 and type 2 wind turbines, since these technologies present low capital and maintenance costs, which are interesting features for small hybrid diesel mini-grids compared to other wind energy technologies. However, the lack of means for controlling the amount of power injected into the mini-grid by these turbines might create some concerns regarding frequency stability.

Droop control is a well know technique for parallel operation of generators, whereby the relationship between power and frequency of the individual generators is required in order to be able to minimize the network frequency disturbance. While this characteristic is usually available for diesel genset (provided by the manufacturer), it is not as obvious to be obtained for uncontrollable power sources such as type 1 and type 2 wind turbines.

In this research work, an approach for obtaining the power-frequency characteristic of type 1 and type 2 wind turbines has been proposed and validated experimentally. It has been shown that wind turbines do present a drooped power-frequency characteristic which can assist with frequency regulation in a passive way. The impact of some parameters of the wind rotor on the power-frequency (droop) characteristics of the turbines has been examined using the wind turbine generic C_P-λ curves. It has been shown that although the value of the pitch angle (β) has an impact on $C_{P\text{-}Max}$ and $\lambda_{CP\text{-}M}$ for 3-blade rotors, it does not result in wind turbines with significantly different power-frequency characteristics. Conversely, the value of β has been found to be having a negligible impact on the C_P-λ curves of 2-blade rotors. However, due to the fact that the 2-blade C_P-λ curve presents a wider range of possible values for λ, the wind turbine could be designed to operate with either low or high values of λ, producing different power-frequency characteristics.

A case study of storage-less hybrid diesel mini-grid operating with variable frequency, high wind penetration and large load variations has been simulated, using an energy flow model and based on models that were experimentally verified. It has been noticed that 2-blade wind turbines with large droop characteristics can be used to reduce the grid

frequency and gen-set output power variations of the hybrid system by approximately 10% during steady state.

A dynamic model of the hybrid system has been developed and used to examine the performance of the proposed designs, when the system is subjected to different transient operating conditions. The overall dynamic response of the system has leaded to the observation that, implementing a droop control in fixed-speed wind turbines could reduce the frequency variations due to load disturbances, as well as the diesel engine torque variations due to wind speed and load variations. However, since the inherent droop characteristic of type 1 wind turbines presents a relatively low droop factor, the impact of the droop control implemented in these turbines was found to be relatively low. Therefore, the implementation of type 2 wind turbines in the hybrid diesel mini-grid has been proposed to overcome the limitations of the type 1 wind turbines.

The performance of a droop controlled type 2 wind turbine for assisting with primary frequency control in the hybrid diesel mini-grid, in a passive way for low cost remote applications has been examined. A simple and effective control approach to increase the droop factor of the type 2 wind turbine, thereby overcoming the limitations of the type 1 WT has been proposed.

As expected, the results of the suggested approach using type 2 WT have shown that the power-frequency droop characteristic introduced in the fixed pitch type 2 WT can reduce to a better extend, the variation of the grid frequency and power supplied by the genset in steady-state, compared to the type 1 WT. In addition to this, the controlled type 2 WT has been able to improve the transient response of the mini-grid, by reducing the frequency excursions that result from load demand and wind speed variations. It has been observed

that with the proposed type 2 WT, the effect of torque variations on the diesel engine shaft could be substantially reduced. The main limitation of the controlled type 2 wind turbine developed in this analysis is the lack of means to estimate quantitatively the power of the WT at a given frequency.

6.2 Future prospects

The following aspects related to the concepts developed in this thesis could bring an insight to the overall research work presented in the thesis.

- Propose a means to estimate quantitatively the power of the type 2 WT, knowing the operating frequency;
- Propose an approach to implement a rotor resistance control that will take into account all possible points of intersection between the power, frequency and rotor resistance at a given wind speed;
- Propose a means to extend the previous aspect so as to include all wind speeds for which the wind turbine is designed. This could be done based on the example given in the appendix;
- Present a cost analysis of the proposed hybrid system in comparison with the cost of typical thermal plans used in remote communities.

BIBLIOGRAPHY

[1] International Energy Agency. Online. <http://www.iea.org>. Accessed on Jan. 27, 2011.

[2] Abu-Elhaija W.S., Muetze A., "Energization Versus Electrification Utililizing Renewables ", *IEEE Power and Energy Society*, pp. 193–195, Jul. 2002.

[3] Thomas Ackermann, *Wind Power in Power Systems,* 16th edition, John Wiley 2009

[4] Hansen, M.O.L. "Basic Rotor Aerodynamics applied to Wind Turbines" Department of Energy Engineering Fluid Mechanics, Technical University of Denmark, Jan. 1998.

[5] Muljadi, E.; Butterfield, C.P. and Handman, D. "Dual-Speed Wind Turbine Generation." *NREL*, Jun. 1996.

[6] Carlin, P.W. Laxson, A.S. and Muljadi, E.B. "The History and State of the Art of Variable-Speed Wind Turbines Technology" *NREL*, Feb. 2001.

[7] Weigand, C.H., Lauw, H.K. and Marckx, D.A. "Variable-Speed Generation Subsystem Using the Doubly Fed Generator." *NREL*, Apr. 1999.

[8] Muller, S. Deicke, M. De Doncker, R.W. "Doubly fed induction generator systems for wind turbines" *IEEE Industry Applications Magazine*, Vol. 8, Issue 3, pp. 26–33, May-Jun. 2002.

[9] Abbey C., Li W., Joos G.,"An online Control Algorithm for Application of a Hybrid ESS to a wind-Diesel", *IEEE Trans. Industrial Electronics*, pp. 3896–3904, Dec. 2010.

[10] Tapas K. S., Debaprasad K., "Design Optimization and Dynamic Performance Analysis of a Stand-Alone Hybrid Wind-Diesel Electrical Power Generation System", *IEEE Trans. Energy Conversion*, Vol. 25, pp. 1209–1217, Dec. 2010.

[11] Datta M., Senjyu T., Yona A., Funabashi T. and Chul-Hwan K., "A Coordinated Control Method for Leveling PV Output Power Fluctuations of PV-Diesel Hybrid Systems Connected to Isolated Power Utility," *IEEE Trans. Energy Conversion*, pp. 153-162, Dec. 2009.

[12] R. Cardenas, R. Pena, M. Perez, J. Clare, G. Asher and F. Vargas, "Vector Control of Front-End Converters for Variable-Speed Wind-Diesel Systems," *IEEE Trans. Industrial Electronics*, Vol. 53, pp. 1127–1336, Aug. 2006.

[13] M. H. Nehrir, B. J. LaMeres, G. Venkataramanan, V. Gerez, and L. A. Alvarado, "An Approach to Evaluate the General Performance of Stand-Alone Wind/Photovoltaic Generating Systems", *IEEE Trans. Energy Conversion*, Vol. 15, pp. 433-439, Dec. 2000.

[14] Uhlen, K., Foss, B.A., Gjosaeter, O.B., "Robust control and analysis of a wind-diesel hybrid power plant," *IEEE Trans. Energy Conversion*, Vol. 9, pp. 701–708, Dec. 1994.

[15] R. B. Cherdid, S. H. Karald, and E. C. Chadi. "Adaptive Fuzzy Control for Wind-Diesel Weak Power System," *IEEE Trans. Energy Conversion*. Vol. 15. No. 1, pp.71-78. Mar. 2000.

[16] Sebastian R., Castro M., Sancristobal E., Yeves F., Peire J., and Quesada J., "Approaching hybrid wind-diesel systems and controller area network" *IEEE Trans. Industrial Electronics*, Vol. 3, pp. 2300–2305, Mar. 2003.

[17] A. Saramourtsis, P. Dokopoulos, A. Bakirtzis, E. Gavanidou. "Probabilistic Evaluation of the Performance of Wind Diesel Energy Systems," *IEEE Trans. Energy Conversion*, Vol. EC-9, No 4, pp. 743-752, Dec. 1994.

[18] G. Contaxis, J. Kabouris, "Short Term Scheduling in a Wind-Diesel Autonomous Energy System," *Paper 91 WM 188-3 PWRS*, Vol. PWRS- 6, No. 3, Aug. 1991.

[19] S. H. Karaki. K. H. Chrdid and R. Ramdan. "Probabilistic Production Costing of Diesel-Wind Energy Conversion System." *IEEE Trans. Energy Conversion.* Vol.15, No.3, pp.284-289, Sep. 2000.

[20] Chinchilla M., Arnaltes S., Burgos J.C., "Control of permanent-magnet generators applied to variable-speed wind-energy systems connected to the grid," *IEEE Trans. Energy Conversion*, 2006, 21(1), pp. 130-135.

[21] T.F. Chang , L. L. Lai, "A Novel Single Phase Self-Regulated Self-Excited Induction Generator using a Three Phase Machine ", *IEEE Trans. Energy conversion*, vol. 16, pp. 204–208, Aug. 2002.

[22] Mipoung O. D., Pillay P., "Generators for rural electrification from renewable energy," *EPEC 2009 IEEE*, pp. 1–7, Oct. 2009.

[23] Stephen J. Chapman, *Electric Machinery Fundamentals*, TK2000.C46 1999, Boston [Mass.]: WCB/McGraw-Hill, C1999.

[24] Roy S.,"Reduction of voltage dynamics in isolated Wind-Diesel units susceptible to gusting", *IEEE Trans. Sustainable Energy*, pp. 84–91, Jul. 2010.

[25] Abbey C., Li W., Joos G.,"An online control algorithm for application of a Hybrid ESS to a Wind-Diesel", *IEEE Trans. Industrial Electronics*, pp. 3896–3904, Dec. 2010.

[26] Tapas K. S., Debaprasad K., "Design optimization and dynamic performance analysis of a stand-Alone hybrid Wind-Diesel electrical power generation system", *IEEE Trans. Energy Conversion*, Vol. 25, pp. 1209–1217, Dec. 2010.

[27] R. Cardenas, R. Pena, M. Perez, J. Clare, G. Asher and F. Vargas, "Vector control of front-end converters for variable-speed Wind-Diesel systems," *IEEE Trans. Industrial Electronics*, Vol. 53, pp. 1127–1336, Aug. 2006.

[28] Uhlen, K., Foss, B.A., Gjosaeter, O.B., "Robust control and analysis of a Wind-Diesel hybrid power plant," *IEEE Trans. Energy Conversion*, Vol. 9, pp. 701–708, Dec. 1994.

[29] Kabouris J., Kanellos F. D.,"Impacts of large-scale wind penetration on designing and operation of electric power systems", *IEEE Trans. Sustainable Energy*, pp. 107–114, Jul. 2010.
[30] X. Wang, H. Dai and R. J. Thomas, "Reliability modeling of large wind farms and electric utility interface systems," *IEEE Trans. Power Apparatus and Systems*, vol. 103, No. 3, pp. 569–575, Mar. 1984.
[31] R. Billinton and G. Bai, "Generation capacity adequacy associated with wind energy," *IEEE Trans. Energy Conversion*, vol. 19, pp. 641-646, Sep. 2004.
[32] R. Karki and R. Billinton, "Cost-effective wind energy utilization for reliable power supply," *IEEE Trans. Energy Conversion*, vol. 19, pp. 435-440, Jun. 2004.
[33] A.K.Al Jabri and A.I. Alolah, "Capacitance requirements for isolated self-excited induction generators," *IEE Proceedings,* Vol. 137, No. 3, pp. 155-159, May 1990.
[34] Malik N. and Mazi A., "Capacitance requirements for isolated self-excited induction generators," *IEEE Trans. EC-2, (1)*, pp. 62-69, 1987.
[35] S. Roy, O. P. Malik and G. S. Hope, "An Adaptive Control Scheme for Speed Control of Diesel Driven Power-Plants," *IEEE Trans. Energy Conversion*, Vol. 6, No. 4, pp. 605-611, Dec. 1991.
[36] R. Hunter and G. Elliot, *Wind-Diesel Systems*, 2005.
[37] B. Wichert, "PV-diesel hybrid energy systems for remote area power generation - A review of current practice and future developments", *Renewable and Sustainable Energy Reviews*, Vol. 1, No. 3, pp. 209-228, 1997.
[38] S. A. Papathanassiou and M. P. Papadopoulos, "Mechanical stresses in fixed-speed wind turbines due to network disturbances," *IEEE Trans. Energy Conversion*, Vol. 16, No. 4, pp. 361-367, Dec. 2001.
[39] J.A. Carta, J. González, and C. Gómez "Operating results of a wind-diesel system which supplies the full energy needs of an isolated village community in the Canary Islands", *Solar Energy*, Vol. 74, No. 1, pp. 53-63, 2003.
[40] R. Sebastian and J. Quesada, "Distributed control system for frequency control in a isolated wind system," *Renewable Energy*, Vol. 31, pp. 285-305, 2006.
[41] "EN50160 European Standard on Voltage Characteristics of Electricity Supplied by Public Distribution Systems," Nov. 1994.
[42] I. Erlich and U. Bachmann, "Grid code requirements concerning connection and operation of wind turbines in Germany," *IEEE Power Engineering Society General Meeting*, Vol. 2, pp. 1253-1257, Jun. 12-16, 2005.
[43] A. Notholt, "Germany's new code for generation plants connected to medium-voltage networks and its repercussion on inverter control," *International Conference on Renewable Energies and Power Quality (ICREPQ'09)*, Valencia, Spain, Apr. 15-17, 2009.

[44] P. Bousseau, R. Belhomme, E. Monnot, N. Laverdure, D. Boëda, D. Roye, and S. Bacha, “Contribution of wind farms to ancillary services”, *CIGRE Plenary Session,* report C6-103, Paris, France, *2006*.

[45] G. Ramtharan, J. B. Ekanayake, and N. Jenkis, “Frequency support from doubly fed induction generator wind turbines,” *IET Renewable Power Generation*, Vol. 1, No. 1, pp. 3-9, 2007.

[46] J. F. Conroy and R. Watson, “Frequency response capability of full converter wind turbine generators in comparison to conventional generation,” *IEEE Trans. Power Systems*, Vol. 23, No. 2, pp. 649-656, May 2008.

[47] D. F. Howard, J. Restrepo, T. Smith, M. Starke, J. Dang, and R. G. Harley, “Calculation of fault current contribution of type I wind turbine-generators,” *IEEE Power and Energy Society*, pp. 1-7, Jul. 24-29, 2011.

[48] J. Morren, S.W.H de Haan, and J. A. Ferreira, “Contributionof DG units to primary frequency control,” *European Transactions Electrical Power*, Vol. 16, pp. 507-521, 2006.

[49] L. Xu and L. Yao, “Power electronics options for large wind farm integration: VSC-based HVDC transmission,” *IEEE Power System Conference and Exposition (PSCE)*, pp. 760-767, 2006.

[50] A. Sumper, O. Gomis-Bellmunt, A. Sundria-Andreu, R. Villafafilla-Robles, and J. Rull-Duran, “Response of fixed speed wind turbines to system frequency disturbances,” *IEEE Trans. Power Systems*, Vol. 24, No. 1, pp. 181-192, Feb. 2009,

[51] M. Behnke, A. Ellis, Y. Kazachkov, T. McCoy, E.Muljadi, W. Price, and J. Sanchez-Gasca, “Development and validation of WECC variable speed wind turbine dynamic models for grid integration studies,” *AWEA’s Wind Power Conference*, Los Angeles, California, Jun. 4–7, 2007.

[52] Md. W. Uddin, Md. Y. Sumon, R. Goswami, Md. R. H. Asif, and K. M. Rahman, "Sensorless peak power point tracking system for small scale wind turbine generators," *IEEE Trans. Energy Conversion*, Vol. 21, No. 1, pp. 257-264, Mar. 2010.

[53] F. Katiraei and C. Abbey, “Diesel plant sizing and performance analysis of a remote wind-diesel microgrid,” *IEEE Power Engineering Society Winter Meeting*, pp. 1-8, 2007.

[54] J. Lefebvre, "Analyse mécanique d’un système éolien-diesel sans stockage basé sur un bilan de puissance", *MSc. Dissertation*, Université du Québec à Rimouski, Dec. 2010.

[55] Torres, M., Lopes, L.A.C., "Frequency control improvement in an autonomous power system: An application of virtual synchronous machines," *Power Electronics and ECCE Asia (ICPE & ECCE)*, *2011 IEEE 8th International Conference*, pp. 2188-2195, May-Jun. 2011.

[56] Johan Morren, Jan Pierik, Sjoerd W.H. de Haan, “Inertia response of variable speed wind turbines,” *Electric Power Systems Research*, pp. 980-987, Jan. 2006.
[57] Mohamed Ridha Khadraoui, Mohamed Elleuch, "Comparison between optislip and fixed speed wind energy conversion systems," *SSD 2008 IEEE*, pp.1–6, Jul. 2008.

LIST OF APPENDIX

APPENDIX-A: Three phase induction generator model:

- *Stator and rotor voltage equations:*

$$V_{ds} = R_s i_{ds} + \frac{d\lambda_{ds}}{dt} - \omega_{syn}\lambda_{qs}$$
$$V_{qs} = R_s i_{qs} + \frac{d\lambda_{qs}}{dt} + \omega_{syn}\lambda_{ds} \quad \text{(A1)}$$

$$0 = R_r i_{dr} + \frac{d\lambda_{dr}}{dt} - (\omega_{syn} - \omega_r)\lambda_{qr}$$
$$0 = R_r i_{qr} + \frac{d\lambda_{qr}}{dt} + (\omega_{syn} - \omega_r)\lambda_{dr} \quad \text{(A2)}$$

Where $\omega_{syn} = 2\pi f_s$ and $\omega_r = \frac{P}{2}\omega_{mec}$

- *Stator and rotor flux equations:*

$$\lambda_{ds} = L_s i_{ds} + L_m i_{dr}$$
$$\lambda_{qs} = L_s i_{qs} + L_m i_{qr} \quad \text{(A3)}$$

$$\lambda_{dr} = L_r i_{dr} + L_m i_{ds}$$
$$\lambda_{qr} = L_r i_{qr} + L_m i_{qs} \quad \text{(A4)}$$

- *Torque and speed equations*

$$T_{em} = \frac{3P}{4}(i_{qs} i_{dr} - i_{ds} i_{qr})$$
$$J\frac{d\omega_{mech}}{dt} = T_{em} - T_{Load} \quad \text{(A5)}$$

APPENDIX-B: Self-excited induction generator model:

- *Stator and rotor voltage equations*

$$V_{s\alpha} = R_s i_{s\alpha} + L_s \frac{di_{s\alpha}}{dt} + L_m \frac{di_{r\alpha}}{dt}$$
$$V_{s\beta} = R_s i_{s\beta} + L_s \frac{di_{s\beta}}{dt} + L_m \frac{di_{r\beta}}{dt} \quad \text{(B1)}$$

$$0 = R_r i_{r\alpha} + L_r \frac{di_{r\alpha}}{dt} + L_m \frac{di_{s\alpha}}{dt} + \omega_r \lambda_{r\beta}$$
$$0 = R_r i_{r\beta} + L_r \frac{di_{r\beta}}{dt} + L_m \frac{di_{s\beta}}{dt} - \omega_r \lambda_{r\alpha} \quad \text{(B2)}$$

- *Rotor flux linkage equations*

$$\lambda_{r\alpha} = L_m i_{s\alpha} + L_r i_{r\alpha} + \lambda_{r\alpha 0}$$
$$\lambda_{r\beta} = L_m i_{s\beta} + L_r i_{r\beta} + \lambda_{r\beta 0} \quad \text{(B3)}$$

- *Capacitor voltages including initial condition*

$$V_{C\alpha} = \frac{1}{C}\int i_{C\alpha} dt + V_{C\alpha 0}$$
$$V_{C\beta} = \frac{1}{C}\int i_{C\beta} dt + V_{C\beta 0} \quad \text{(B4)}$$

Equations (B1) to (B4) can be written in matrix form for no load condition as follows.

$$\begin{bmatrix} 0 \\ 0 \\ 0 \\ 0 \end{bmatrix} = \begin{bmatrix} R_s + \frac{dL_s}{dt} & 0 & \frac{dL_m}{dt} & 0 \\ 0 & R_s + \frac{dL_s}{dt} & 0 & \frac{dL_m}{dt} \\ \frac{dL_m}{dt} & \omega_r L_m & R_r + \frac{dL_r}{dt} & \omega_r L_r \\ -\omega_r L_m & \frac{dL_m}{dt} & -\omega_r L_r & R_r + \frac{dL_r}{dt} \end{bmatrix} \begin{bmatrix} i_{s\alpha} \\ i_{s\beta} \\ i_{r\alpha} \\ i_{r\beta} \end{bmatrix} + \begin{bmatrix} V_{C\alpha} \\ V_{C\beta} \\ \omega_r \lambda_{r\beta 0} \\ -\omega_r \lambda_{r\alpha 0} \end{bmatrix} \quad \text{(B5)}$$

The state space form of the above matrix can be derived as follows.

$$A\frac{dI_G}{dt} + BI_G + V_G = 0 \quad \text{(B6)}$$

Where,

$$A = \begin{bmatrix} L_s & 0 & L_m & 0 \\ 0 & L_s & 0 & L_m \\ L_m & 0 & L_r & 0 \\ 0 & L_m & 0 & L_r \end{bmatrix} \quad V_G = \begin{bmatrix} V_{C\alpha} \\ V_{C\beta} \\ \omega_r \lambda_{r\beta 0} \\ -\omega_r \lambda_{r\alpha 0} \end{bmatrix} \quad \text{(B7)}$$

$$B=\begin{bmatrix} R_s & 0 & 0 & 0 \\ 0 & R_s & 0 & 0 \\ 0 & \omega_r L_m & R_r & \omega_r L_r \\ -\omega_r L_m & 0 & -\omega_r L_r & R_r \end{bmatrix} \quad \text{(B8)}$$

$$I_G=\begin{bmatrix} i_{s\alpha} \\ i_{s\beta} \\ i_{r\alpha} \\ i_{r\beta} \end{bmatrix}$$

(B9)

Using matrix inversion, equation (B6) can be solved for the current derivatives.

$$\frac{dI_G}{dt}=-A^{-1}BI_G-A^{-1}V_G \quad \text{(B10)}$$

$$\frac{di_{s\alpha}}{dt}=-\frac{L_r}{L}(R_s i_{s\alpha}+V_{C\alpha})+\frac{L_m}{L}[\omega_r(L_m i_{s\beta}+L_r i_{r\beta}+\lambda_{r\beta 0})+R_r i_{r\alpha}]$$
$$\frac{di_{s\beta}}{dt}=-\frac{L_r}{L}(R_s i_{s\beta}+V_{C\beta})-\frac{L_m}{L}[\omega_r(L_m i_{s\alpha}+L_r i_{r\alpha}+\lambda_{r\alpha 0})-R_r i_{r\beta}] \quad \text{(B11)}$$

$$\frac{di_{r\alpha}}{dt}=\frac{L_m}{L}(R_s i_{s\alpha}+V_{C\alpha})-\frac{L_s}{L}[\omega_r(L_m i_{s\beta}+L_r i_{r\beta}+\lambda_{r\beta 0})+R_r i_{r\alpha}]$$
$$\frac{di_{r\beta}}{dt}=\frac{L_m}{L}(R_s i_{s\beta}+V_{C\beta})+\frac{L_s}{L}[\omega_r(L_m i_{s\alpha}+L_r i_{r\alpha}+\lambda_{r\alpha 0})-R_r i_{r\beta}] \quad \text{(B12)}$$

$$\frac{di_{r\alpha}}{dt}=\frac{L_m}{L}(R_s i_{s\alpha}+V_{C\alpha})-\frac{L_s}{L}[\omega_r(L_m i_{s\beta}+L_r i_{r\beta}+\lambda_{r\beta 0})+R_r i_{r\alpha}]$$
$$\frac{di_{r\beta}}{dt}=\frac{L_m}{L}(R_s i_{s\beta}+V_{C\beta})+\frac{L_s}{L}[\omega_r(L_m i_{s\alpha}+L_r i_{r\alpha}+\lambda_{r\alpha 0})-R_r i_{r\beta}] \quad \text{(B13)}$$

Where $L=L_s L_r-L_m{}^2$

Assuming resistive loads connected across the generator, the load voltage and load current can be modelled as follows.

$$\frac{dv_{L\alpha}}{dt}=\frac{1}{C}i_{C\alpha}$$
$$\frac{dv_{L\beta}}{dt}=\frac{1}{C}i_{C\beta} \quad \text{(B14)}$$

$$i_{L\alpha}=\frac{v_{L\alpha}}{R_L}$$
$$i_{L\beta}=\frac{v_{L\beta}}{R_L} \quad \text{(B15)}$$

APPENDIX-C: Single phase capacitor start induction generator model:

$$\begin{bmatrix} f_{dr}^s \\ f_{qr}^s \end{bmatrix}=\begin{bmatrix} \cos\theta_r & -\sin\theta_r \\ \sin\theta_r & \cos\theta_r \end{bmatrix}\begin{bmatrix} f_{dr}^r \\ f_{qr}^r \end{bmatrix} \quad \text{(C1)}$$

$$V_{ds}^{'}=(\frac{N_{qs}}{N_{ds}})V_{ds}$$
$$i_{ds}^{'}=(\frac{N_{ds}}{N_{qs}})i_{ds} \quad \text{(C2)}$$

$$R_{ds}^{'}=(\frac{N_{qs}}{N_{ds}})^2 R_{ds}$$
$$L_{lds}^{'}=(\frac{N_{qs}}{N_{ds}})^2 L_{lds} \quad \text{(C3)}$$

$$L_{mq}=N_{qs}^2 p_g$$
$$L_{md}^{'}=L_{mq}=(\frac{N_{qs}}{N_{ds}})^2 N_{ds}^2 p_g \quad \text{(C4)}$$

$$R_r^{'}=(\frac{N_{qs}}{N_r})^2 R_r$$
$$L_{lr}^{'}=(\frac{N_{qs}}{N_r})^2 L_{lr} \quad \text{(C5)}$$

$$\lambda_{dr}^{',s}=(\frac{N_{qs}}{N_r})\lambda_{dr}^s$$
$$\lambda_{qr}^{',s}=(\frac{N_{qs}}{N_r})\lambda_{qr}^s \quad \text{(C6)}$$

$$V_{dr}^{',s}=(\frac{N_{qs}}{N_r})V_{dr}^s$$
$$V_{qr}^{',s}=(\frac{N_{qs}}{N_r})V_{qr}^s \quad \text{(C7)}$$
$$i_{qr}^{',s}=(\frac{N_r}{N_{qs}})i_{qr}^s$$

- *Voltage equations*

$$V_{ds}^{'} = R_r^{'} i_{ds}^{'} + \frac{d\lambda_{ds}^{'}}{dt}$$
$$V_{qs} = R_{qs} i_{qs} + \frac{d\lambda_{qs}}{dt} \quad \text{(C8)}$$

$$V_{dr}^{'s} = R_r^{'} i_{dr}^{'s} + \frac{d\lambda_{dr}^{'s}}{dt} + \omega_r \lambda_{qr}^{'s}$$
$$V_{qr}^{'s} = R_r^{'} i_{qr}^{'s} + \frac{d\lambda_{qr}^{'s}}{dt} - \omega_r \lambda_{dr}^{'s} \quad \text{(C9)}$$
$$V_{Cs}^{'} = \frac{1}{C}\int i_{ds}^{'s}$$

- *Flux equations*

$$\lambda_{qs} = X_{lqs} i_{qs} + \lambda_{mq}$$
$$\lambda_{ds}^{'} = X_{lds}^{'} i_{ds}^{'} + \lambda_{md}^{'} \quad \text{(C10)}$$

$$\lambda_{mq} = X_{mq}(i_{qs} + i_{qr}^{'s})$$
$$\lambda_{md}^{'} = X_{mq}(i_{ds}^{'s} + i_{dr}^{'s}) \quad \text{(C11)}$$

$$\lambda_{qr}^{'s} = X_{lr}^{'} i_{qr}^{'s} + \lambda_{mq}$$
$$\lambda_{dr}^{'s} = X_{lr}^{'} i_{dr}^{'s} + \lambda_{md}^{'} \quad \text{(C12)}$$

- *Torque and speed equations*

$$T_{em} = \frac{P}{2}(\lambda_{ds}^{'} i_{qs} - \lambda_{qs} i_{ds}^{'})$$
$$J\frac{d\omega_r}{dt} = T_{em} + T_{Load} - T_{damp} \quad \text{(C13)}$$

- *Open circuit condition*

$$i_{ds}^{'} = 0$$
$$\lambda_{ds}^{'} = \lambda_{md}^{'} = X_{mq} i_{dr}^{'s} \quad \text{(C14)}$$
$$i_{dr}^{'s} = \frac{\lambda_{dr}^{'s}}{X_{lr}^{'} + X_{mq}}$$

$$V_{ds}^{'} = X_{mq}\frac{di_{dr}^{'s}}{dt}$$
$$V_{ds}^{'} = \frac{X_{mq}}{X_{lr}^{'} + X_{mq}}\frac{d\lambda_{dr}^{'s}}{dt} \quad \text{(C15)}$$

APPENDIX-D: Permanent magnet synchronous generator system model:

- *Voltage equations:*

$$V_{ds} = -R_s i_{ds} - \omega_m \lambda_{qs} + \frac{d\lambda_{ds}}{dt}$$
$$V_{qs} = -R_s i_{qs} + \omega_m \lambda_{ds} + \frac{d\lambda_{qs}}{dt} \quad \text{(D1)}$$

- *Flux equations:*

$$\lambda_{ds} = L_{ds} i_{ds} + \lambda_f$$
$$\lambda_{qs} = L_{qs} i_{qs} \quad \text{(D2)}$$

where λ_f is the flux produced by the permanent magnet.

- *Torque and speed equations:*

$$T_{em} = \frac{3P}{2}(\lambda_{ds} i_{qs} - \lambda_{qs} i_{ds})$$
$$J\frac{d\omega_r}{dt} = T_{em} - T_{Load} \quad \text{(D3)}$$

with P the number of pole of the machine

- *Generator side converter*

The power converter shown in Fig.2.20 can be modelled as a fundamental frequency converter. The generator terminal voltages in the dq reference frame can be expressed in terms of the dc-link voltage as follows.

$$V_{ds} = m_1 V_{DC}\cos\theta$$
$$V_{qs} = m_1 V_{DC}\sin\theta \quad \text{(D4)}$$

Where, m_1 *is the modulation index of the converter and* V_{DC} *the dc-link voltage. The angle* θ *is obtained by controlling the generator frequency trough the active power control, meanwhile the modulation index* m_1 *is obtained by controlling the terminal voltage of the generator as shown below.*

$$\frac{d\theta}{dt} = \omega_b(\omega_m - f) \quad \text{(D5)}$$

ω_b *is the base speed of the permanent magnet machine and* ω_m *the grid speed.* f *can be obtained by controlling the active power and the modulation index by controlling the stator voltages shown in the following figures.*

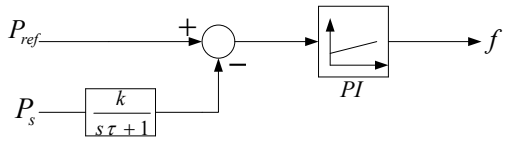

Fig D1: *Active power control scheme*

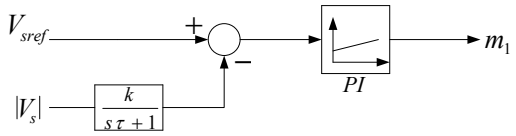

Fig D2: *Stator voltage control scheme*

$$\left|V_s\right| = V_{ds}^2 + V_{qs}^2 \tag{D6}$$

- *DC link model:*

The model of the dc-link can be derived using the following equations where the converter is assumed to operate as a fundamental frequency current source.

$$I_v = C\frac{dV_{DC}}{dt} \tag{D7}$$

I_v *is the generator side converter current through the capacitor.* I_v *can be obtained from the power supplied to the capacitor by the generator.*

$$I_v = \frac{V_{qs}i_{qs} + V_{ds}i_{ds} - P_{sloss}}{V_{DC}} \tag{D8}$$

$$\frac{dV_{DC}}{dt} = \frac{1}{CV_{DC}}(V_{qs}i_{qs} + V_{ds}i_{ds} - P_{sloss}) \tag{D9}$$

Where P_{sloss} *represents the converter losses. Equation (D9) represents the dynamic equation of the dc-link voltage.*

APPENDIX-E: Single phase split phase induction generator model

- *voltage equations:*

$$V_{ds}^{'} = R_r^{'}i_{ds}^{'} + \frac{d\lambda_{ds}^{'}}{dt}$$
$$V_{qs} = R_{qs}i_{qs} + \frac{d\lambda_{qs}}{dt} \tag{E1}$$

$$V_{dr}^{',s} = R_r^{'}i_{dr}^{',s} + \frac{d\lambda_{dr}^{',s}}{dt} + \omega_r\lambda_{qr}^{',s}$$
$$V_{qr}^{',s} = R_r^{'}i_{qr}^{',s} + \frac{d\lambda_{qr}^{',s}}{dt} - \omega_r\lambda_{dr}^{',s} \tag{E2}$$

- *flux equations:*

$$\lambda_{qs} = X_{lqs}i_{qs} + \lambda_{mq}$$
$$\lambda_{ds}^{'} = X_{lds}^{'}i_{ds}^{'} + \lambda_{md}^{'} \tag{E3}$$

$$\lambda_{qr}^{',s} = X_{lr}^{'}i_{qr}^{',s} + \lambda_{mq}$$
$$\lambda_{dr}^{',s} = X_{lr}^{'}i_{dr}^{',s} + \lambda_{md}^{'} \tag{E4}$$

$$\lambda_{mq} = X_{mq}(i_{qs} + i_{qr}^{',s})$$
$$\lambda_{md}^{'} = X_{mq}(i_{ds}^{',s} + i_{dr}^{',s}) \tag{E5}$$

- *torque and speed equations:*

$$T_{em} = \frac{P}{2}(\lambda_{ds}^{'}i_{qs} - \lambda_{qs}i_{ds}^{'})$$
$$J\frac{d\omega_r}{dt} = T_{em} + T_{Load} - T_{damp} \tag{E6}$$

- *open circuit condition:*

$$i_{ds}^{'} = 0$$
$$\lambda_{ds}^{'} = \lambda_{md}^{'} = X_{mq}i_{dr}^{',s}$$
$$i_{dr}^{',s} = \frac{\lambda_{dr}^{',s}}{X_{lr}^{'} + X_{mq}} \tag{E7}$$

$$V_{ds}^{'} = X_{mq}\frac{di_{dr}^{',s}}{dt}$$
$$V_{ds}^{'} = \frac{X_{mq}}{X_{lr}^{'} + X_{mq}}\frac{d\lambda_{dr}^{',s}}{dt} \tag{E8}$$

APPENDIX-F: Fatigue failure estimation of type 1 WT in the droop controlled hybrid min-grid

In Chapter 3, it has been shown that fixed speed WTs can be implemented in the hybrid mini-grid to improve the frequency regulation while reducing the level of stress experience by the diesel genset. However, the lack of converter used to interface the wind generator and the mini-grid makes the wind turbine generator to be directly connected to the mini-grid. Thus, all frequency variations taking place in the network will be directly transmitted into the wind turbine drive train. A useful dimension of the application considered in this research work will be to propose an approach (or technique) to estimate the life time of the turbine drive train based on the loading conditions of the WT in the hybrid mini-grid. This is useful for remote communities, since these locations are usually prone to little available technical expertise. In addition to this, when the technical expertise is available nearby, travel conditions can introduce lengthy delays in repair, thus mandating longest possible times between failures. So a method to predict the system fatigue failure could help replacing the turbine parts at the required time, thereby avoiding sudden breakdown of the wind system In this appendix, the effect of load variations on fixed speed wind turbines operating in the droop controlled hybrid diesel mini-grid is examined. A model used to predict the mechanical stress transmitted into the turbine drive train is proposed, along with a simple approach how to estimate the number of cycle to a fatigue failure the drive train can be subjected to, based on the type and level of the WT shaft loading.

a) Mechanical stress model

When a shaft is subjected to a torque or twisting, a shearing stress is produced in the shaft. The shear stress varies from zero in the axis to a maximum at the outside surface of the shaft. The maximum shear stress in a solid circular shaft can be estimated using the following equations:

$$\sigma = T_{shft} \times \frac{r}{I_P} \tag{F1}$$

$$I_P = \frac{\pi}{32}\left(D^4 - d^4\right) \tag{F2}$$

where σ is the shear stress, T_{shft} the twisting moment, r the radius of the shaft and I_p the polar moment of inertia of the shaft. The polar moment of inertia is a measure of an object's ability to resist torsion. D represents the shaft outside diameter and d the shaft inside diameter (neglected in this analysis). From basic rotating shaft design theory, proper shaft sizing can be determined using the following equation (assuming shafts with keyway):

$$D = \sqrt[3]{\frac{1.33 \times 10^6 P}{n_{shaft}}} \tag{F3}$$

where P is the horse power, n_{shaft} the shaft speed in revolution per minute (rpm) and D the diameter of the shaft in mm. For the case considered in this analysis, the diameter of the high speed shaft (D_{HS}) and that of the low speed shaft (D_{LS}) can be estimated as follows (a safety factor of 1.5 has been applied):

$$D_{HS} = 1.5 \times \sqrt[3]{\frac{1.33 \times 10^6 \times 100}{1800}} \approx 63mm \tag{F4}$$

$$D_{LS} = 1.5 \times \sqrt[3]{\frac{1.33 \times 10^6 \times 100}{\frac{1800}{22}}} \approx 176mm \tag{F5}$$

The model used to predict the mechanical stress transmitted into the turbine drive train can be implemented as illustrated in the figure below using equations (F1) to (F3).

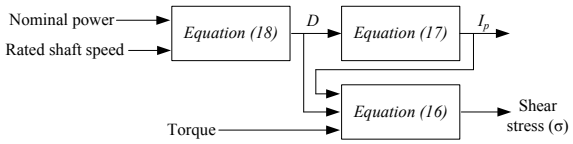

Figure F1. Model of the mechanical stress on the drive train shaft

This model is used to analyze a case study of the turbine drive train loading as the load demand varies. The following figures are used to explain the assumed case study.

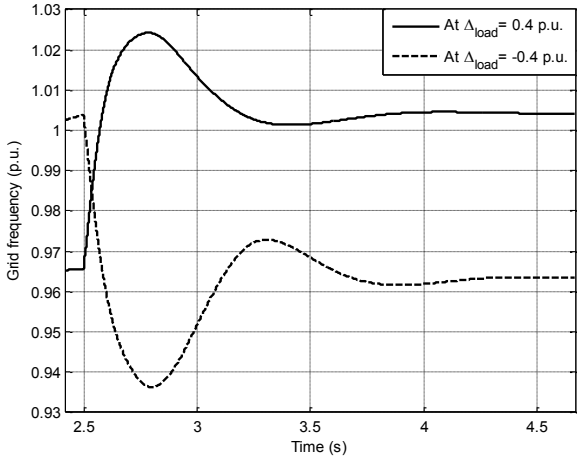

Figure F2. Grid frequency disturbance due to load variations

Figure F2 represents the Grid frequency disturbance due to load variations. The load is increased and decreased by the same amount. The resulting stress responses are shown in the Figures below.

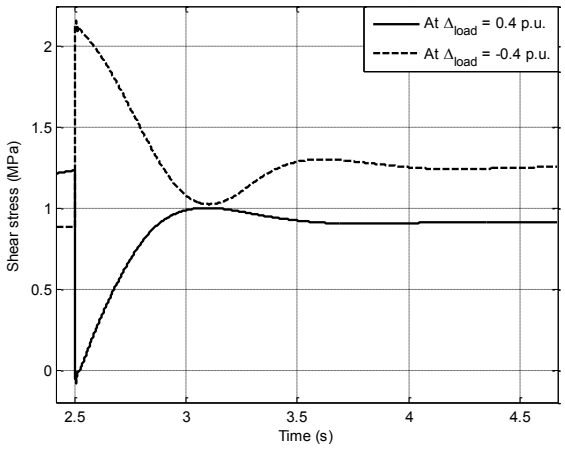

Figure F3. Shaft loading on the high speed side of the drive

Figure F3 is a representation of the resulting shaft loading on the high speed side of the drive train when the load varies. It can be seen from this figure that the mechanical stress experienced by the drive train due to load variation of same magnitude is nearly similar as the load increases and decreases, but in opposite direction.

Figure F4 represents the resulting shaft loading on the low speed side of the drive train when the load varies. One can see from this figure that the high frequency components that are present in the stress on the high speed side have been filtered. This is due to the damping effect of the drive train which has an inherent low pass filter characteristic.

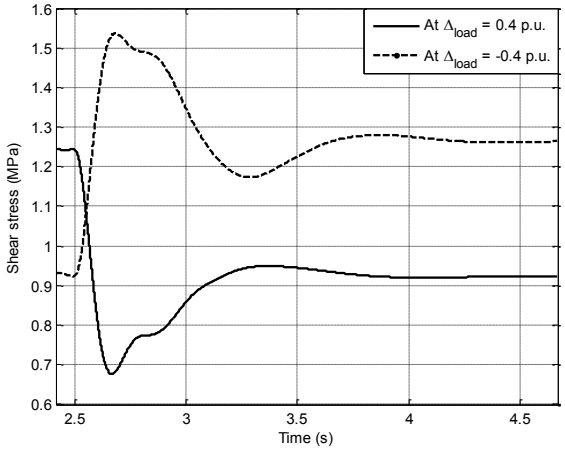

Figure F4. Shaft loading on the low speed side of the drive

In the following part of this analysis, the main focus will be on the stress transmitted to the low speed side. This is the one experienced by the entire drive train as the stress is transmitted from the high speed side to the low speed side of the drive train.

The mechanical stress shown in Figure 10 can be classified as one of the non sinusoidal time varying stresses. This type of stress is generally experienced by machine parts when they are subjected to time varying loading. The main components of such a stress can be described using the following figure. To simplify the analysis, only the stress due to load decrease has been reproduced.

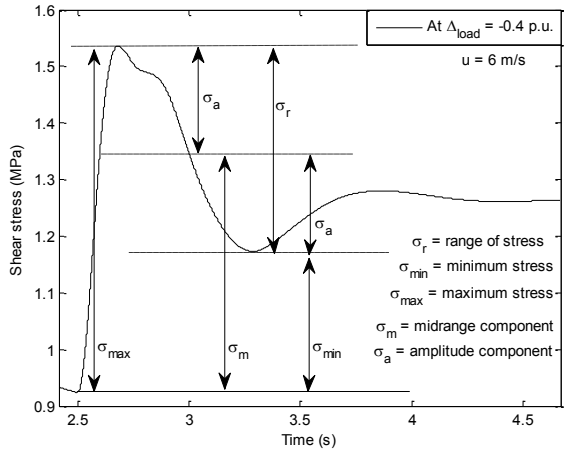

Figure F5. Main components of the non sinusoidal time varying stress

The following relations can be derived based on Figure F5.

$$\sigma_a = \frac{\sigma_{\max} - \sigma_{\min}}{2} \quad \text{(F6)}$$

$$\sigma_m = \frac{\sigma_{\max} + \sigma_{\min}}{2} \quad \text{(F7)}$$

The stress ratio and the amplitude ratio can be estimated using the following relations:

$$R = \frac{\sigma_{\min}}{\sigma_{\max}} \quad \text{(F8)}$$

$$A = \frac{\sigma_a}{\sigma_m} \quad \text{(F9)}$$

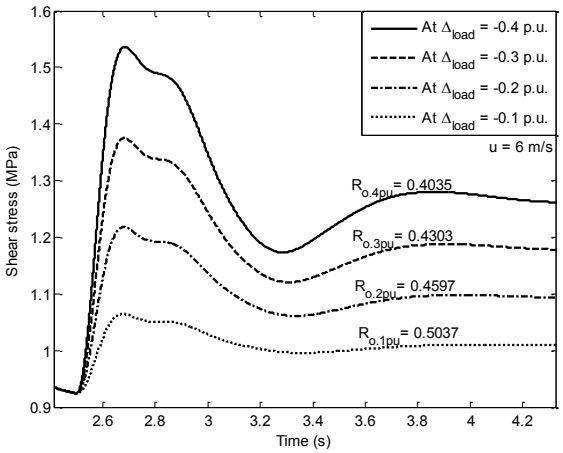

Figure F6. Stress on the low speed side at different shaft loadings

Figure F6 represents the stress transmitted to the low speed side of the drive train at different shaft loadings, along with their respective stress ratios. It results from this figure that, as the load variation increases, the stress ratio decreases. High stress ratio would be beneficial for the system since it results in low transient in the stress experienced by the shaft.

b) Effect of Shaft Loading on the Drive Train Life Time

Rotating shafts that are subjected to stresses that vary with time or fluctuate between different levels, experience relatively earlier fatigue failure over a period of time. Fatigue failure is a complicated phenomenon which is only partially understood. There are basically three fatigue life methods used in design and analysis to predict when a cyclically loaded machine component will possible fail in fatigue over a period of time:

- *The stress-life method based on stress levels only;*
- *The strain-life method based on the plastic deformation at localized regions where the stresses are considered for life estimates;*
- *The fracture mechanics method based on the assumption that a crack is already present and detected;*

Detailed information on the individual approaches can be found in literatures. In either approach, important characteristic parameters of the material constituting the shaft are required. The S-N (strength-life) diagram providing the fatigue strength (S_f) versus cycle life (N) of a material is generally available for different types of material. In this section, the effect of the load variation on the life time of the turbine drive train is briefly examined. The case study presented here will be based on the loading of the low speed shaft when Δ_{load} =-0.4 p.u. and Δ_{load} =-0.1 p.u.. These cases are clearly represented in the figures below.

It is assumed in this analysis that, the turbine shaft is made of steel and undergoes cyclic loading such as the one represented in Fig. 13 and Fig. 14. The objective is to estimate the number of cycles to a fatigue failure the shaft will be subjected to.

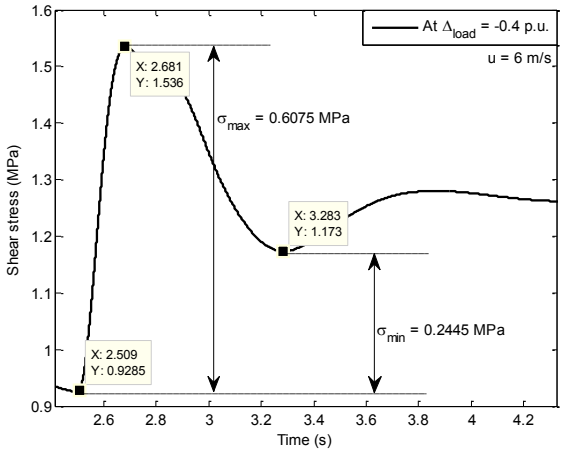

Figure F7. Case study 1: stress on the low speed side when Δ_{load} = -0.4 p.u.

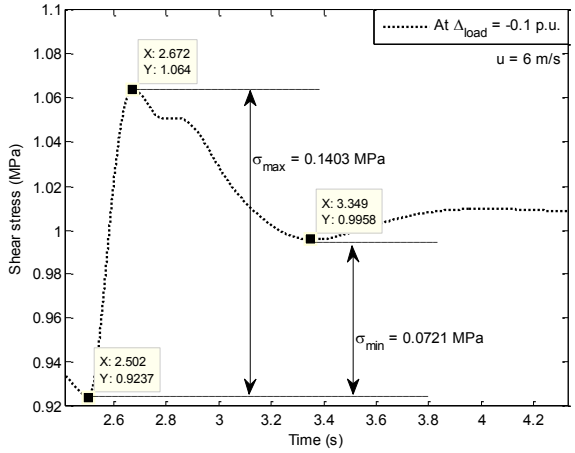

Figure F8. Case study 2: stress on the low speed side when Δ_{load} = -0.1 p.u.

Case study 1:

From equations (F6), (F7) and Figure F7 the followings parameters can be calculated.

$$\sigma_{a1} = \frac{\sigma_{\max} - \sigma_{\min}}{2} = \frac{0.6075 - 0.2445}{2} = 0.1815\ MPa \quad \text{(F10)}$$

$$\sigma_{m1} = \frac{\sigma_{\max} + \sigma_{\min}}{2} = \frac{0.6075 + 0.2445}{2} = 0.4260\ MPa \quad \text{(F11)}$$

From the material (steel) properties, S_{ut} = 551 MPa, S_y = 448MPa and f = 0.9, where S_{ut} is the minimum tensile strength of the material, S_y the yield strength of the material and f the fatigue strength fraction of S_{ut} at 10^3 cycles.

In real operating condition of machines, the endurance of the material used will be affected by the surface condition, size, loading, temperature, and miscellaneous items. To account for theses effects, a fully corrected endurance limit (S_e) is recommended (S_e= 275MPa for steel). The number of cycles of the shaft subjected to a stress such as the one represented in Fig. 13 can be calculated as follows F7:

$$N = \left(\frac{S_f}{a}\right)^{\frac{1}{b}} \quad \text{(F12)}$$

$$a = \frac{(S_{ut} f)^2}{S_e} = \frac{(0.9 \times 551.58)^2}{275.79} = 893\ MPa \quad \text{(F13)}$$

$$b = -\frac{1}{3}\log\left(\frac{S_{ut} f}{S_e}\right) = -\frac{1}{3}\log\left(\frac{0.9 \times 551.58}{275.79}\right) = -0.08 \quad \text{(F14)}$$

$$S_{f1} = \frac{\sigma_a}{1 - \frac{\sigma_m}{S_{ut}}} = \frac{0.1815}{1 - \frac{0.4260}{551.58}} = 0.1816 \quad \text{(F15)}$$

$$N_1 = \left(\frac{0.1816}{893.55}\right)^{\frac{-1}{0.0851}} = 2.4226 \times 10^{43} cycles \quad \text{(F16)}$$

Case study 2:

The shaft material is assumed to be the same as in case 1. Thus, constants a and b are unchanged since these constants depend totally on the material properties.

$$\sigma_{a2} = \frac{\sigma_{\max} - \sigma_{\min}}{2} = \frac{0.1403 - 0.0721}{2} = 0.0341\ MPa \quad \text{(F17)}$$

$$\sigma_{m2} = \frac{\sigma_{\max} + \sigma_{\min}}{2} = \frac{0.1403 + 0.0721}{2} = 0.1062\ MPa \quad \text{(F18)}$$

$$S_{f2} = \frac{\sigma_{a2}}{1 - \frac{\sigma_{m2}}{S_{ut}}} = \frac{0.0341}{1 - \frac{0.1062}{551.58}} = 0.0341\ MPa \quad \text{(F19)}$$

$$N_2 = \left(\frac{0.0341}{893.55}\right)^{\frac{-1}{0.0851}} = 8.3114 \times 10^{51} cycles \quad \text{(F20)}$$

$$N_2 = 343.08 \times 10^6 \times N_1 \quad \text{(F21)}$$

It results from these case studies that the stress resulting from load variations increases with the level of network disturbance. The high is the

stress level, the shorter is the number of cycle before breakdown.

APPENDIX-G: WT droop factor adjustment at variable wind speed

In Chapter 5, an approach to obtain a relationship between the external rotor resistance, grid frequency and injected power for which the wind system operates in the selected frequency range at a given wind speed is presented. A case study similar to the one presented in this Chapter is illustrated in the figure below, using Table G.1. Figure G.1 represents the power frequency curves of the wind system at 12 m/s and different rotor resistances, where the blue line represents a desired operating droop curve at 12 m/s wind speed.

Table G.1 Case study of power-frequency variation of the WT at different rotor resistances

f (Hz)	u = 12 m/s			
	$R_{r\_t} = R_r$	$R_{r\_t} = 5R_r$	$R_{r\_t} = 10R_r$	$R_{r\_t} = 15R_r$
58	77.67	46.48	32.64	25.58
59	76.41	45.62	31.96	25.08
60	74.96	44.74	31.35	24.57
61	73.64	43.84	30.73	24.05
62	72.29	42.94	30.09	23.58
s_{p-u} (kW/Hz)	----	----	----	----

The desired droop line shown in Figure G.1 can be described using the following equation.

$$P_{WT}(f) = P_{u-f\max} + s_{p-u}(f_{\max} - f) \qquad \text{(G1)}$$
$$= 23.5854 + 13.519(62 - f)$$

Where $P_{u\text{-}fmax}$ is the injected power at a given wind speed for maximum grid frequency and $s_{P\text{-}u}$ is the slope of the curve which varies with the wind speed. It appears from Figure G.1 that the desired droop curve of the turbine intersects the power- frequency curves of the wind generator at the individual rotor resistances, and the point of intersection (I_1 or I_2) is unique for every frequency point. Thus, for a given slope (s_P) and a given power at maximum grid frequency (P_{max}), it is possible to obtain the desired droop curve one might want the wind system to operate at. In addition to this, if all the possible points of intersection of the assumed droop curve with the power- frequency curves at the individual rotor resistances are known, it will be possible to obtain the external rotor resistance required for which the wind system would operate on the desired curve.

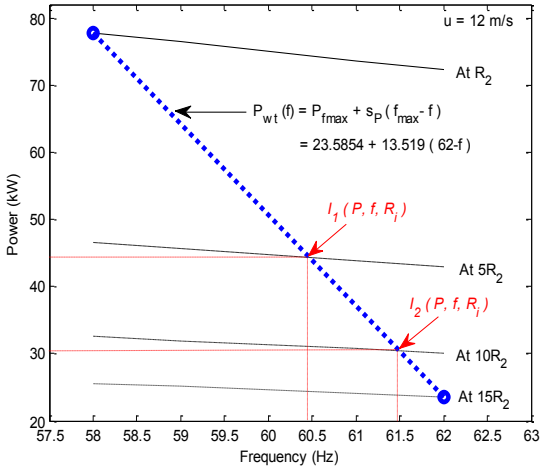

Figure G.1 Power-frequency curve of the wind generator at 12 m/s and different rotor resistances

In order to achieve this, it is suggested to use data points with reduced step variation in the rotor resistance, since in such a case the curve fitting will be more consistent. Thus, Table G.2 will be assumed rather than Table G.1. In Table G.2, a step variation of R_r is used instead of 5 R_r as in Table G.1.

Table G.2 Power-frequency curve of the wind generator at 12 m/s with variable rotor resistance

f (Hz)	u = 12 m/s														
	$R_{r\_t} = R_r$	$R_{r\_t} = 2R_r$	$R_{r\_t} = 3R_r$	$R_{r\_t} = 4R_r$	$R_{r\_t} = 5R_r$	$R_{r\_t} = 6R_r$	$R_{r\_t} = 7R_r$	$R_{r\_t} = 8R_r$	$R_{r\_t} = 9R_r$	$R_{r\_t} = 10R_r$	$R_{r\_t} = 11R_r$	$R_{r\_t} = 12R_r$	$R_{r\_t} = 13R_r$	$R_{r\_t} = 14R_r$	$R_{r\_t} = 15R_r$
58	77.67	65.53	57.27	51.23	46.48	42.70	39.58	36.83	34.64	32.64	30.92	29.31	27.98	26.69	25.58
59	76.41	64.36	56.30	50.20	45.62	41.88	38.71	36.18	33.93	31.96	30.26	28.76	27.37	26.17	25.08
60	74.96	63.16	55.19	49.27	44.74	41.05	38.01	35.43	33.21	31.35	29.68	28.19	26.82	25.64	24.57
61	73.64	62.07	54.17	48.32	43.84	40.21	37.21	34.75	32.56	30.73	29.08	27.61	26.26	25.10	24.05
62	72.29	60.82	53.02	47.36	42.9	39.45	36.49	34.06	31.90	30.09	28.47	27.03	25.77	24.62	23.58
$s_{p\text{-}u}$ (kW/Hz)	---	---	---	---	---	---	---	---	---	---	---	---	---	---	---

The 3-D plot of the data given in Table 6.2 with R_r = 0.03281 Ω is represented in the figure below.

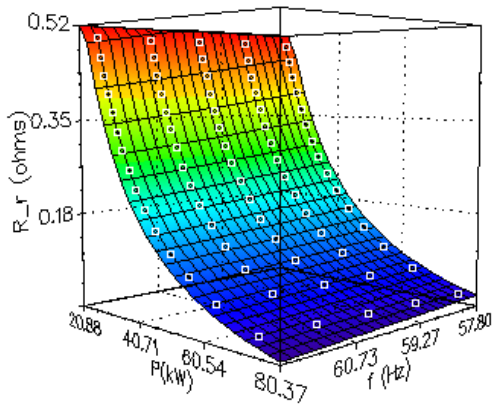

Figure G.2 Rotor resistance variation versus frequency and power variations using the data of Table G.2

From Figure G.2, all the possible points of intersection between the power, the external rotor resistance and the grid frequency at 12 m/s wind speed can be clearly seen (white dots). The relationship between the external rotor resistance, the grid frequency and the injected power can be obtained using a 3-D equation that fits better the trajectory of these points of intersection. The closest relation obtained is given in the equation below, where constants k_1, k_2, k_3, k_4, k_5 and k_6 can be obtained using a multi variable curve regression optimization program.

$$R_r(f, P_{wt}) = \frac{k_1 + k_2 \ln(f) + k_3 \ln(P_{wt})}{1 + k_4 f + k_5 P_{wt}} + k_6 \quad \text{(G2)}$$

where k_1= -5.9596; k_2= 8.9617; k_3= 4.66; k_4= -1.9107; k_5= -5.6145; k_6= -3.1427.

$$R_r(f, P_{wt}) = \frac{-5.9596 + 8.9617 \ln(f) + 4.66 \ln(P_{wt})}{1 - 1.9107 f - 5.6145 P_{wt}} - 3.1427 \quad \text{(G3)}$$

The errors obtained using equation (G3) to fit the curve shown in Figure G.2 is represented in the figures below:

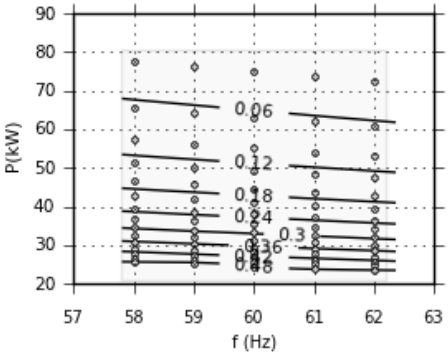

Figure G.3 Contour plot of Rr (f, Pwt) characteristic

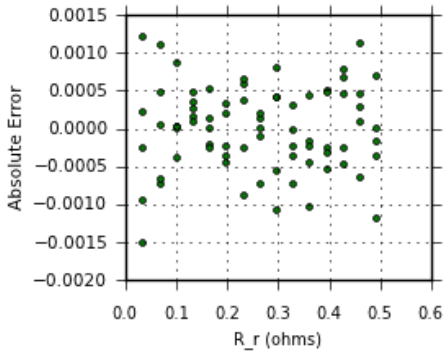

Figure G.4 Absolute error vs. rotor resistance plot

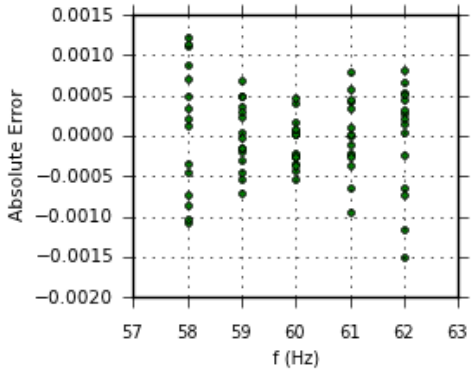

Figure G.5 Absolute error v.s. frequency plot

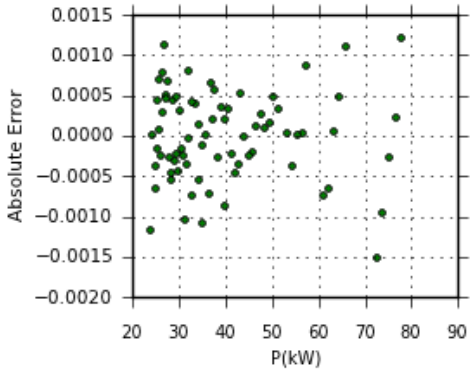

Figure G.6 Absolute error vs. power plot

The absolute errors shown in Figure G.4 to Figure G.6 are relatively small. Thus, equation (G3) provides a good description of the relationship between the external rotor resistance, injected power and grid frequency for the data considered in Table G.2.

The model of the case study presented in this Section can be represented as shown in the figure below.

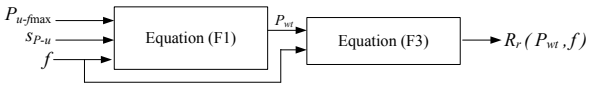

Figure G.7 Model of the rotor resistance variation vs. grid frequency and injected power at 12 m/s

a) At variable wind speed

The model presented in the previous subSection can be extended as shown in this Section to take into account a possible operation of the controlled WT for a given wind speed range. It is assumed that data points such as those represented in Table G.2 are available for each wind speed in the entire wind speed range. All the data at the individual wind speeds need to be fitted using the approach shown in the previous subsection such that all the curve fitting equations will have the same general form given in equation (G2). It is expected that, constants k_1 to k_6 at the individual wind speeds will have different values. The model represented in Figure G.7 can be extended for the selected wind speed range by inserting a look-up table that does the interpolation at a given wind speed to find the corresponding k_i constants, as illustrated in the following figure.

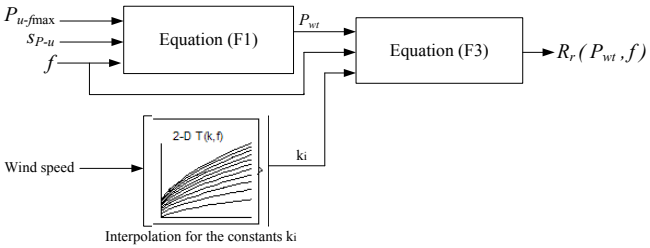

Figure G.8 Model of the rotor resistance variation versus grid frequency and injected power for a given wind speed range

For a given wind speed, the model shown in Figure G.8 interpolates for the constants k_i. It is assumed that parameters $P_{u\text{-}fmax}$ and $s_{P\text{-}u}$ are selected based on the wind speed at which the WT operates. If this condition is satisfied, the model should be able to predict accurately the external rotor resistance required for the desired operating point. Thus, by integrating this model conveniently in the model developed in Chapter 5 to generate the duty cycle of the IGBT switch, the proposed type 2 WT will be able to operate in any given wind speed range, providing that all

parameters of the model have been selected and set properly.

APPENDIX-H: Parameters of the individual machine types

TABLE A

THREE PHASE INDUCTION MACHINE PARAMETERS

Parameter	Value
Stator resistance(Ω)	1.4
Rotor resistance(Ω)	1.03
Stator leakage inductance (H)	2.675e-3
Rotor leakage inductance (H)	4.011e-3
Magnetizing inductance (H)	0.112
Nominal power (HP)	2
Number of pole	4
Synchronous frequency (Hz)	60
Capacitance for self-excitation (uF)	72
Nominal voltage (V)	208

TABLE B

PERMANENT MAGNET MACHINE PARAMETERS

Parameter	value
Nominal power (HP)	3.5
Nominal voltage (V)	208
Converter resistance(mΩ)	2.5
Stator winding resistance(Ω)	1.4
Stator d-axis leakage inductance (H)	5.6e-3
Stator q-axis leakage inductance (H)	9e-3
Moment of inertia (kg m^2)	6.5e-3
Number of pole	4
Synchronous frequency (Hz)	60
Permanent Magnet flux (Wb)	0.1546

TABLE C

CAPACITOR START INDUCTION MACHINE PARAMETERS

Parameter	value
Nominal power (HP)	15
Nominal voltage (V)	230
Main winding stator resistance(Ω)	0.575
Main winding rotor resistance(Ω)	1.1728
Auxiliary winding stator resistance(Ω)	2.0325
Auxiliary winding stator leakage inductance (H)	1.33e-3
Main winding stator leakage inductance (H)	1.15e-3
Main winding rotor leakage inductance (H)	0.8703e-3
Main winding mutual inductance (H)	0.0275
Moment of inertia (kg m2)	24.6e-3
Number of pole	4
Turn ratio (Nqs/Nds)	1/2.18
Synchronous frequency (Hz)	60
Capacitor impedance (Ω)	4.8-j*4.3

TABLE D

SPLIT PHASE INDUCTION MACHINE PARAMETERS

Parameter	value
Nominal power (HP)	1/4
Nominal voltage (V)	110
Main winding stator resistance(Ω)	2.02
Main winding rotor resistance(Ω)	4.12
Auxiliary winding stator resistance(Ω)	7.14
Auxiliary winding stator leakage inductance (H)	8.5e-3
Main winding stator leakage inductance (H)	7.4e-3
Main winding rotor leakage inductance (H)	5.6e-3
Main winding mutual inductance (H)	0.1772
Moment of inertia (kg m2)	7.3e-3
Number of pole	4
Turn ratio (Nqs/Nds)	1/1.18
Synchronous frequency (Hz)	60

TABLE E

PARAMETERS OF THE THREE PHASE INDUCTION MACHINE USED AS SINGLE PHASE GENERATOR

Parameter	Value
Stator resistance(Ω)	1.45
Rotor resistance(Ω)	5.5
Stator leakage reactance (Ω)	4.184
Rotor leakage reactance (Ω)	4.184
Magnetizing reactance (Ω)	70.87
Nominal power (HP)	5
Number of pole	4
Synchronous frequency (Hz)	60
Nominal voltage (V)	380

TABLE F

WIND TURBINE PARAMETERS USED IN CHAPTER 4

Parameter	Value
Rated power	100 Hp
Rated wind speed	12 m/s
Cut-in wind speed	6m/s
Rated grid frequency	60Hz
Grid frequency variation	+/- 3.33%

TABLE G

INDUCTION GENERATOR PARAMETERS USED IN CHAPTER 4

Parameter	Value
Rated power	100 HP
Rated voltage	460 V
Stator phase resistance	0.03957 Ω
Rotor phase resistance	0.02215 Ω
Stator and rotor phase reactance	0.1467 Ω
Magnetizing reactance	6.27 Ω
Number of poles	4
Base frequency	60 Hz
Moment of inertia	1.3 kg.m^2

TABLE H

WIND SYSTEM PARAMETERS USED IN CHAPTER 3

Parameter	**value**
3-blade wind rotor with β = 0°	
Nominal power	5 HP
Nominal wind speed	10m/s
Blade diameter	5.6m
Moment of inertia	4.5Kg-m^2
Air density	1.25 Kg/m^3
Gear box ratio (K_{gb})	6.8
Induction generator	
Nominal power	5 HP
Stator phase resistance	1.45Ω
Rotor phase resistance	5.5Ω
Stator and rotor phase reactance	4.184Ω
Magnetizing reactance	70.87Ω
Number of poles	4
Base frequency	50Hz

TABLE I

WIND TURBINE DRIVE TRAIN PARAMETERS

Parameter	**value**
Rotor moment of inertia (kg.m^2)	1300
Shaft stiffness on generator side (Nm/rad)	5252
Damping coefficient on generator side (Nms/rad)	4.11

TABLE J

WIND SYSTEM PARAMETERS USED IN CHAPTER 5

Parameter	**value**
2-blade fixed-pitch wind rotor	
Rated power	100 HP
Rated wind speed	12 m/s
Cut-in wind speed	6 m/s
Rated grid frequency	60 Hz
Grid frequency range	58Hz-62Hz
Rotor radius	10.4m
Pitch angle	0°
Gear box ratio (K_{gb})	1:7.8
Wound rotor Induction generator	
Rated power	100 HP
Rated voltage	460 V
Stator phase resistance	0.0646 Ω
Rotor phase resistance	0.03281 Ω
Stator phase inductance	0.587 mH
Rotor phase inductance	0.9751 mH
Magnetizing inductance	22.5 mH
Number of poles	4
Base frequency	60 Hz

TABLE K

DIESEL ENGINE PARAMETERS

Parameter	**value**
Engine torque constant (k_{eng})	1
Actuator constant (k_a)	1.0
Engine inertia (J)	0.88 kg.m^2
Actuator time constant (τ_a)	0.05-0.2
Engine dead time (τ_{eng})	0.011s
Engine friction coefficient (Nms)	0.03